AERONUTRONIC

A DIVISION OF

Ford Motor Company

Publication No. U-1458
Dated November 1961

SPECIAL PROGRAMS OPERATIONS

Submitted to:

Chief
Bureau of Ships
Code 420
Department of the Navy
Washington, D. C.

Contract No. NObs 84364
Index No. SF 0130207
Task 1714

TECHNICAL REPORT

PROGRAM FOR REDUCTION OF HYDRO-SKIMMER POWER REQUIREMENTS

16000

Prepared by:
W. L. Rawlings

D. H. Seiveno

Approved by:
M. F. Southcote, Manager
Air Transportation

AERONUTRONIC
A DIVISION OF Ford Motor Company
FORD ROAD / NEWPORT BEACH, CALIFORNIA

SECTION I

SUMMARY

An experimental program for the development of a flexible flap for hydroskimmer type vehicles is described. A successful flexible flap configuration was developed. Calculations indicate that power requirements may be reduced by a factor of approximately 3 to 1.5 on a typical hydroskimmer vehicle operating at 60 knots. Recommendations are made for further development.

Data from a large-scale, two-dimensional model over a flat ground plane show that rigid flaps that extend both sides of the jets provide a substantial power saving over an unflapped model of otherwise identical configuration. Tests with various ratios of inner to outer flap length show that little performance is gained through the use of inner flaps.

Dynamic tests of a series of different flexible flaps attached to the above model, but with the model mounted over a moving wave train, have demonstrated that a successful flexible flap configuration can be constructed. The power requirements of a typical hydroskimmer vehicle operating in two different sea states are predicted both with and without flaps.

TABLE OF CONTENTS

SECTION II

INTRODUCTION

HOVERING POWER

Three primary parameters affect hovering power at constant gross weight. Hovering power:

1. increases approximately linearly with vehicle height;
2. decreases inversely with vehicle base area; and
3. is proportional to the square root of the planform loading.

Figure 2-1 shows hovering horsepower required per foot of altitude for a ton of gross weight as a function of planform area for an annular jet type vehicle of circular planform with variable "optimum" geometry. If the height above the ground is doubled, there is twice as much gap between vehicle and ground to be sealed. Hence, to double the height, twice the power is required.

The second point to be seen is the fundamental effect of size on power required for a given amount of lift. The large reduction in power required as the size increases is evident. The reason is apparent from a consideration of the simple momentum theory. The lift that is generated depends on the area, which increases with the square of the diameter. The perimeter which determines the power required, varies directly with the diameter. For example, if the diameter is doubled, the area, and therefore the lift, increases by a factor of 4, whereas the perimeter, and therefore the power required increases by only a factor of 2. As a result, the horsepower per unit lift is reduced by a factor of 2. The thing to note is the inherent increase in efficiency of air-cushion vehicles as the size increases (assuming height remains constant).

HOVERING POWER
CIRCULAR PLANFORM

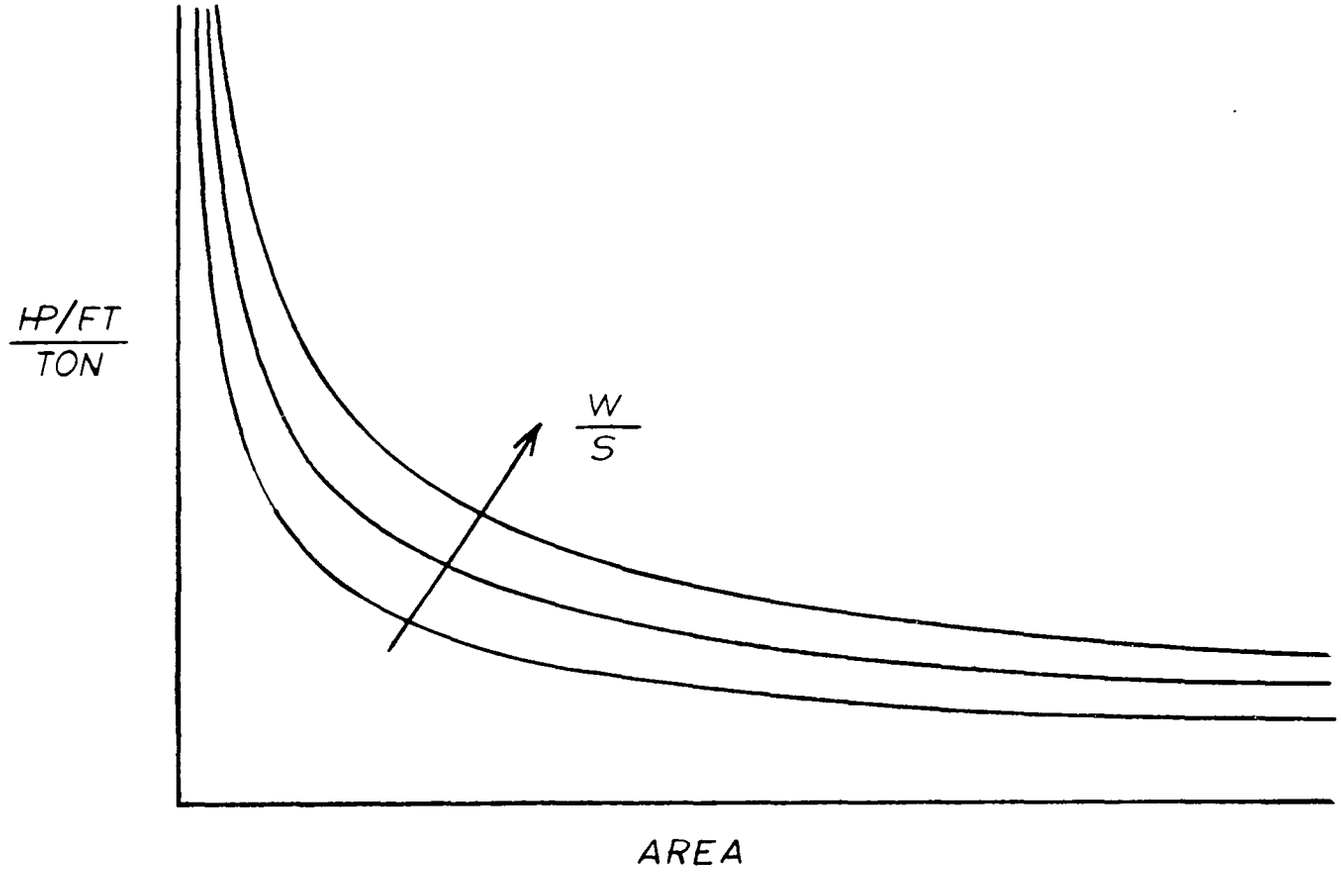

FIG. 2-1

The third point demonstrated is the effect of planform loading. The planform loading is roughly proportional to base pressure which is directly proportional to jet total pressure (for a given jet thickness and height). Therefore doubling the planform loading requires approximately double the jet total pressure and results in doubling the lift for a given area. Now, power required is proportional to the product of the jet total pressure and the volume flow, and volume flow is proportional to the square root of jet total pressure. Power is thus proportional to jet total pressure to the (3/2) power. Doubling the planform loading thus increases power by the ratio of $2^{3/2}$. However, as noted before, the lift has also doubled. The ratio of power per ton of lift is then, $2^{3/2}/2$ or $2^{1/2}$ times the previous ratio. Power required per ton is seen to be proportional to the square root of the planform loading.

The flexible flaps described in this report offer a method for reducing the effective aerodynamic height while sufficient vehicle clearance height is maintained to insure that the vehicle base contacts the water only infrequently.

FORWARD MOTION

As forward velocity is increased, cushion power (that power required for lift) decreases somewhat due to the change in static pressure distribution around the vehicle. In this report it is assumed that full dynamic pressure is recovered along the front of the vehicle and that the pressure along the rear of the vehicle is one-half of dynamic pressure lower than ambient. This means that as velocity increases, progressively less power is required to sustain a given base pressure at the front of the vehicle, and vice-versa at the rear. Since the static pressure changes more at the front than at the rear, a net decrease in cushion power with velocity results. This is shown on Figure 2-2.

Momentum drag is defined as the product of jet mass flow and the difference between vehicle velocity and the horizontal component of jet velocity. Although the jet mass flow decreases with velocity (due to the lowered cushion power requirements), the velocity change increases more rapidly. This results in the rapid increase in momentum drag with vehicle velocity that is shown in Figure 2-2.

FIG. 2-2

POWER REQUIRED

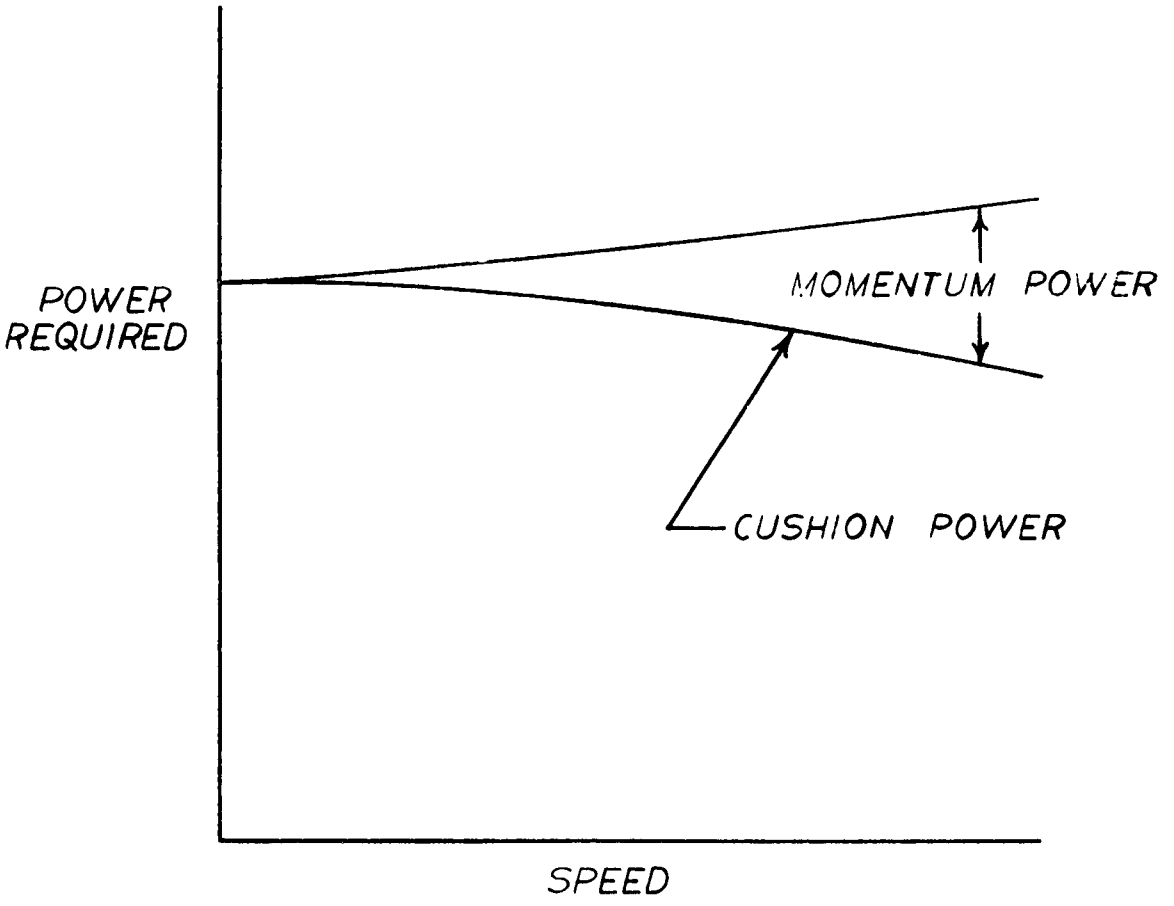

Power is required to overcome several other drag forces (aerodynamic drag, wave drag, skeg drag, internal flow system loss factors). These forces change only slightly, if at all, when flaps are installed on a vehicle, so will not be discussed further here. The installation of flaps on a vehicle will reduce effective height, and hence jet thickness. The reduced jet thickness requires a lower jet volume flow which lowers both cushion power and momentum drag.

PROGRAM PHILOSOPHY

At the high speeds (above about 50 knots) being considered for hydroskimmer type vehicles, water waves will appear solid to a flexible flap. This permits the simulation of the motion of flexible flaps over water with solid waves. Several advantages accrue through the use of solid waves. These are:

1. A much simpler testing procedure may be utilized.
2. Test parameters may be more closely controlled.
3. Both of the preceding advantages result in lower costs.

Therefore, the program approach was to create a severe dynamic environment for the flaps through the use of a solid wave system.

SECTION III

NOMENCLATURE

b	Beam, model or vehicle	ft
C	Discharge coefficient	-
C_b	Base pressure coefficient $= \frac{p_b}{p_{t_j}}$	
$\bar{C}_r$	Jet reaction coefficient $= \frac{\int_0^{t_e} \left(p_j + 2q_j\right) dt}{p_{t_j} \quad t_e}$	-
$\bar{C}_v$	Jet velocity coefficient $= \frac{\bar{V}_j}{V_{j_o}}$	-
D	Drag	lb
$H.P._{Aero + W.D.}$	Horsepower required to overcome aerodynamic and wave drag	-
$H.P._{Aero + W.D. + Skeg}$	Horsepower required to overcome aerodynamic, wave and skeg drag	-
$H.P._{F.D.}$	Horsepower required to overcome flap drag, exclusive of friction	-
$H.P._{F.F.D.}$	Horsepower required to overcome flap friction drag	-
$H.P._c$	Horsepower required to sustain lift	-
$H.P._m$	Horsepower required to overcome momentum drag	-

h	Height (flap tip to wave trough or ground)	ft
h_b	Height (base to wave trough or ground)	ft
h'	Integrated average height above sine wave (h' or h_b')	ft
ℓ	Flap length	ft
L	Lift, vehicle or flap	lb
M	Moment at flap balance strain gage locations	in-lb
p_b	Base pressure (gage)	lb/ft^2
p_o	Ambient pressure	lb/ft^2
p_j	Jet static pressure (gage)	lb/ft^2
p_{t_j}	Jet total pressure (gage)	lb/ft^2
q	Dynamic pressure	lb/ft^2
Q	Jet volume flow	ft^3/sec
R	Jet reaction force	lb
S_b	Base area	ft^2
S_j	Jet area	ft^2
t_e	Jet exit width	ft
V	Velocity	ft/sec
W	Wave height, trough to crest	ft
x	Jet shape parameter = $(te/h)(1 + \sin \theta)$	-
θ	Angle between vertical and jet centerline	-
ρ	Mass density of air	$lb\text{-}sec^2/ft^4$

SECTION IV

LIST OF ILLUSTRATIONS

SECTION V

TEST EQUIPMENT

Previously Fabricated Equipment

During a previous government sponsored air-cushion program, Aeronutronic fabricated a test stand of considerable flexibility. This stand is shown in Figure 5-1. The angle iron tower supports a 30 HP electrical motor and a Chicago Airfoil Centrifugal Blower, the pressure-flow capabilities of which are illustrated in Figure 5-2. These characteristics permit large scale experiments over a wide range of simulated vehicle planform loadings. The split flow ducting beneath the blower is fitted with two baffles in each passage to control the discharge total pressure at both ends of the simulated vehicle base.

The cart into which the jets discharge is a two-dimensional flow channel two feet wide and open at each end. It is particularly suitable for hydroskimmer investigations because of the two-dimensionality of the jet flow in hydroskimmers. The ground board in the channel is adjustable in both height and attitude.

Equipment for Preparatory Investigation

In anticipation of this contract program, Aeronutronic performed a series of tests to investigate the potential performance advantages offered by the use of flexible flaps. The configuration shown in Figure 5-1 was modified by the installation of vertical, two inch thick jets. Extensions were fabricated for both the inner and outer nozzle walls. A sketch of the installation of these extensions is shown in Figure 5-3, which also illustrates the nomenclature. The lengths of these extensions are tabulated below.

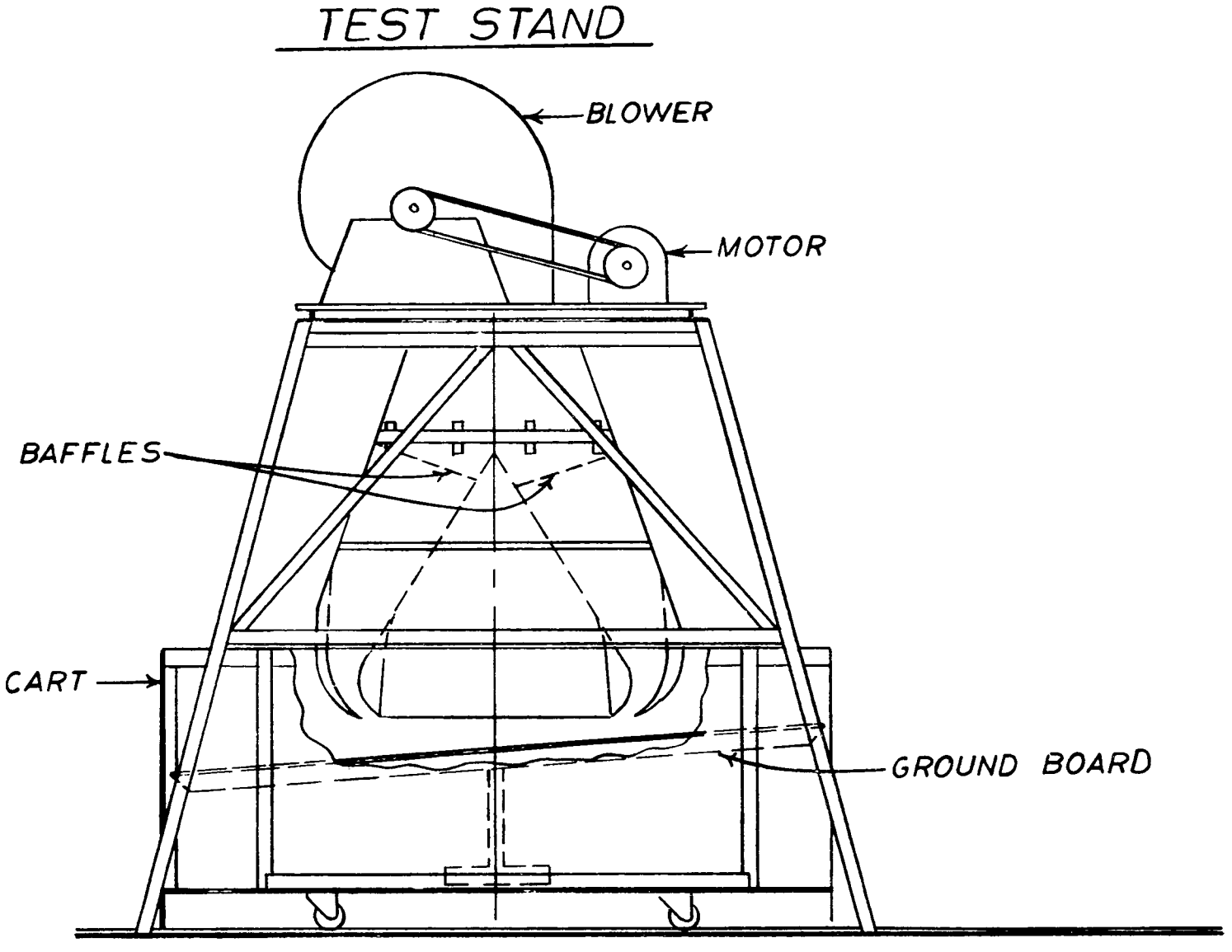

FIG. 5-1

AVAILABLE PRESSURE VS. FLOW

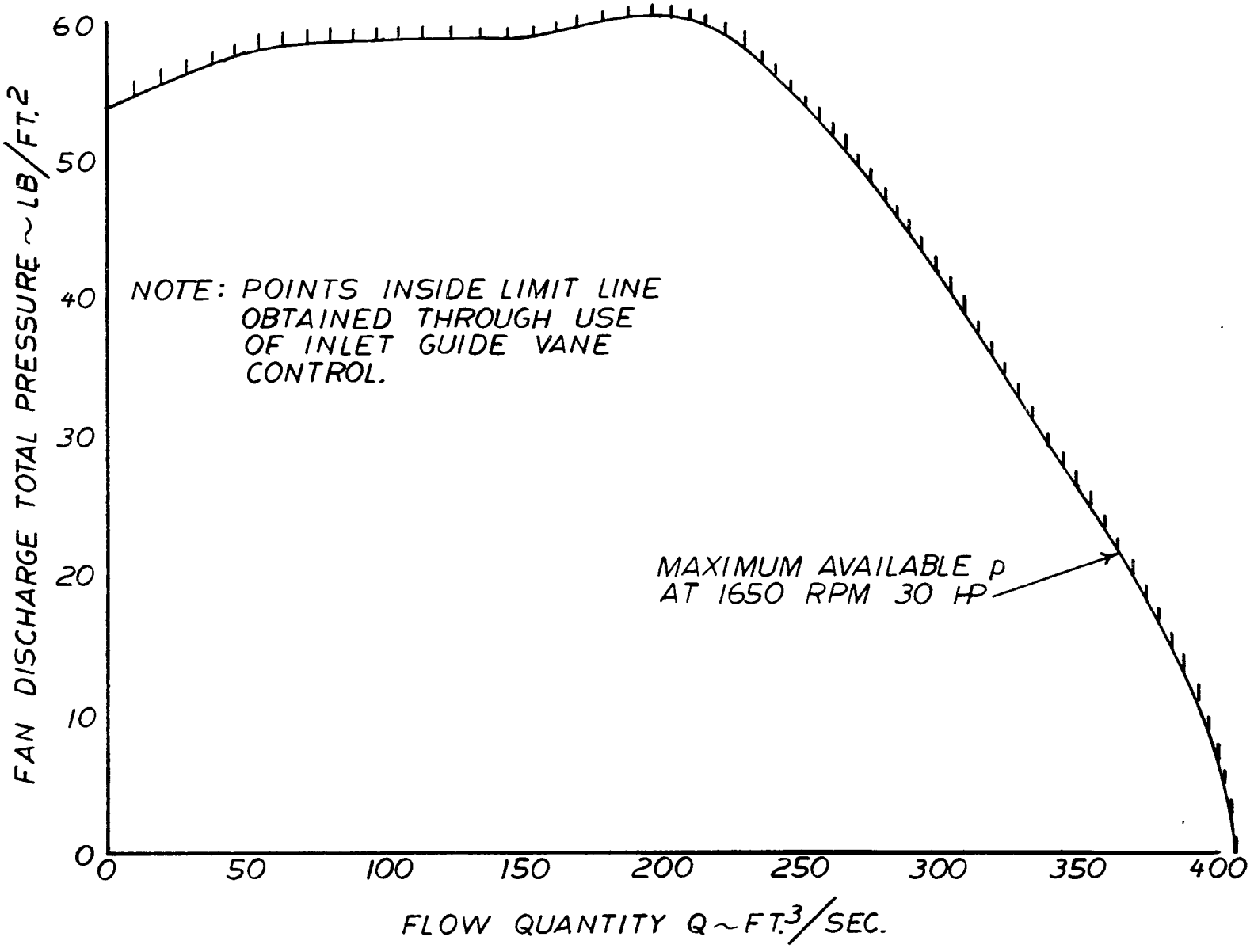

FIG. 5-2

RIGID FLAP NOMENCLATURE

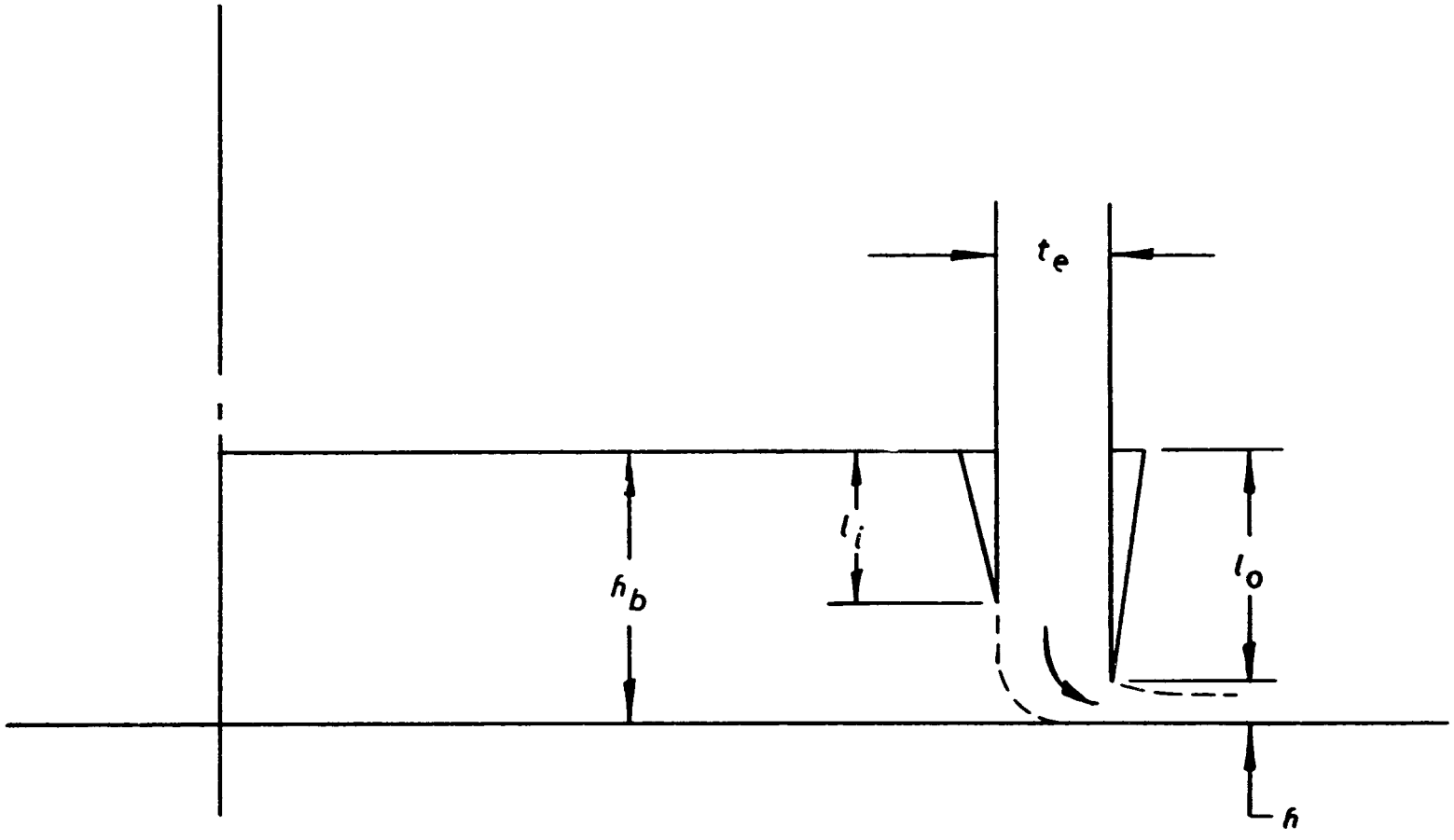

FIG. 5-3

Nozzle Extension Lengths

Length (inches)	Inner Wall	Outer Wall
	1	1
	2	2
	3	3
	4	4
	6	6
	8	8
	12	12

The combinations of outer and inner nozzle walls tested are described in a later section of this report.

Both jets were surveyed by the use of ten-probe pressure rakes, each of which had five total head probes and five static head probes. The total probe openings were at the same streamwise station as the static probe openings so that the two readings could properly be compared.

Figure 5-4 shows schematically the location of all the pressure instrumentation used in the tests. The numbers by the taps show the order in which the taps were connected to the 50 tube, 100 inch manometer. The data on the manometer board were recorded on a 4" x 5" speed graphic camera with a polaroid back using positive transparency film. In this fashion, the data records were available in permanent form very soon after the run. They could be examined immediately to insure accurate and clearly legible records.

Flexible Flap Test Equipment

Wave Simulator

One major item was fabricated for the flexible flap tests and several modifications were made to the test stand.

The major construction item was a moving wave system which traveled within the two dimensional flow cart. Figure 5-5 is a schematic sketch of the installation. The wave is cut from a flexible urethane elastomer foam. The wave is segmented due to difficulties which arose in stretching of the neoprene protective cap sheet when the wave went around the large pulleys at the ends of the machine. The method of bonding the wave

PRESSURE INSTRUMENTATION LOCATION

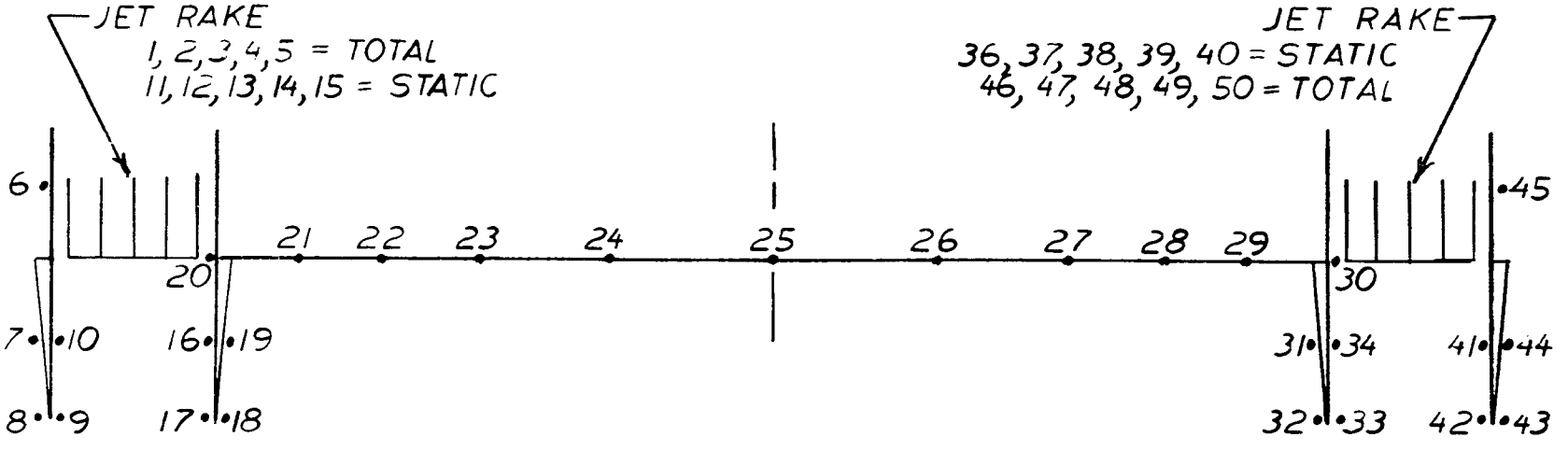

STATIC TAP NO. 7, 10, 16, 19, 31, 34, 41, 44
USED ONLY IN EXTENSIONS
6 INCHES OR LONGER

FIG. 5-4

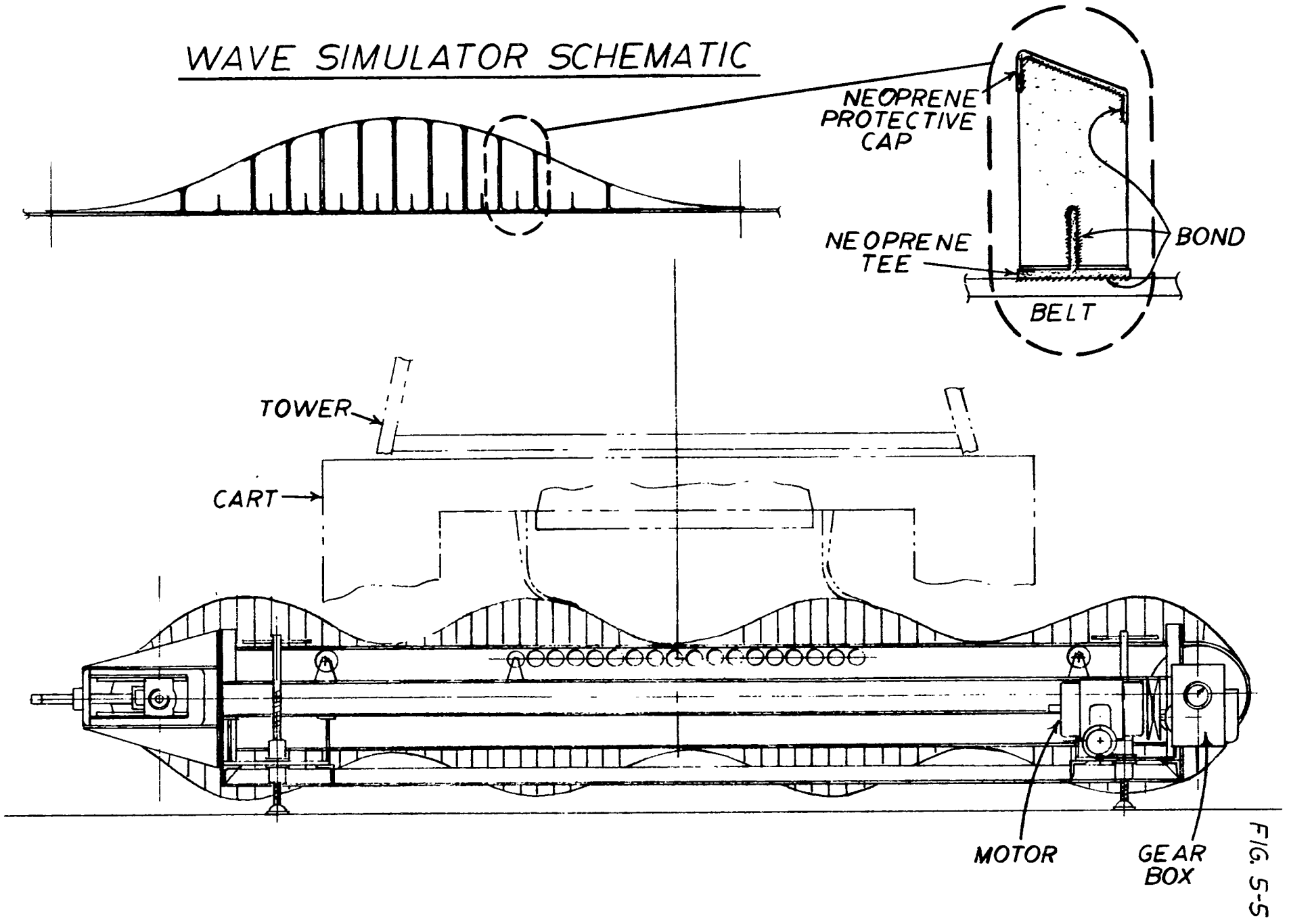
WAVE SIMULATOR SCHEMATIC
NEOPRENE PROTECTIVE CAP
NEOPRENE TEE
BOND
BELT
TOWER
CART
MOTOR
GEAR BOX

FIG. 5-5

segments to the belt is also shown for one segment. This bonding technique permitted the wave to negotiate the pulley turns with no deformation strain on any of the segments. Thus, the protective cap sheets underwent no strain and could be firmly bonded in place.

The wave shape is sinusoidal with a length to height ratio of 7:1. The wave is in phase with the jets; i.e., the wave length is the same as the distance between jet centerlines, 50 inches. The entire wave system is adjustable in its vertical location through the use of the screw jacks at the four corners.

Motive power is supplied by a 5 horsepower electric motor with a "Rotocone" variable diameter sheave on the drive shaft. A 5:1 speed reduction gear box is driven by either of two interchangeably installed, fixed diameter sheaves which in turn are driven by the Rotocone. Using the two different diameter sheaves permits a wave system speed variation of 1 to 5 cycles per second. The entire system is reversible in direction through a forward-reverse starter switch. The frictional drag between flap and wave was reduced by greasing the wave.

The outer walls of the jet were replaced with considerably stronger structure. The previously used walls were mere aerodynamic fairings and were not considered strong enough to withstand the dynamic impact loads which were predicted. The aerodynamic contour of the original walls was retained.

Instrumentation

Nine Dynisco DPT85-1, $\pm$ 0.5 psi differential pressure transducers were obtained for this test. Two of these transducers were attached to jet total pressure probes and two were attached to jet static pressure probes. These probes measured pressure on the jet centerlines. Aeronutronic's familiarity with the flow pattern in the test stand (see Reference 1) made it possible to determine average jet static and total pressures by this simple procedure.

The other five transducers were installed in the base of the model. They were attached to a sliding rack which could be moved to either of two positions for measuring pressures. Thus, with five transducers, base pressures could be measured at 10 stations.

The strain beams originally designed are three component balances, intended to measure lift, drag and moment caused by impact of the wave on the flap. Two such beams were made. Unfortunately, the deformation of these beams under load was such that the noise in the system was of the same magnitude as the signal, and the data readout was difficult to interpret. This was particularly true of the lift channel. Accordingly, the lift channel was not used.

A twelve channel Minneapolis Honeywell Visicorder Oscillograph was used for recording the data. The instrumentation described actually required 4 channels for strain measurement, 4 for jet total and static pressures and 10 for base pressures (2 positions of the 5 station track) for a total of 18 channels. In addition, one channel was required to act as a wave position indicator. Whenever a wave crest passed a jet centerline, a magnetic pickup sensed the passage of a metal nut imbedded in the wave. This caused a pip on the Visicorder record.

All these channels were recorded as follows. The "bow" strain beam was switched into the Visicorder and the 2 position transducer track was moved to its foremost position. The air was turned on and the wave machine started while the Visicorder recorded the bow beam, 4 jet pressures and 5 base pressures. The stand was shut down and the stern beam was switched into the recorder to replace the bow beam and the transducer track was moved to its aftmost position. The recording process was then repeated. Thus, the twelve channel recorder produced 24 channels of information; 4 channels of strain measurement (2 twice), 10 of base pressure (5 twice), 8 of jet pressures (4 twice) and 2 of wave position (1 twice).

In addition to the aforementioned difficulty in interpretation of the strain channel data, a further difficulty was encountered in the reduction of the test data. In order to permit free travel of the wave system through the cart, there was a small clearance allowed between the edge of the belt and the sides of the cart. Leakage through this narrow clearance was greater than anticipated. The exact difference could not be determined. It was, therefore, deemed advisable to repeat some of the tests which appeared to be the most valuable.

For these tests, a new strain beam was made which had sufficient output to give a clearly defined signal. This beam is sketched in Figure 5-6.

FIG. 5-6

FLAP BALANCE

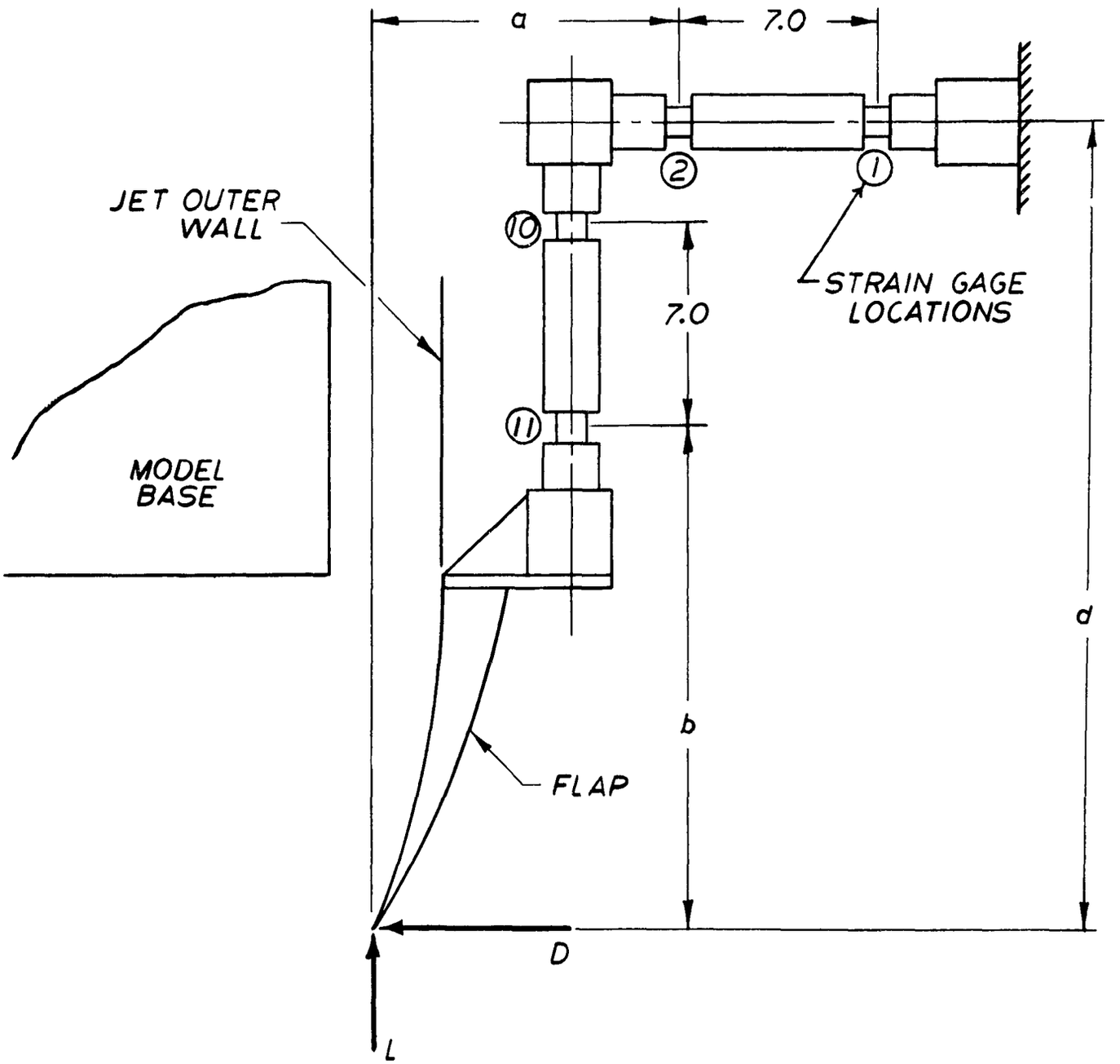

Further, it was seen possible to reduce the amount of pressure instrumentation in the base region without reducing the effectiveness of the data analysis. Three pressure transducers were mounted permanently in the base; one in the center of the base and one at each end as close to the end as the 2 inch diameter of the transducer permitted. In addition, a parallel set of instrumentation was set up using the previously mentioned manometer board. Each transducer tap was matched by a corresponding manometer pressure tap placed as close as possible without interference. Under static conditions this gave a good check of the transducer output by an independent instrumentation system. Data interpretation in the second series of tests was facilitated by the use of a 36 channel Visicorder Oscillograph with 12 inch wide paper. This permitted the 12 channels recorded to be spread out over a much wider area.

The leakage problem was effectively reduced by the installation of a combination of sliding and non-sliding seals. The sliding seals were installed in the cart underneath the belt. The seals were in intimate contact with the belt thus providing an efficient seal. Teflon tape was used to reduce friction forces between the belt and the seals. Unfortunately, the friction was great enough to reduce the maximum speed capability of the belt to 3½ cycles per second. In the test section where the belt is supported by an array of closely spaced rollers, this type seal could not be used. Strips of flexible urethane foam were forced between the wave machine rails and the sides of the cart to reduce the leakage in this region. These seals were not completely effective, but a simple correction for the leakage was devised and will be discussed later.

Flexible Flap Models

Two basic concepts of flexible flap were evolved during this program. Two variations of one of these and one of the second were tested. The first basic concept is of a flexible foam core on which a skin of elastomeric sheet material is bonded. The foam core may be one of several materials as may be the skin. The core may also be of composite construction to provide various bending and/or buckling characteristics. The same may be said of the skin. For example, fiberglas cloth may be used to make "sandwich" type skin in various combinations of thicknesses. Several combinations were given preliminary evaluation during this program.

The two variations of this concept actually tested in the dynamic wave facility are shown in Figure 5-7. They are constructed of flexible urethane foam and covered with urethane elastomer sheet. The only difference in these two variations is in the width of the flap sections. The larger of the two variations is essentially four of the smaller sections bonded together with alternate half length and full length ribs rather than all full length ribs. This provides a built in weak point where the flap will buckle when subject to a load at the tip. Thus only half the flap will buckle rather than all of the flap.

The second basic concept utilizes the principle of lateral buckling of a beam. For a thorough discussion of this principle, see Reference 4. Two flexible rods (for example, fiberglas) are imbedded in a rod of solid urethane elastomer as illustrated in Figure 5-8. The base pressure loads the beam about its major structural axis. As loads greater than the beam's buckling strength are applied, the beam rotates and bends about its minor structural axis. The slope of the load vs. deflection curve is much less after the rotation than before, and the applied load will increase only slightly beyond this point as sketched below.

The specimens fabricated and tested are of the geometry shown in Figure 5-8. The rods are bonded to the mounting block with major axes parallel. Two flaps were made up of 64 such rods each to fit into the two foot wide test section.

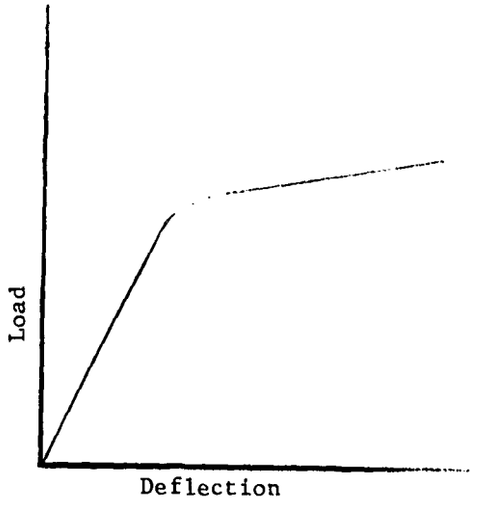

FOAM CORE FLAP TEST SPECIMENS

FACES 1/16" THICK
SIDES AND RIBS 1/32" THICK
FLEXIBLE OPEN CELL URETHANE FOAM CORE

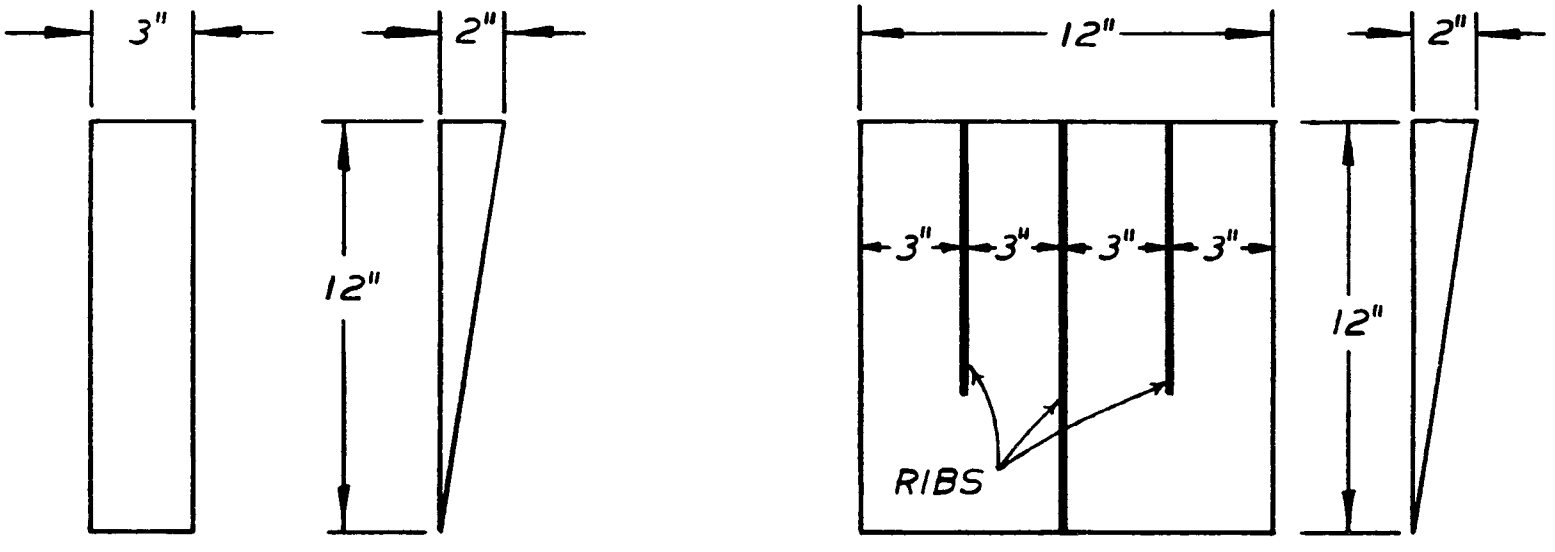

FIG. 5-7

FIBERGLAS REINFORCED URETHANE ROD

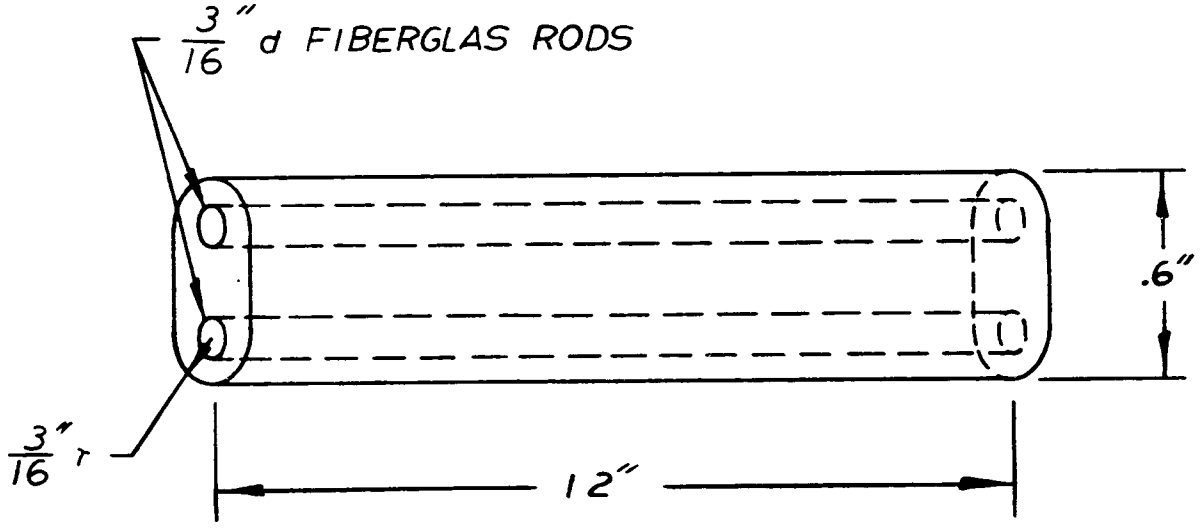

FIG. 5-8

SECTION VI

DATA ANALYSIS METHODS

Vehicle Performance Data

Pressure data were reduced to the form originally proposed by Stanton-Jones in Reference 2 and extended in Reference 3. With this method base pressure, jet reaction and jet velocity are expressed in the usual coefficient form, but are presented as functions of the parameter

$$x = (te/h)\ (1 + \sin\theta)$$

rather than the previously used parameter te/h. When x is used as the independent variable, the jet efflux angle θ is eliminated as a parameter and only one line appears for all jet angles. Theoretical equations for the three performance coefficients are listed below in terms of x.

$$C_b = \frac{P_b}{\bar{P}_{t_j}} = 1 - e^{-2x}$$

$$\bar{C}_r = \frac{\bar{P}_j + 2\bar{q}_j}{\bar{P}_{t_j}} = 1 + \frac{1}{2x}\left(1 - e^{-2x}\right)$$

$$\bar{C}_v = \frac{\bar{V}_j}{\bar{V}_{j_o}} = \sqrt{\frac{\bar{q}_j}{\bar{P}_{t_j}}} = \frac{1}{x}\left(1 - e^{-2x}\right)$$

The validity of x as a correlation parameter is demonstrated in Figures 6-1, 6-2, and 6-3 which present C_b, $\bar{C}_r$ and $\bar{C}_v$ data

FIG. 6-1

BASE PRESSURE COEFFICIENT

AERONUTRONIC DATA COMPARED TO
STANTON JONES EXPONENTIAL THEORY
SINGLE JET DATA FROM REF. 1
DOUBLE JET DATA FROM
UNPUBLISHED AERONUTRONIC WORK

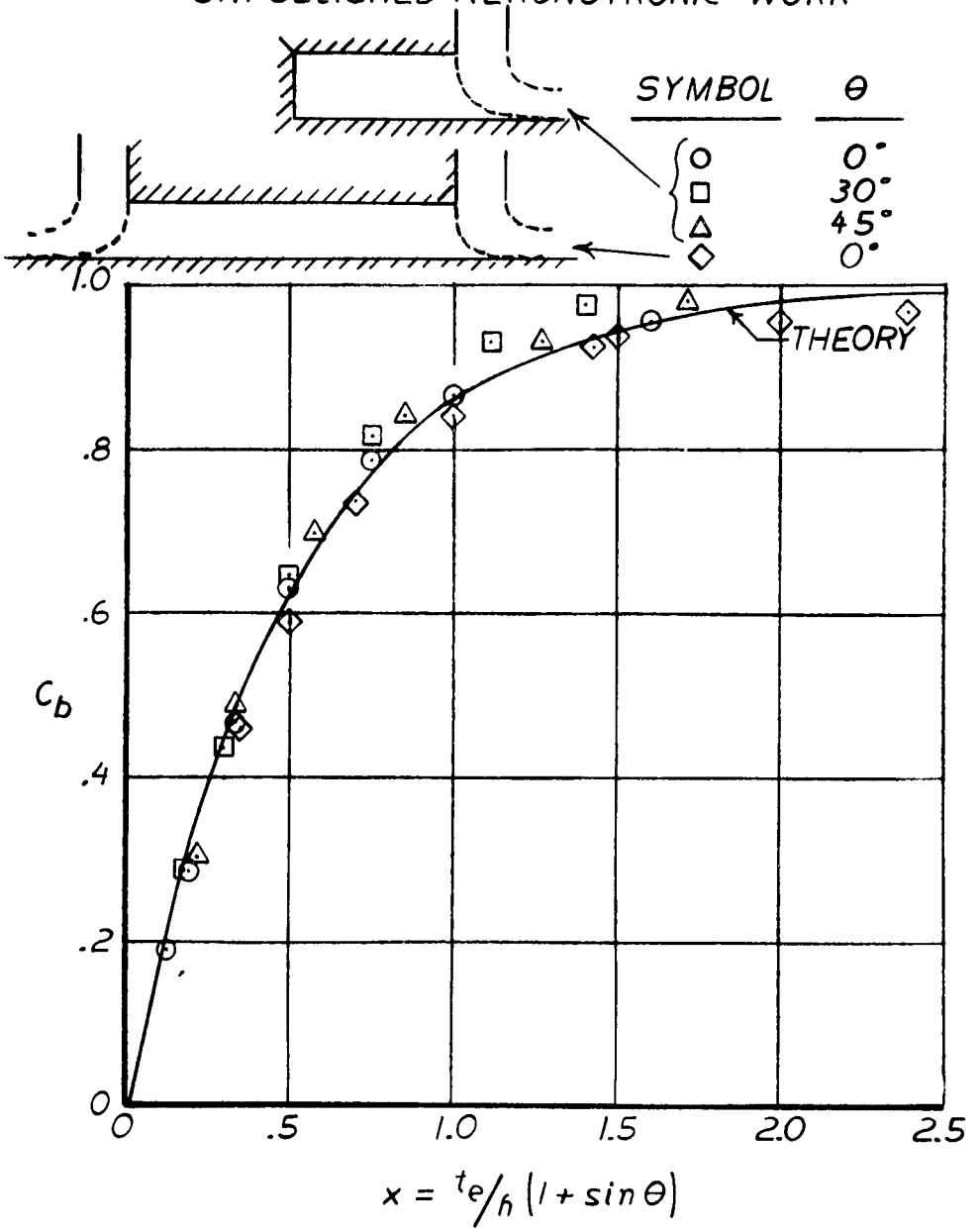

FIG. 6-2

JET VELOCITY COEFFICIENT

AERONUTRONIC DATA COMPARED TO
STANTON JONES EXPONENTIAL THEORY
DATA FROM REF. 1

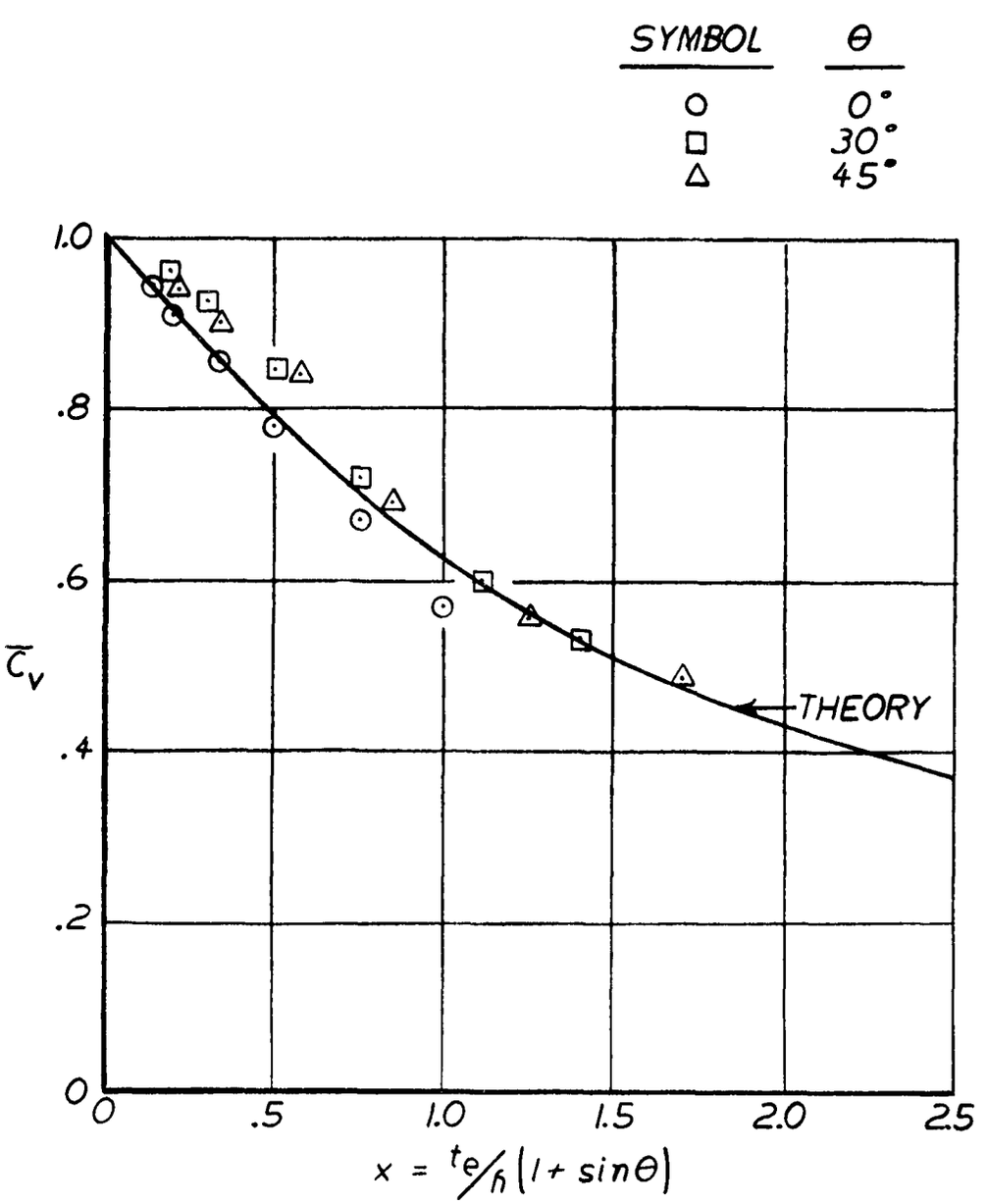

FIG. 6-3

JET REACTION COEFFICIENT

AERONUTRONIC DATA COMPARED TO
STANTON JONES EXPONENTIAL THEORY
DATA FROM REF. 1

SYMBOL	θ
○	0°
□	30°
△	45°

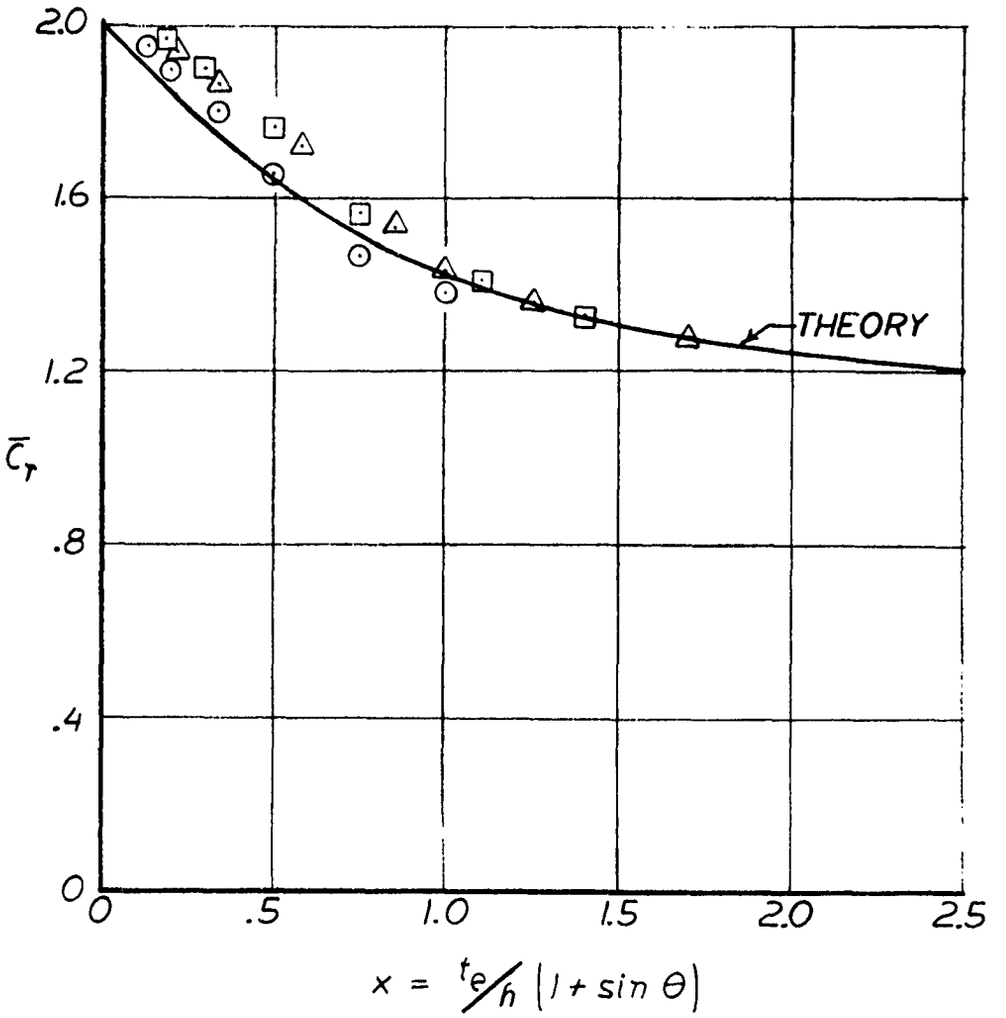

from Reference 1 plotted against x. Correlation was shown in Reference 3 using data from Reference 1. Figures 6-1 through 6-3 include additional data and are included herein for convenient reference.

Dynamic data were averaged over several cycles by drawing a straight line through the oscillograph traces in such a way that the pressure oscillations traced equal areas on each side of the straight line. A typical oscillograph record is shown on Figure 6-4.

Height as used in discussing the coefficient data herein differs from the usual definition in two significant ways:

1. The bottom of the vehicle is taken as the lower edge of the flap rather than as the base.

2. When the ground surface undulates, height is measured either from the wave troughs or as an integrated average height over one cycle.

The height nomenclature is illustrated in Figure 6-5a.

It will be shown in the first part of Section VII that for better data correlation the height of a flapped vehicle should be measured from the ground to the lower tip of the flap rather than to the vehicle base. Although the coefficients C_b, $\overline{C}_r$ and $\overline{C}_v$ do not look as impressive when plotted in this manner, experimental data correlates much better.

When considering the height of a flapped vehicle above a wavy surface, two problems present themselves; first, the height is constantly varying as the vehicle moves over a wave, and second, height may be zero for part of the cycle if the flap comes into contact with the wave surface. Defining height as an integrated average over one wave cycle will account for the continuous variation in height with wave position and will also account for contact between the flaps and wave during any portion of the cycle. The integrated average height was determined from the equation

$$h' = \frac{\int_0^Z h_z \, dz}{Z}$$

where the terms are as noted in Figure 6-5b.

FIG. 6-4

TYPICAL OSCILLOGRAPH RECORD

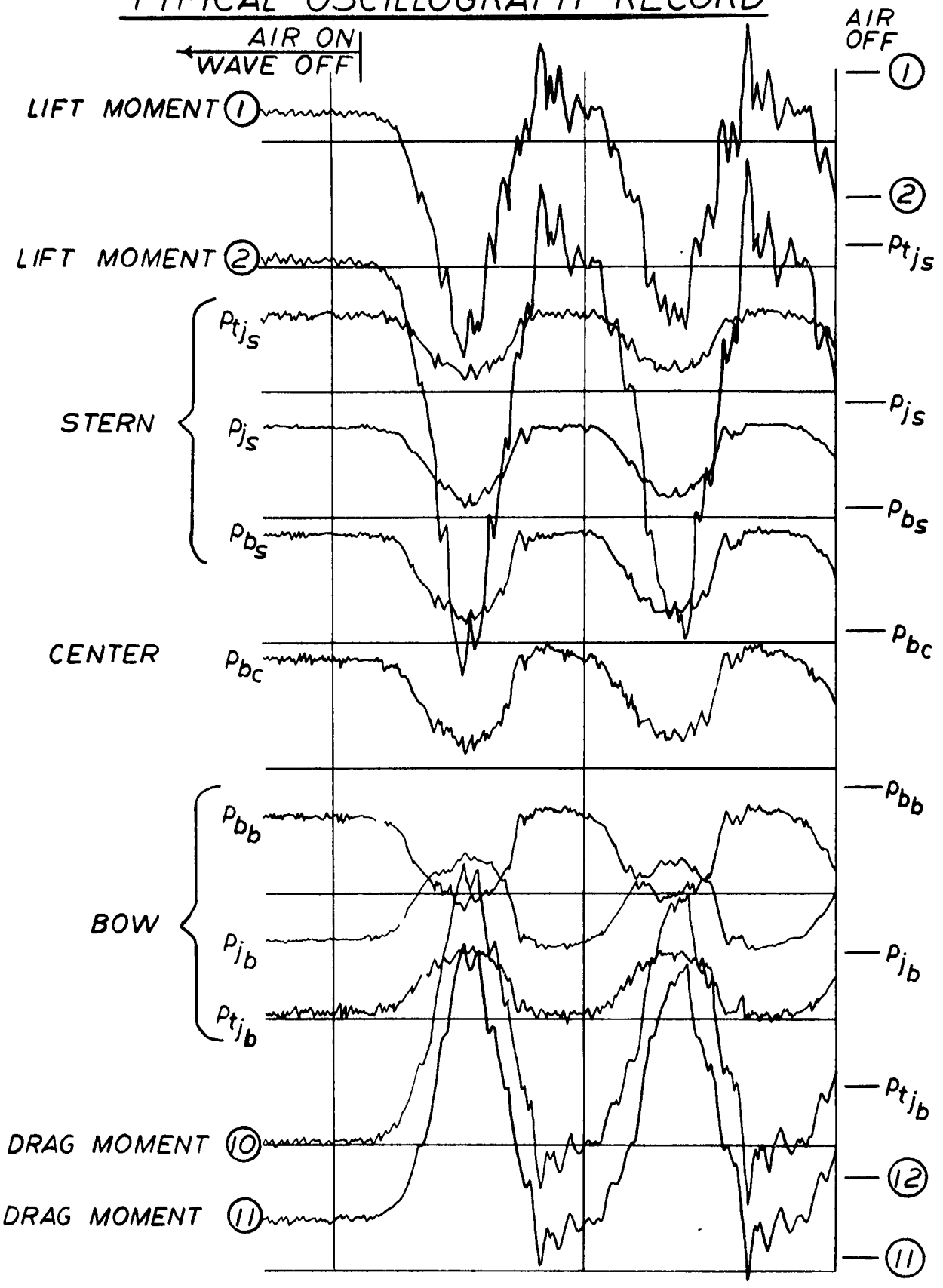

FIG. 6-5

WAVE AND FLAP HEIGHT NOMENCLATURE

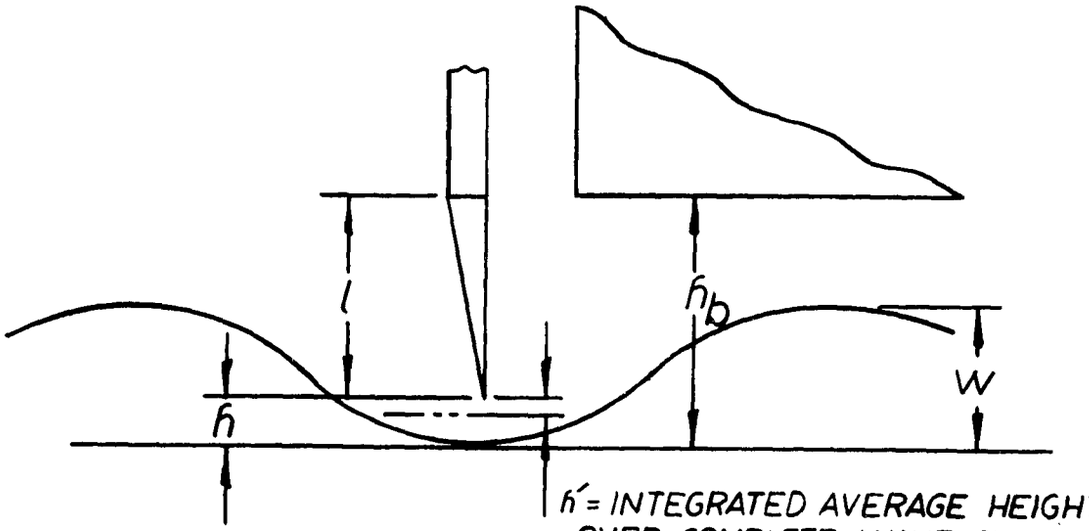

h' = INTEGRATED AVERAGE HEIGHT OVER COMPLETE WAVE CYCLE

$$= \frac{\int_0^Z h_z \, dz}{Z}$$

NOMENCLATURE FOR DETERMINATION OF INTEGRATED AVERAGE HEIGHT

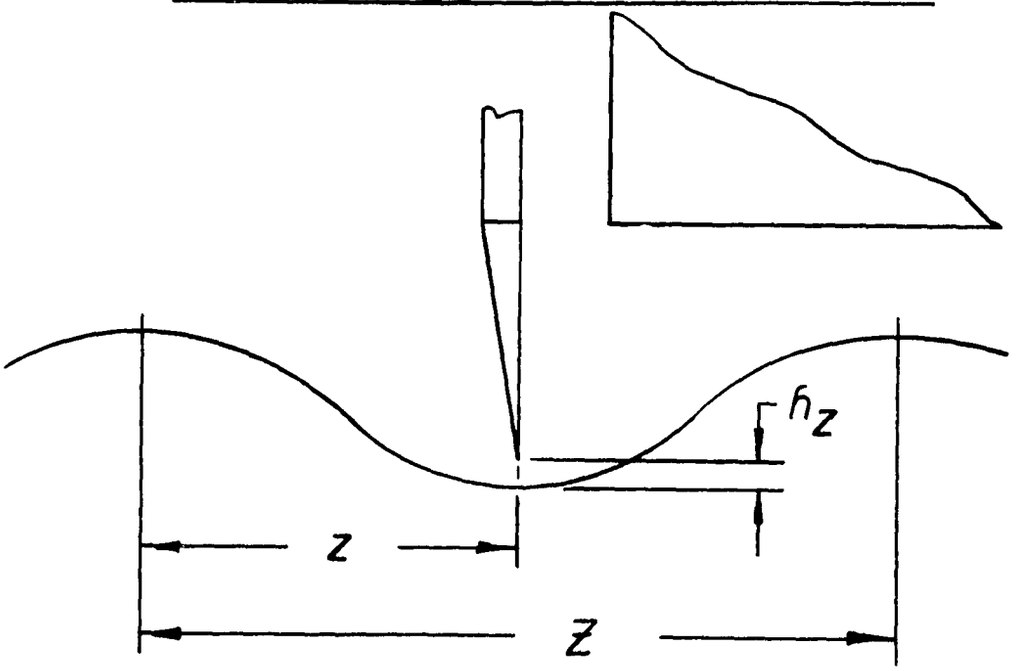

As the flap is lowered into a wave trough, $\bar{x}'$ (based upon h') will increase very rapidly because the actual height h is zero for an increasingly larger portion of the wave cycle. If the performance coefficients C_b, $\bar{C}_r$ and $\bar{C}_v$ are plotted as functions of x' they will approach an asymtote much less rapidly than as functions of x. For this reason, pressure, reaction and velocity coefficients are presented as functions of x where h is measured to the wave trough. Separate curves, Figures 6-6 and 6-7 are presented for relating h and x to the integrated averages h' and x'. Performance coefficients based upon integrated average heights may be obtained by converting x' to x (Figure 6-7) and then entering the performance coefficient curves with the x from Figure 6-7.

When the flap tip is very close to the wave trough or the ground, or when the integrated average height to the flap tip is very small, the flow no longer behaves as an annular jet. Most of the air leaks out between the flap rods and the flow is that of a plenum with a very low discharge coefficient. The flow data will, therefore, be presented in discharge coefficient form in addition to the jet flow velocity coefficient. The discharge coefficient (C) based on base height, h_b, base pressure, p_b, is

$$C = \frac{Q}{2h_b\, b\sqrt{\frac{2}{\rho}\, p_b}}$$

Flap Lift and Drag Data

Flap lift and drag forces were determined from four flap balance strain gage readings. The balance is illustrated in Figure 5-6 The arrangement of the strain gages on the balance is such that both lift and drag may be calculated directly and, if necessary, the location of the resultant force located. When a flap load is applied at an arbitrary location, the moment equations at the various strain gage locations are

$$\left.\begin{aligned} M_1 &= L\,(a + 7) + D\,(d) \\ M_2 &= L\,(a) + D\,(d) \end{aligned}\right\} \text{ Lift strain gage locations}$$

$$\left.\begin{aligned} M_{10} &= L\,(c) + D\,(b + 7) \\ M_{11} &= L\,(c) + D\,(b) \end{aligned}\right\} \text{ Drag strain gage locations}$$

FIG. 6-6

FLAP TO TROUGH HEIGHT COMPARED TO INTEGRATED AVERAGE FLAP TO WAVE HEIGHT

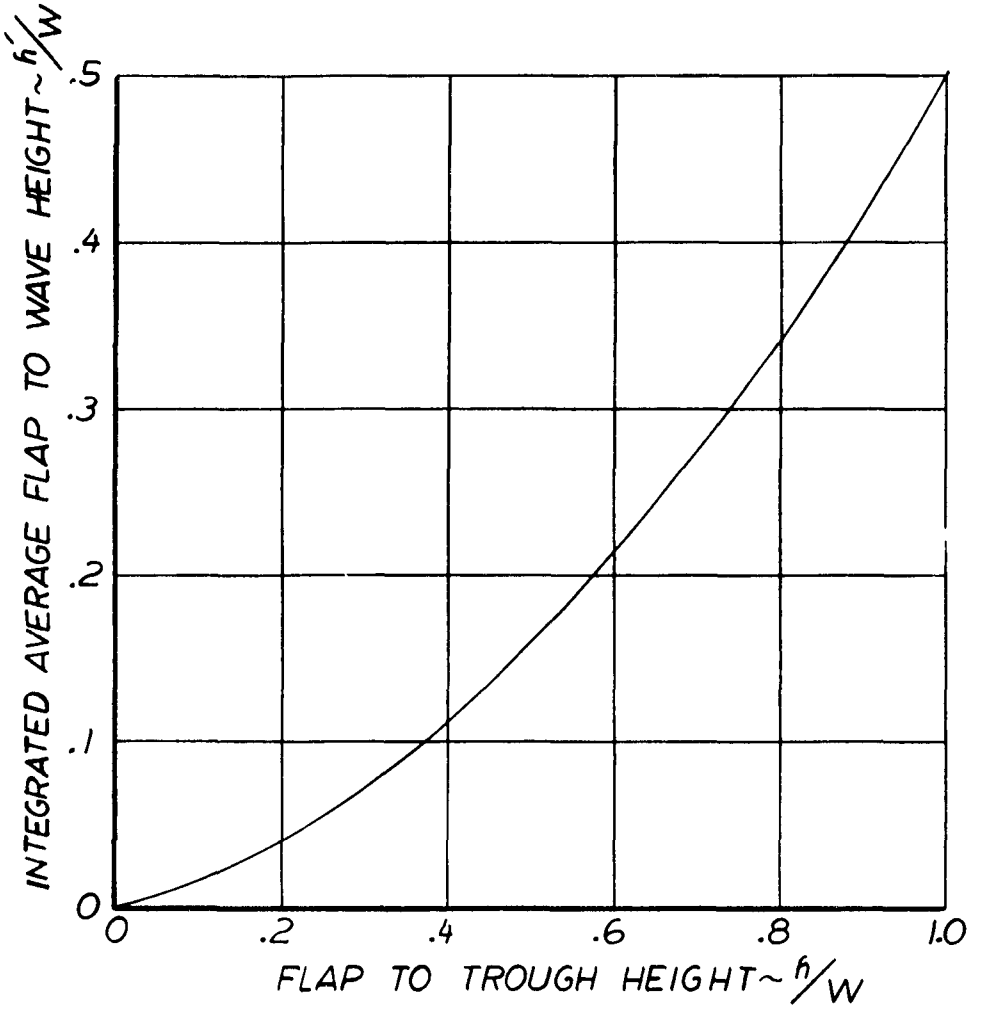

FIG. 6-7

FLAP TO TROUGH x COMPARED TO INTEGRATED AVERAGE x'

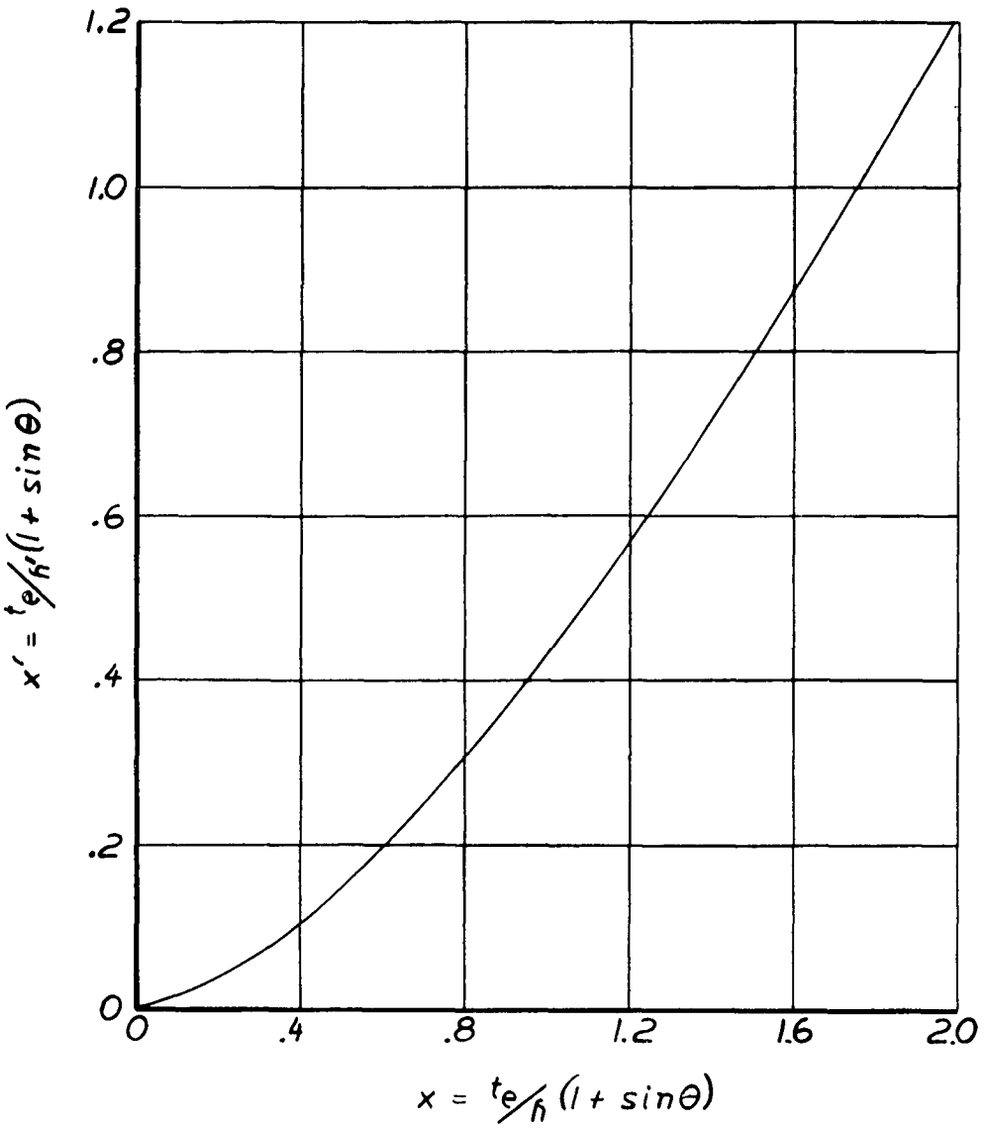

If one of the lift moment equations is subtracted from the other and the resulting equation solved for lift, the expression below results. The equivalent expression for drag may be determined in the same way and is also listed.

$$L = \frac{M_1 - M_2}{7}$$

$$D = \frac{M_{10} - M_{11}}{7}$$

Hence, it is seen that the balance yields flap forces independently of the point of force application. The above equations were used for reducing all flap force data.

The requirement that the flap balance be fitted into a restricted area dictated that the spacing between strain gages of a given moment pair (either lift or drag) be held to 7 inches. This spacing, combined with the location of the balance with respect to the flap loading location, resulted in the two moments of each pair being of nearly equal value. Compounding the difficulty of determining a small difference between large moments was the extremely oscillatory character of the momert traces on the oscillograph tapes. These oscillations were due partly to flap rebound after the initial flap-wave impact and partly to rebound as the flap sprang free from the back side of the wave.

The above problems emphasize the necessity for very careful oscillograph trace readings. Each moment channel was averaged by graphically determining the area between the moment trace and a reference line and by then determining the average moment value from

$$\Delta h = \frac{S}{\Delta x}$$

where Δh is the distance from the reference line to the average moment line, S is the area noted above, and Δx is the length of the area considered. In all cases the moment readings were averaged over three cycles and independently checked by another person. It will be shown in Section VII that even with such care considerable data scatter resulted.

A fundamental problem in the design of a flap element is that of providing strength to support the vehicle base pressure while also providing sufficient flexibility so that the flap will deflect on impact.

The parameters of a pure deflection system (EI for deflection, E and material allowable stress for strength) impose certain natural functional limitations which make the use of such a system for flap elements difficult (See Section VII "Flexible Flap Models," discussion of fatigue failures). Such systems have not been ruled out but are considered to be in an area which needs further exploration.

To circumvent the problems of a pure deflection system, a lateral buckling flap element was developed. The flap element configuration discussed herein (Figure 5-8) supports the base pressure loading about the major structural axis. As loads greater than that due to base pressure are applied to the element, it rotates and bends about the minor structural axis. While bending about the minimum axis, the structural rods within the flap element are bending about a common axis which permits maximum deflections without structural failure.

In the following paragraphs methods are presented for: (a) determining the rod cross section required for a given length of flap to withstand a particular applied pressure, (b) extending the measured drags to the above flap for different values of flap tip-to-trough height and wave height. The rods are assumed to be of the same cross sectional proportions.

In order to extend the results of the wave drag tests to various flap lengths and pressures for a first order parametric approximation, two relationships are required. One relationship expresses the flap element section size in terms of the element width a, length ℓ , and the base pressure p_b (p_b in psi). The second relationship expresses tip drag D in terms of D_{basic}, p_b and ℓ , where tip drag is defined as the critical tip load which initiates element buckling. Both relationships are derived below.

From Reference 4 the following relationship may be determined for the critical loading of a lateral buckling cantelever beam:

$$p_b = \frac{12.85}{a\ell^3}\sqrt{EIJG}$$

where ap_b is the load per inch of length which initiates buckling. The flap element investigated in this program (Figure 5-8) was constructured from two fiberglas rods encased in a body of polyurethane. Since the polyurethane does not have a significant linear stress-strain range, the value of EIJG was determined experimentally. EIJG was evaluated by loading several short flap elements until they buckled, and then substituting the critical loads and flap lengths into the equation for the critical end load (Reference 4),

$$F_{cr} = \frac{4.013}{\ell^2}\sqrt{EIJG}$$

For the flap cross-section tested,

$$\sqrt{EIJG} = 25 \text{ lb in}^2$$

To put the two desired relationships in parametric form, it need only be remembered that I and J have units of in^4 and that E and G are material constants. Using the element width a as the typical dimension

$$I = k_1 a^4$$

$$J = k_2 a^4$$

$$E = k_3$$

$$G = k_4$$

or

$$\sqrt{EIJG} = \sqrt{k_1 k_2 k_3 k_4 \quad a^8}$$

$$= K a^4$$

Therefore,

$$K a^4 = 25$$

For the flap element size used in these tests, a was 0.375 inch so that

$$K = 1270$$

and

$$\sqrt{EIJG} = 1270 a^4$$

If $\sqrt{EIJG}$ in the pressure equation is replaced with $1270 a^4$,

$$p_b = 16{,}300 \left(\frac{a}{\ell}\right)^3$$

If $\sqrt{EIJG}$ is eliminated between the original p_b and F_{cr} equations,

$$F_{cr} = .312 \, p_b a \ell$$

Substituting

$$a = \ell \left(\frac{p_b}{16,300} \right)^{1/3}$$

$$D = F_{cr} = .0123 \ell^2 p_b^{4/3}$$

This relation is analytical except for the evaluation of $\sqrt{EIJG}$. It is used later with the measured drag to correct for unknowns in the system in the following manner. The ratio is formed between the analytical drag equation (above) and the actual measured drag (called "basic" drag) with the test flap length and pressure substituted.

$$\frac{D}{D_{basic}} = \frac{.0123 \ell^2 p_b^{4/3}}{.0123 \left(\ell^2 p_b^{4/3} \right)_{test}}$$

where D_{basic} is the integrated average drag over one cycle, and p_b of the test is the maximum value attained during the tests (0.7 psi)

$$D = .0141 D_{basic} \ell^2 p_b^{4/3}$$

A preliminary attempt has been made to present flap force data in terms of a flap "wave penetration parameter." This parameter is the percentage of flap length that protrudes below the wave peaks, or

$$\frac{W-h}{\ell} = \frac{W}{\ell} \left(1 - \frac{h}{W} \right)$$

This form is convenient for predicting the effect of flap protrusion into the wave troughs. When used with the equation developed earlier for correcting drag for flap length and base pressure, it is felt that flap forces may be predicted accurately enough for preliminary estimates.

Effect of Flaps on Vehicle Performance

The effect of installing flexible flaps on a hydroskimmer vehicle will be shown by using the data generated during this program to predict the change in total power required that could be expected if flaps were installed on a typical vehicle. The hydroskimmer vehicle proposed to Bu Ships by Aeronutronic in Reference 5 was used as a basis for comparison. Pertinent vehicle specifications are tabulated below. Several geometry changes were made for simplification of this analysis. The conditions differing from the vehicle of Reference 5 are noted by an asterisk.

Gross Weight	45,000	lb
Base Length	50	ft
Base Width	20	ft
*Height of Base Above Skeg Bottom	4.5	ft
Flap Tip Above Skeg Bottom	0.25	ft
Bow Jet Angle (θ_b)	45^o	
Stern Jet Angle (θ_s)	25^o	
Skeg Jet Angle (θ_{sk})	45^o	

*Jet Thicknesses Fore and Aft
Variable with q
*No Interventing Jets
*Identical p_{t_j} in Fore and Aft Jets
*Skeg Jets Optimized for 30 Knots
*Separate Air Supply for Skeg Jets

Two other assumptions in this analysis that differed from Reference 5 are:

1. Cushion power was based upon jet exit conditions (internal ducting losses are omitted).
2. 100% overall efficiency was assumed in estimating thrust power.

The effect of flaps can be clearly demonstrated without the inclusion of these losses. In this manner, the discussion of flaps may be made without being colored by dispute as to the particular efficiency analysis which might be made herein.

Wave drag, aerodynamic drag and skeg drag were taken directly from Reference 5. Flap friction drag is an uncertain quantity because of two things: the flap wetted area and the inclination of the friction force from the horizontal. Both are dependent on flap penetration into the waves, wave shape and direction of vehicle motion relative to the waves. Friction drag was estimated by assuming a force inclination of 45^o, a wetted length of 0.5 ft and the corresponding friction drag coefficient (Reference 6) of 0.003. This estimate also assumes operation over a state 3 sea as defined on page 6-11, item 3.

Cushion power estimates were made by two separate analyses. The first examined power requirements according to annular jet methods, and the second assumed plenum chamber characteristics. In forward motion the static pressure at the outer edge of the jet is different from ambient static due to the nature of the flow around the vehicle. The static pressure at the bow jet was assumed to be fully stagnated; i.e., p_o at the bow is equal to flight q. At the stern jet p_o was assumed equal to a negative (1/2) q. These are the same assumptions as in Reference 5.

Due to the effect of the static pressure distribution on the total pressure required to support a given base pressure, the solution of the lift equation for total pressure is implicit. When hovering, the static pressure is constant around the vehicle and the solution for jet total pressure is explicit. The manner in which this solution was effected was to assume several values of x of the bow jet and several values of total pressure at each x. The selection of the total pressures to provide the required lift was guided by the pressure required at zero velocity. The effect of q is to reduce p_t required, and p_t values were selected to bracket the required lift. Lift was plotted against total pressure at constant x of the bow and the pressure required for the given lift was read off this plot. With this total pressure the volume flow, momentum drag and power were established for each x of the bow. Power required was then plotted against x to determine minimum power required.

The values of x at which the total power minimized were all less than 1.0. From

$$x = \frac{te}{h} (1 + \sin \theta)$$

it can be seen that the jet thickness is less than the height to the flap tip, or about 0.10 to 0.2 feet. When these thicknesses are examined in relation to the height of the base (or the length of flexible flap) it appears unlikely that the jet will retain its "jet-like" qualities down to the tip of the flap. There will be considerable viscous mixing of these thin jets with the base region air and air will also be leaking out through the flaps (referring specifically to the urethane rods). In the limit when the flaps are actually touching the wave surface most of the time the annular jet description of the flow loses all significance. The flow is then analogous to a plenum chamber with a low discharge coefficient.

For the condition at which the vehicle will be analyzed it is believed more appropriate to use the plenum flow analysis.

The lift is then

$$L = p_b S_b$$

and

$$Q_{bow} = Ch_b b \sqrt{\frac{2}{\rho}} \sqrt{p_b - q}$$

$$Q_{stern} = Ch_b b \sqrt{\frac{2}{\rho}} \sqrt{p_b + \frac{1}{2} q}$$

The low volume flows in this plenum chamber will permit low plenum inlet velocities with attendant low dumping losses. The base pressure will be very nearly equal to plenum total pressure. In this analysis it is assumed that

$$p_t = p_b$$

The momentum drag and air power required can thus be determined.

When the vehicle is operating over a rough sea, considerable leakage areas develop under the skegs when the vehicle passes over a wave trough. If the plenum air is allowed to escape through these troughs, it flows with a discharge coefficient of about 0.6. This results in a severe cushion power penalty and high momentum drag. It was, therefore, assumed that the skegs have jets at the bottom, inclined inward at 45°. These jets could have been designed to optimum thickness and to cause zero momentum drag at all velocities through the use of variable rearward deflection of the jets. However, since the main purpose of this report is to demonstrate the effect of flexible flaps and not to design an optimum vehicle, a fixed side jet geometry optimized for a forward speed of 30 knots was assumed. This resulted in a thrust from the side jets at velocities less than 30 knots and a drag at velocities greater than 30 knots. A separate power source was assumed to supply the side jet air. The higher total pressure requirements of the side jets (in relation to the plenum) could thus be satisfied.

Four operating conditions were analyzed to show flap effects on performance. They are:

1. No flaps installed and the vehicle operating over a flat, calm sea. The skegs were assumed to seal the cushion perfectly at the side but to create no drag. In this condition the side jets are not in use. Theoretical curves of C_b, $\overline{C}_v$ and $\overline{C}_r$ were used since the annular jet analysis is valid in this case. For example see Figures 6-1, 6-2, and 6-3.

2. Flaps installed and the vehicle operating over a flat, calm sea. Again the skegs were assumed to skim the surface causing no drag. The clearance from the flap tips to the flat sea was assumed to be 0.25 ft. The discharge coefficient curves were used for finding volume flow.

3. No flaps installed and the vehicle operating over a state three sea. The average wave height, trough to crest, was 2.6 feet and the vehicle was assumed to be operating at a height such that the skegs were continuously at the wave mean line. The average wave length in this sea condition is approximately 60 feet, but for the purpose of this demonstration, was assumed to equal the vehicle base length, 50 feet. With the skegs at the wave mean height line there was leakage area under the skeg through the trough of the wave. This leakage area was sealed by the skeg jets discussed previously. Again, the theoretical curves of Stanton Jones were used, Figures 6-1, 6-2, and 6-3.

4. Flaps installed and the vehicle operating in the same state three sea as in the previous description, with the flap tips 0.25 feet above the wave mean line in their undeflected position. Again, the leakage area through the wave trough was sealed by the skeg jets.

SECTION VII

RESULTS AND DISCUSSION

PREPARATORY INVESTIGATION

In preparation for the flexible flap investigation Aeronutronic conducted a test program to explore the power savings potentially available through the use of such flaps. This was done using rigid flaps over a solid ground plane. Figure 5-3 shows schematically the installation of these rigid extensions and illustrates the nomenclature used herein.

The tests were made at three values of the ratio of ℓ_i / ℓ_o (0, 0.5 and 1.0) and two of h/h_b (0.25 and 0.5). Figures 7-1, 7-2, and 7-3 clearly demonstrate the increase in performance caused by extending flaps with the base at a given height. C_b is significantly increased while $\overline{C}_v$ is decreased. The reduction in $\overline{C}_r$ is of minor importance since jet reaction lift is only a small portion of net vehicle lift, especially with the small jet thicknesses required to attain a given lift while using flaps.

These figures show that a given base pressure (hence, approximately, lift) can be attained with either lower total pressures or thinner jets. Volume flow also has an attendant reduction through either of these reductions. Significant power reductions thereby result as will later be illustrated.

Graphic as these figures are, the height of the base above the ground is not the proper engineering parameter to use in correlating the data for the three coefficients C_b, $\overline{C}_v$ and $\overline{C}_r$. As will be demonstrated, the use of the height to the flap tips makes it possible to use a single line on these charts for varying ratios of h/h_b.

FIG. 7-1

BASE PRESSURE COEFFICIENT

RIGID FLAP DATA COMPARED TO
STANTON-JONES EXPONENTIAL THEORY

$l_i/l_o = 0$

$\theta = 0°$ $\quad t_e = 2$ IN.

HEIGHT MEASURED TO BASE

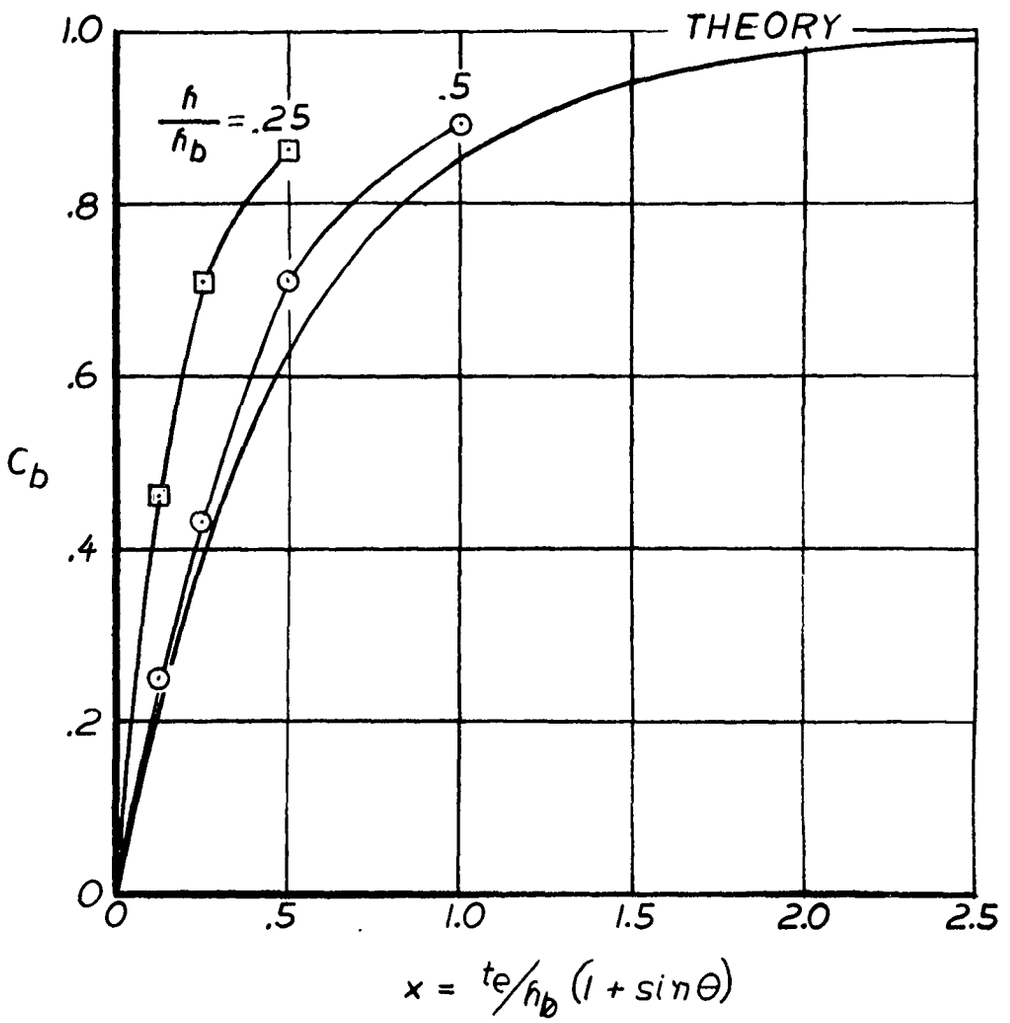

FIG. 7-2

JET VELOCITY COEFFICIENT

RIGID FLAP DATA COMPARED TO
STANTON-JONES EXPONENTIAL THEORY

$l_i/l_o = 0$

$\theta = 0°$ $t_e = 2$ IN.

HEIGHT MEASURED TO BASE

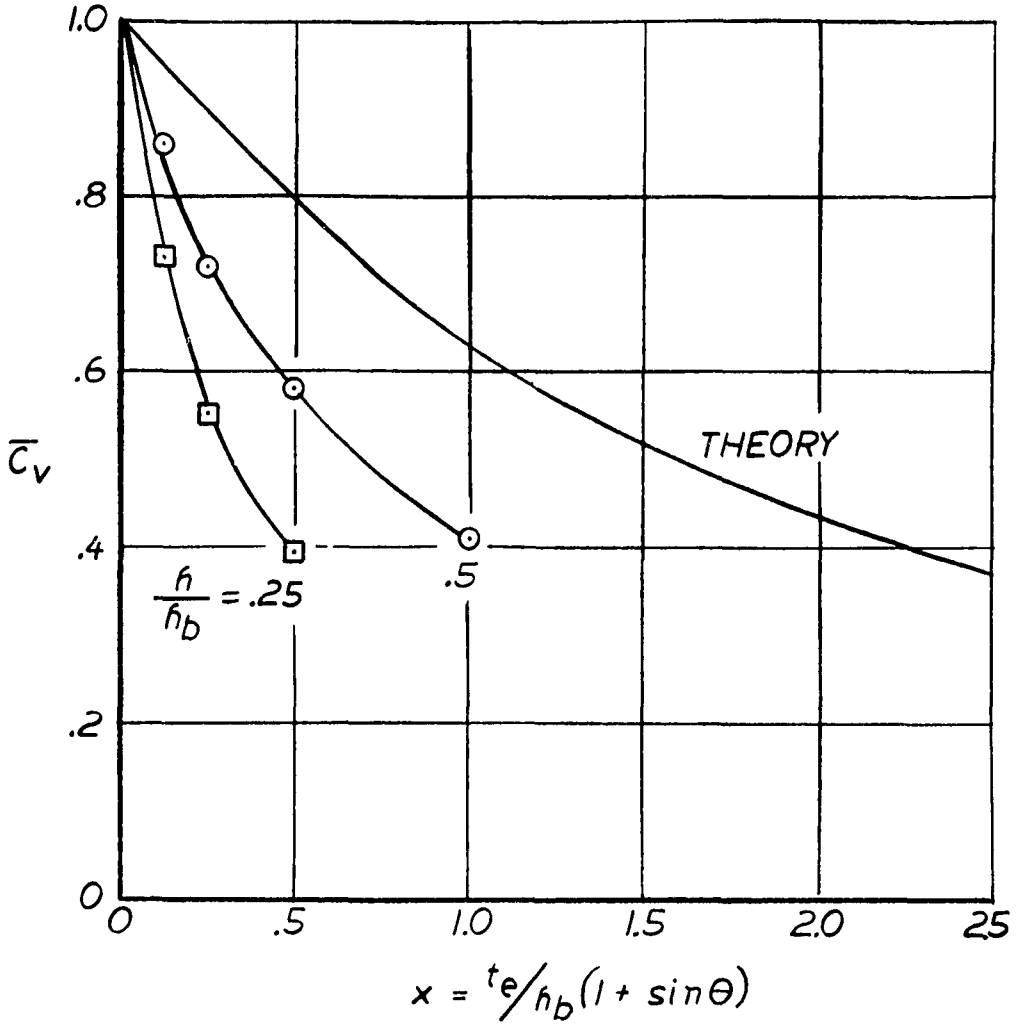

FIG. 7-3

JET REACTION COEFFICIENT

RIGID FLAP DATA COMPARED TO
STANTON JONES EXPONENTIAL THEORY

$l_i/l_o = 0$

$\theta = 0°$ $t_e = 2$ IN.

HEIGHT MEASURED TO BASE

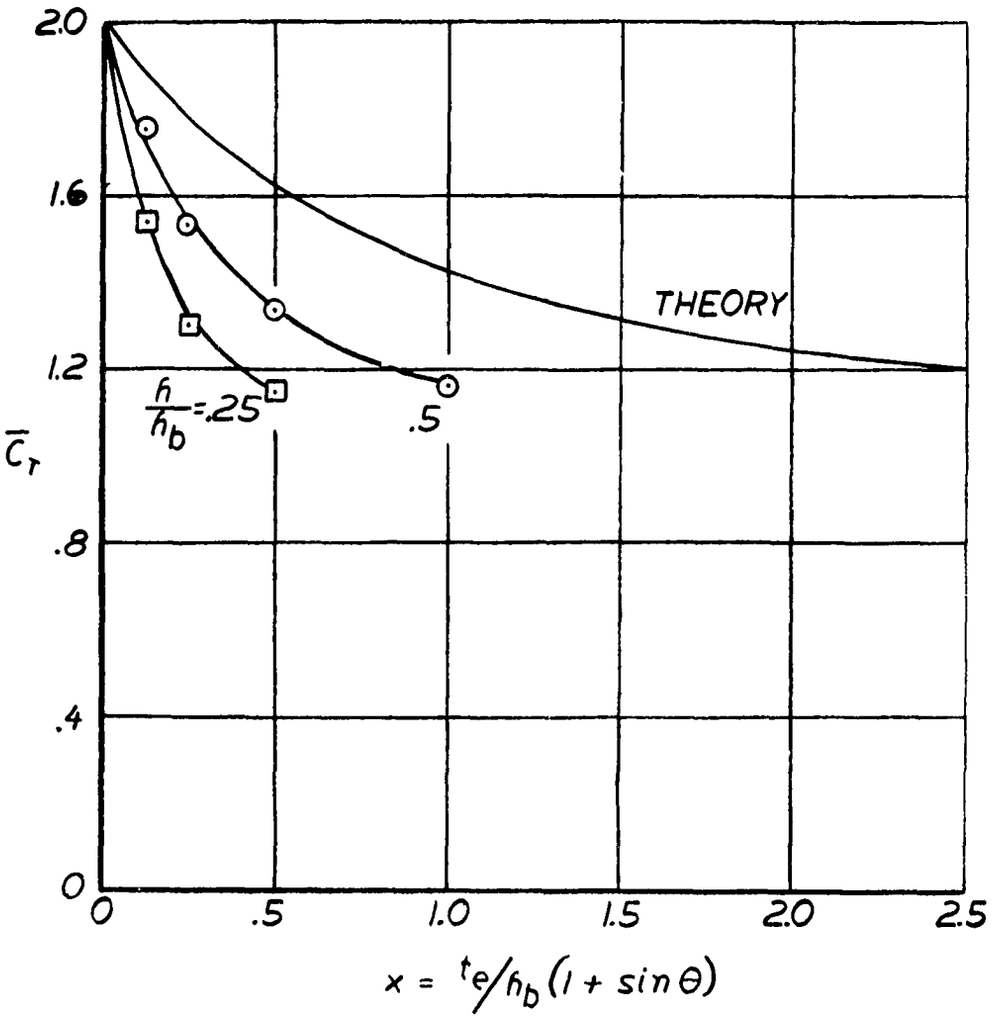

Using the height to the flap tips (h) rather than height to the base (h_b), Figures 7-4 through 7-12 show the three coefficients for constant values of ℓ_i / ℓ_o on each figure. The data curves on these figures are for h/h_b of 0.25 and 0.5. These curves could well be represented by a single line, especially at low values of x. For this reason the results of the flexible flap tests will be presented as a function of height measured to the flap tip.

The results from the rigid flap program have been carried through to a demonstration of the power savings available through the use of the "ground effect power factor", G. This parameter is the ratio of power required for an air-cushion vehicle to hover to that required for a ducted fan to hover out of the ground effect with the same weight and planform area.

The data shown in the preceding figures were used to determine minimum G for a hydroskimmer type vehicle over a range of vehicle height to length ratios. Since the intent of this procedure is to demonstrate power savings rather than correlate data, G is plotted in Figure 7-13 against base height to vehicle length ratio.

There are two things to note in this figure. The first is that putting flaps on a vehicle results in power requirements approximately the same as if the base of the unflapped vehicle were lowered to the height of the tip of the flaps. The second is that only second order differences in power required occur between the full length inner flap condition and no inner flap condition. Appreciable savings in flap system weight and complexity thereby result. Based on this result, consideration was given only to an outer wall flap in the flexible flap program.

FLEXIBLE FLAP PROGRAM

Section V showed the flaps built and tested in this program. The foam core flaps were eliminated from present consideration about midway through the test runs. When the flaps buckled under load, the sides and ribs caused local stress concentrations in the faces of the flaps in the immediate vicinity of the side and ribs. Due to the elastomeric nature of the urethane skins, it was anticipated that these local stress concentrations would not be any problem.

FIG. 7-4

BASE PRESSURE COEFFICIENT

RIGID FLAP DATA COMPARED TO
STANTON-JONES EXPONENTIAL THEORY
$\theta = 0°$ $t_e = 2$ IN.

$l_i/l_o = 0$

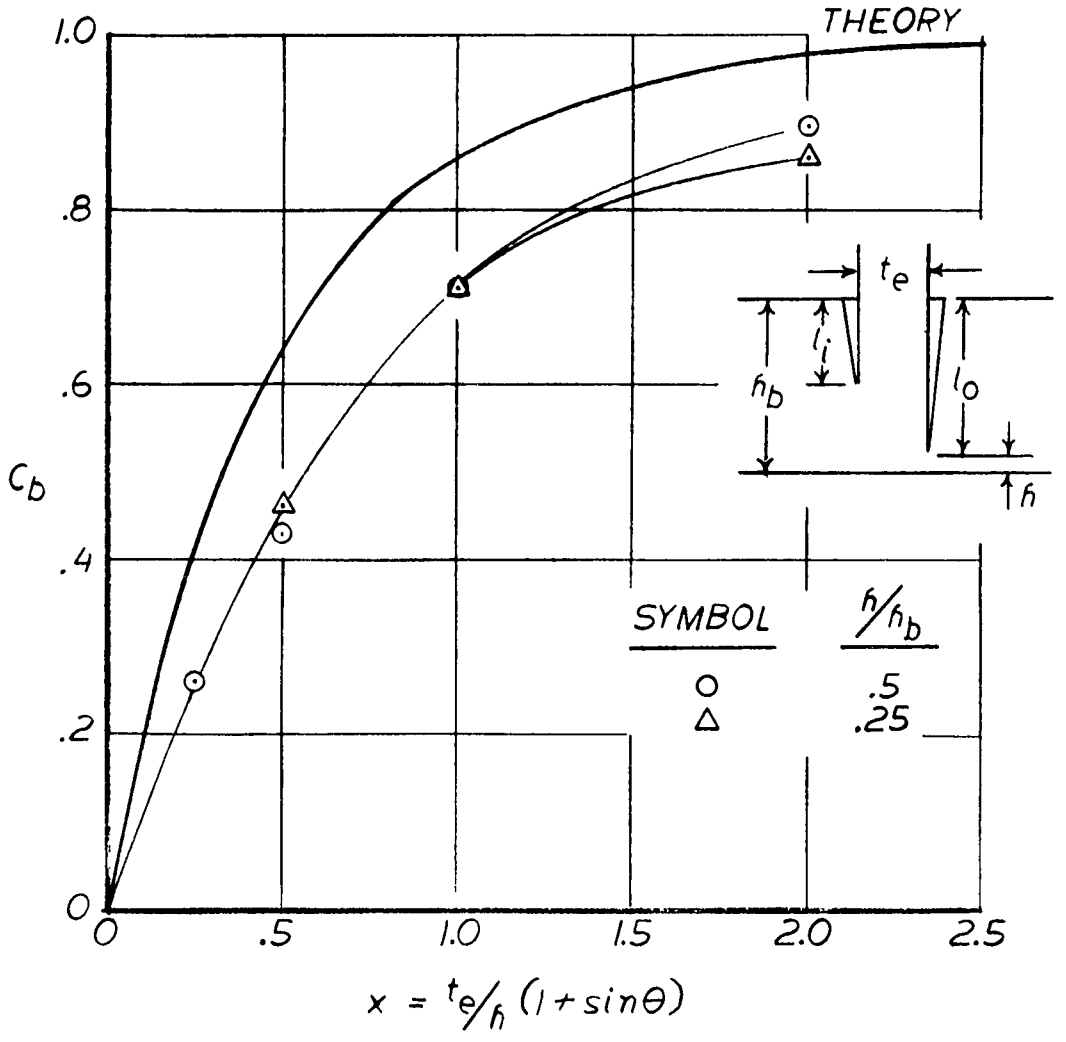

FIG. 7-5

BASE PRESSURE COEFFICIENT

RIGID FLAP DATA COMPARED TO
STANTON-JONES EXPONENTIAL THEORY
$\theta = 0°$ $t_e = 2$ IN.

$l_i/l_o = .5$

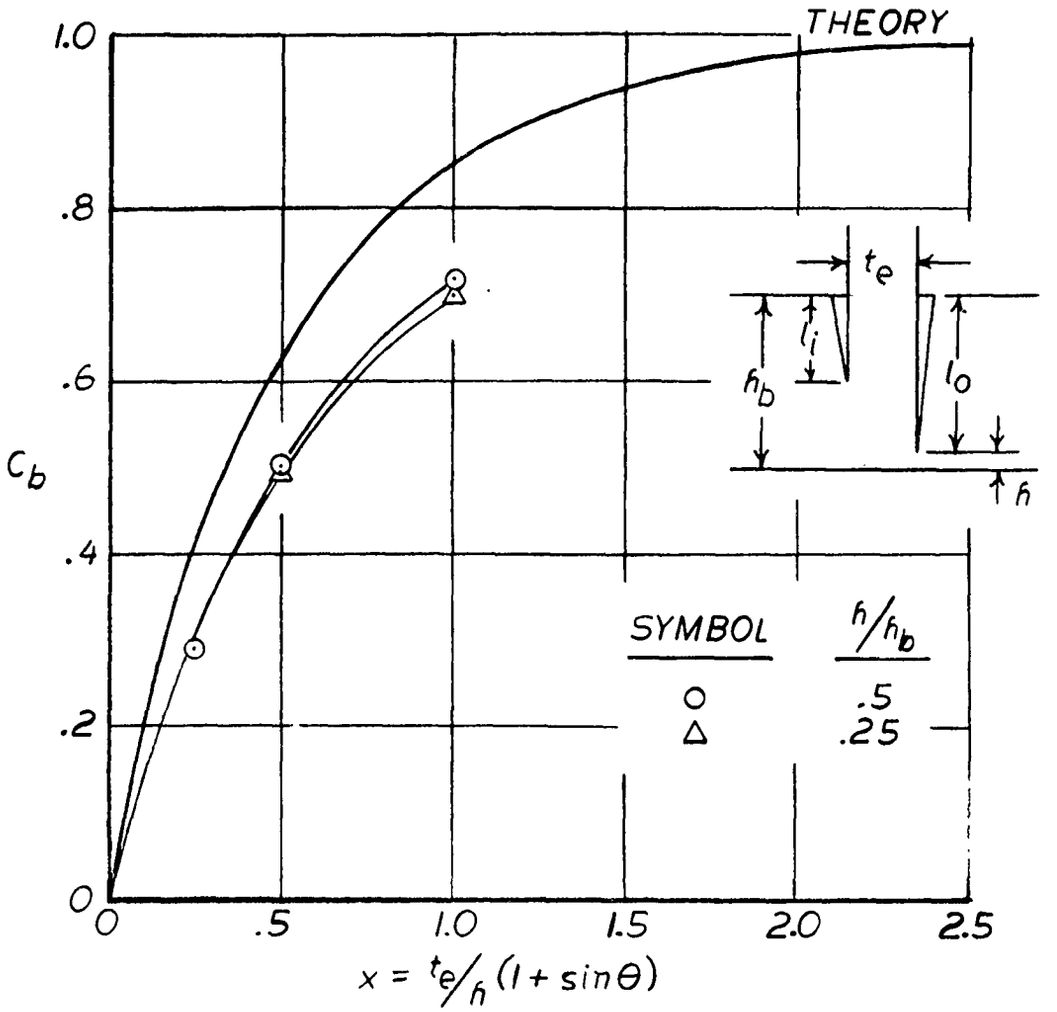

FIG. 7-6

BASE PRESSURE COEFFICIENT

RIGID FLAP DATA COMPARED TO
STANTON-JONES EXPONENTIAL THEORY
$\theta = 0°$ $t_e = 2$ IN.

$l_i/l_o = 1.0$

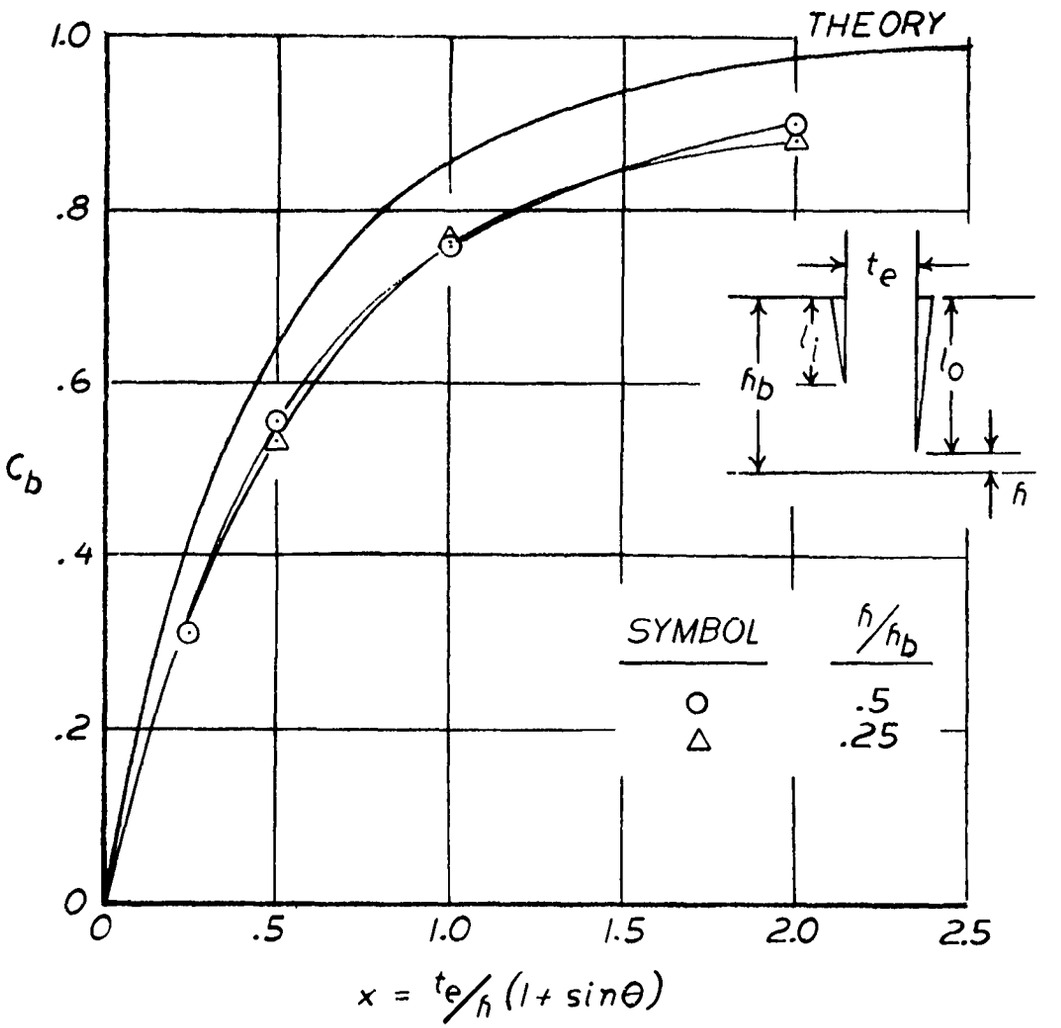

FIG. 7-7

JET VELOCITY COEFFICIENT

RIGID FLAP DATA COMPARED TO
STANTON-JONES EXPONENTIAL THEORY
$\theta = 0°$ $t_e = 2$ IN.

$l_i/l_o = 0$

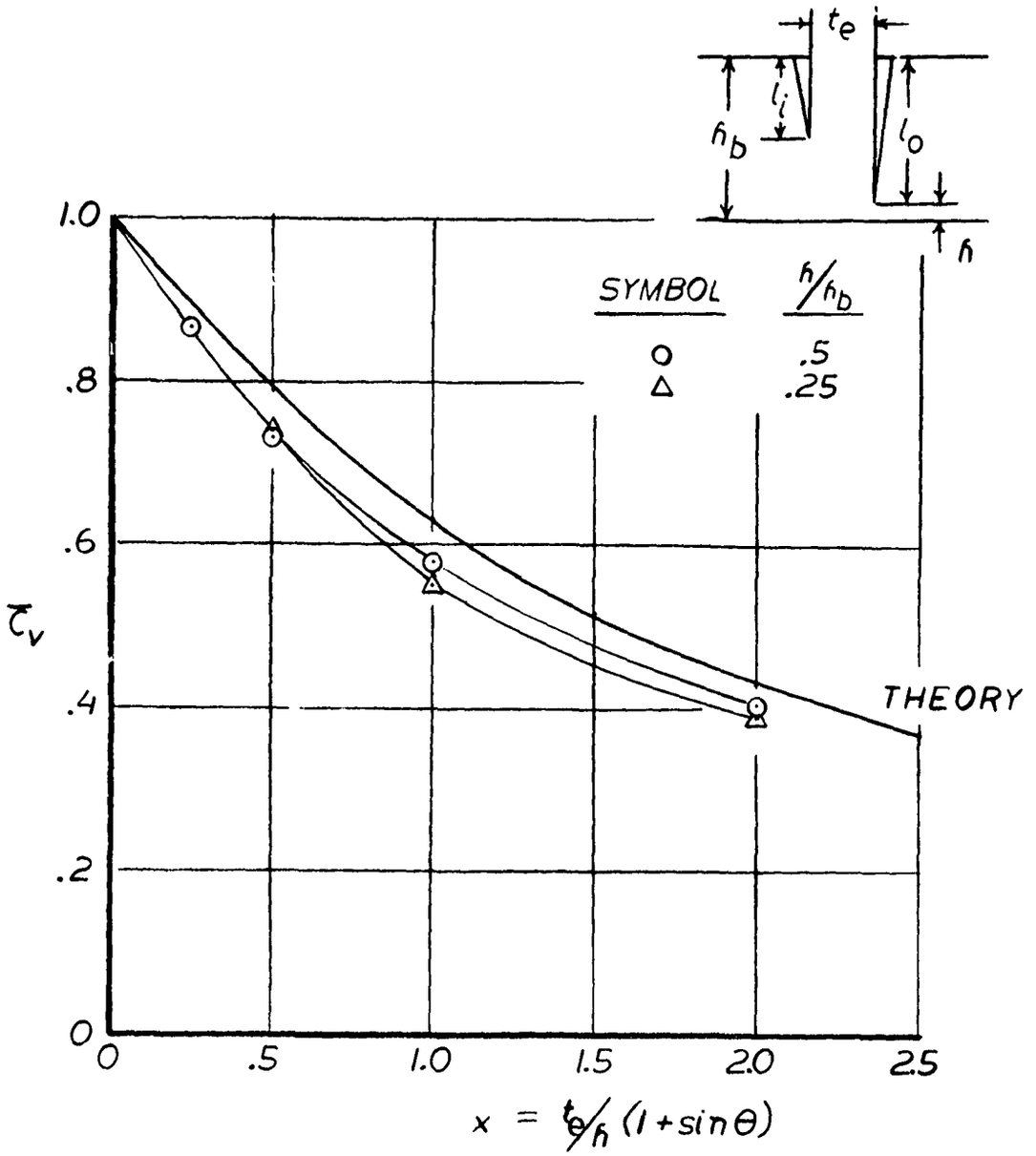

FIG. 7-8

JET VELOCITY COEFFICIENT

RIGID FLAP DATA COMPARED TO
STANTON-JONES EXPONENTIAL THEORY
$\theta = 0°$ $t_e = 2$ IN.

$l_i/l_o = .5$

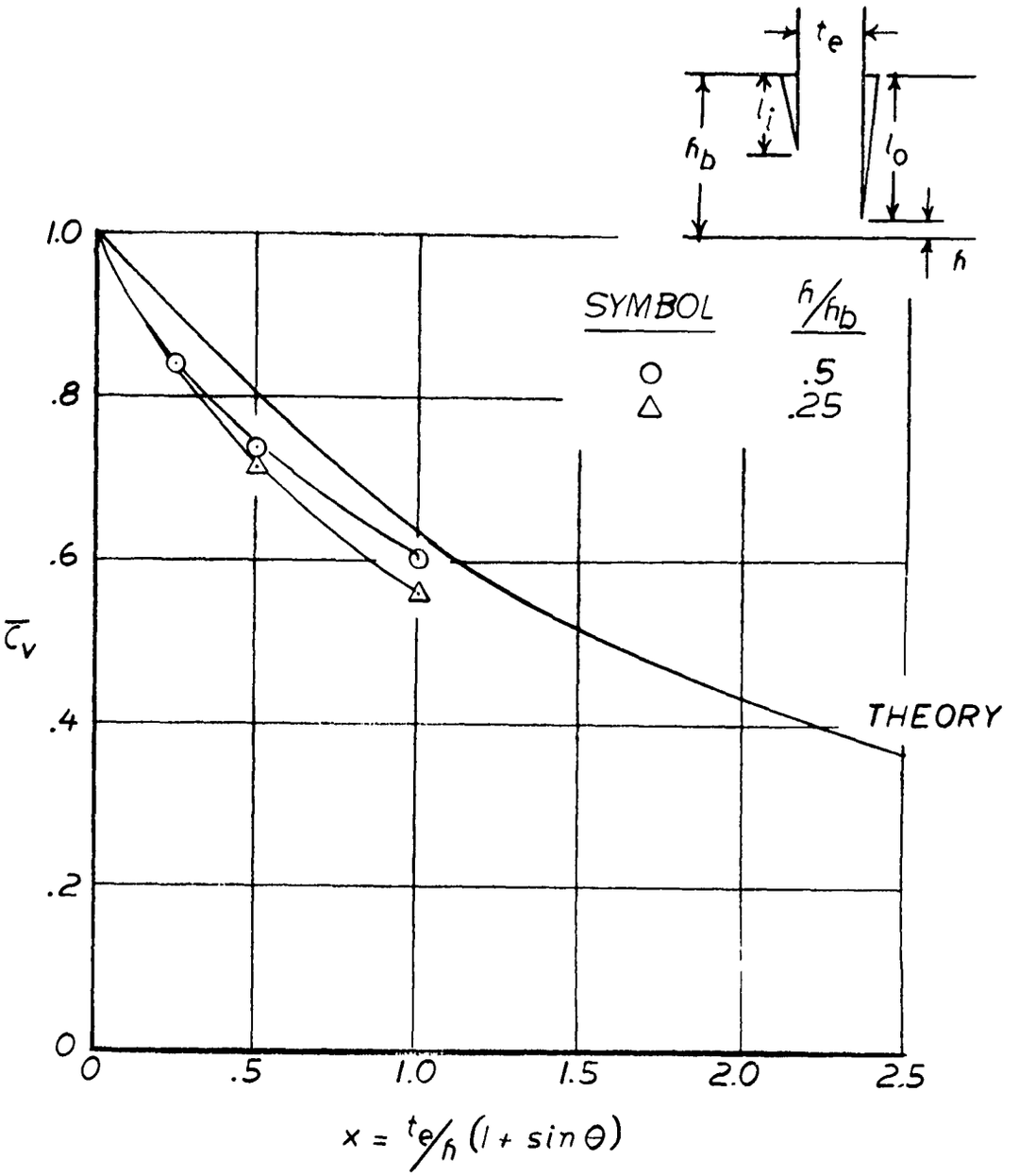

FIG. 7-9

JET VELOCITY COEFFICIENT

RIGID FLAP DATA COMPARED TO
STANTON-JONES EXPONENTIAL THEORY
$\theta = 0°$ $t_e = 2$ IN.

$l_i/l_o = 1.0$

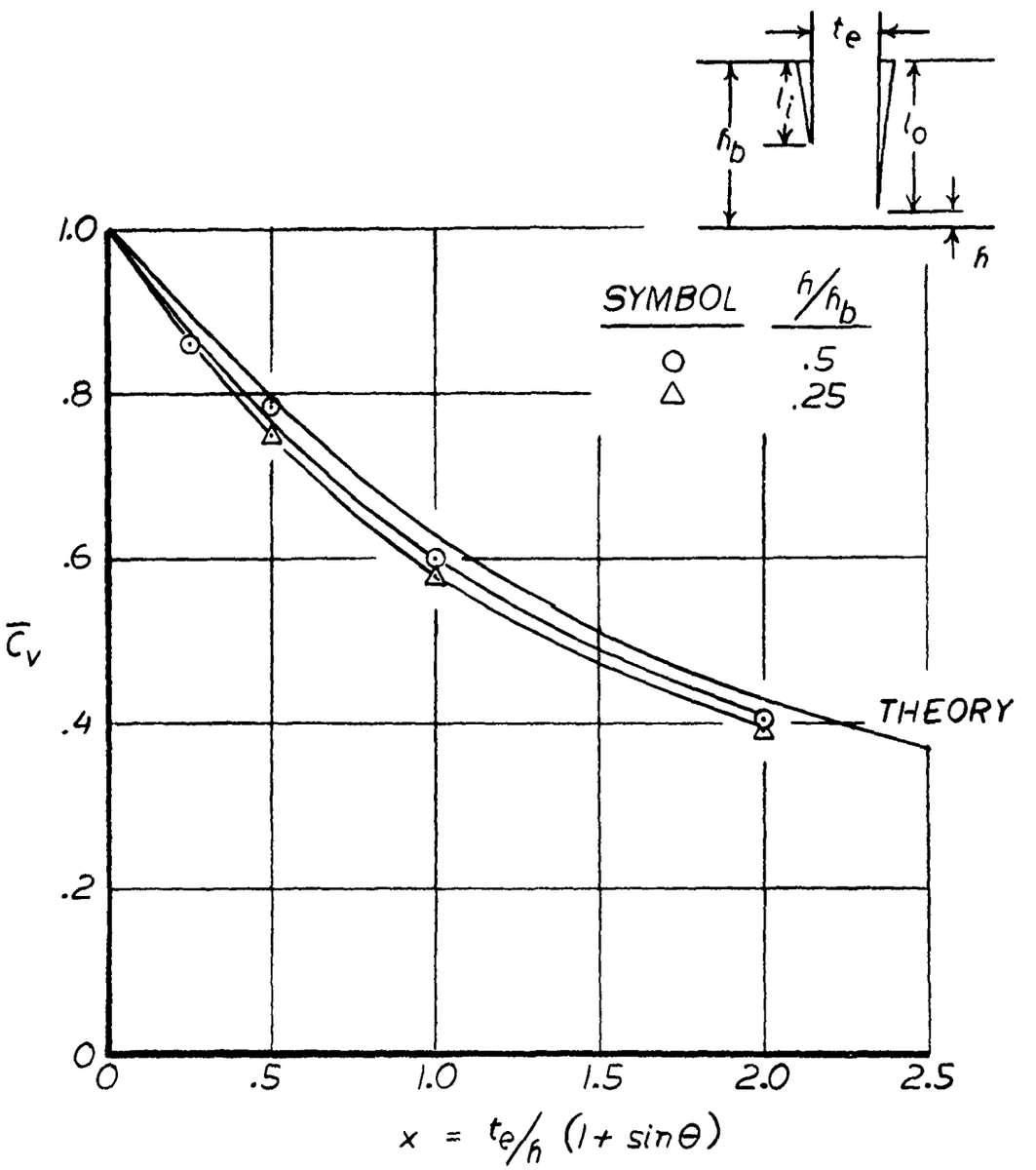

FIG. 7-10

JET REACTION COEFFICIENT

RIGID FLAP DATA COMPARED TO
STANTON-JONES EXPONENTIAL THEORY
$\theta = 0°$ $t_e = 2$ IN.

$l_i/l_o = 0$

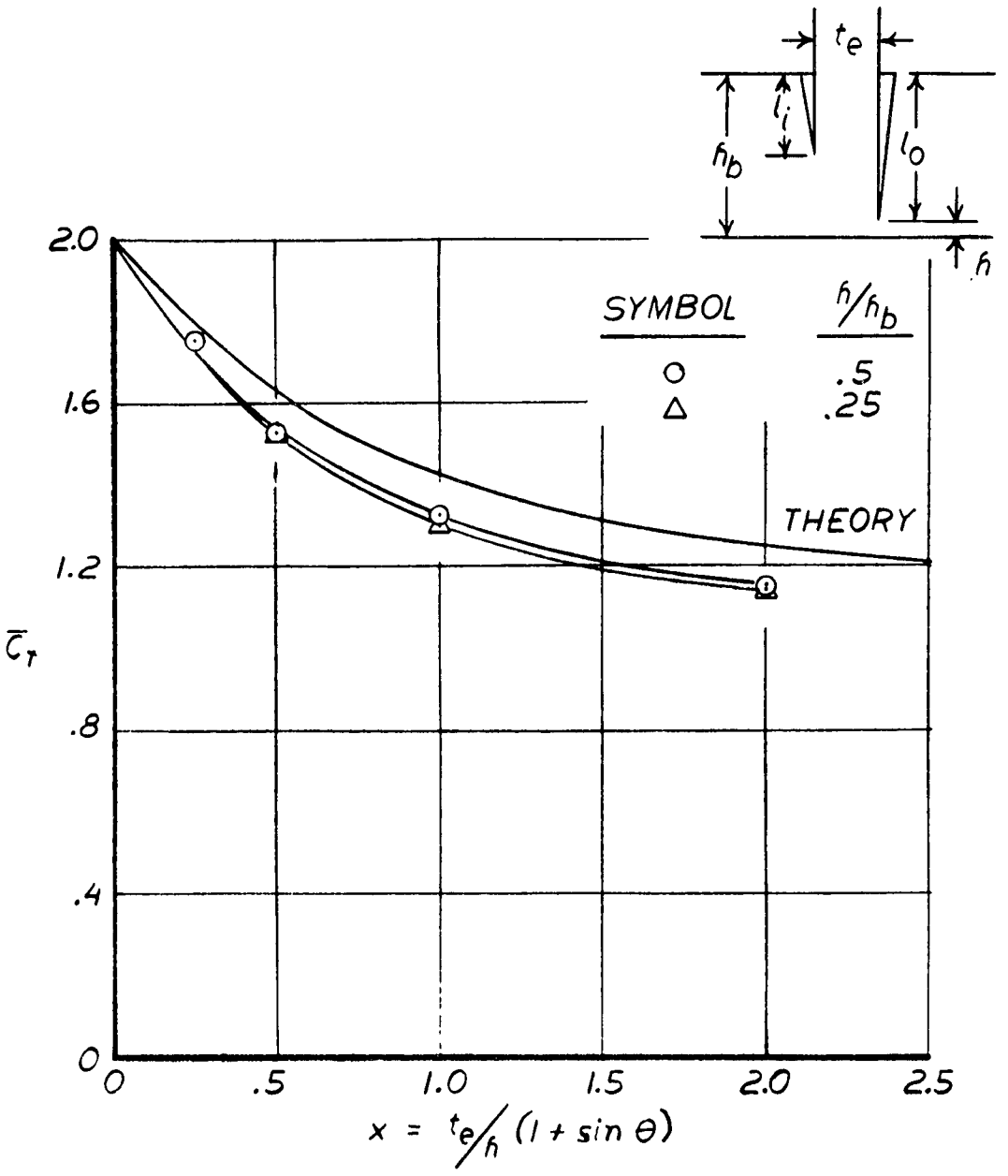

FIG. 7-11

JET REACTION COEFFICIENT

RIGID FLAP DATA COMPARED TO
STANTON-JONES EXPONENTIAL THEORY
$\theta = 0°$ $t_e = 2$ IN.

$l_i/l_o = .5$

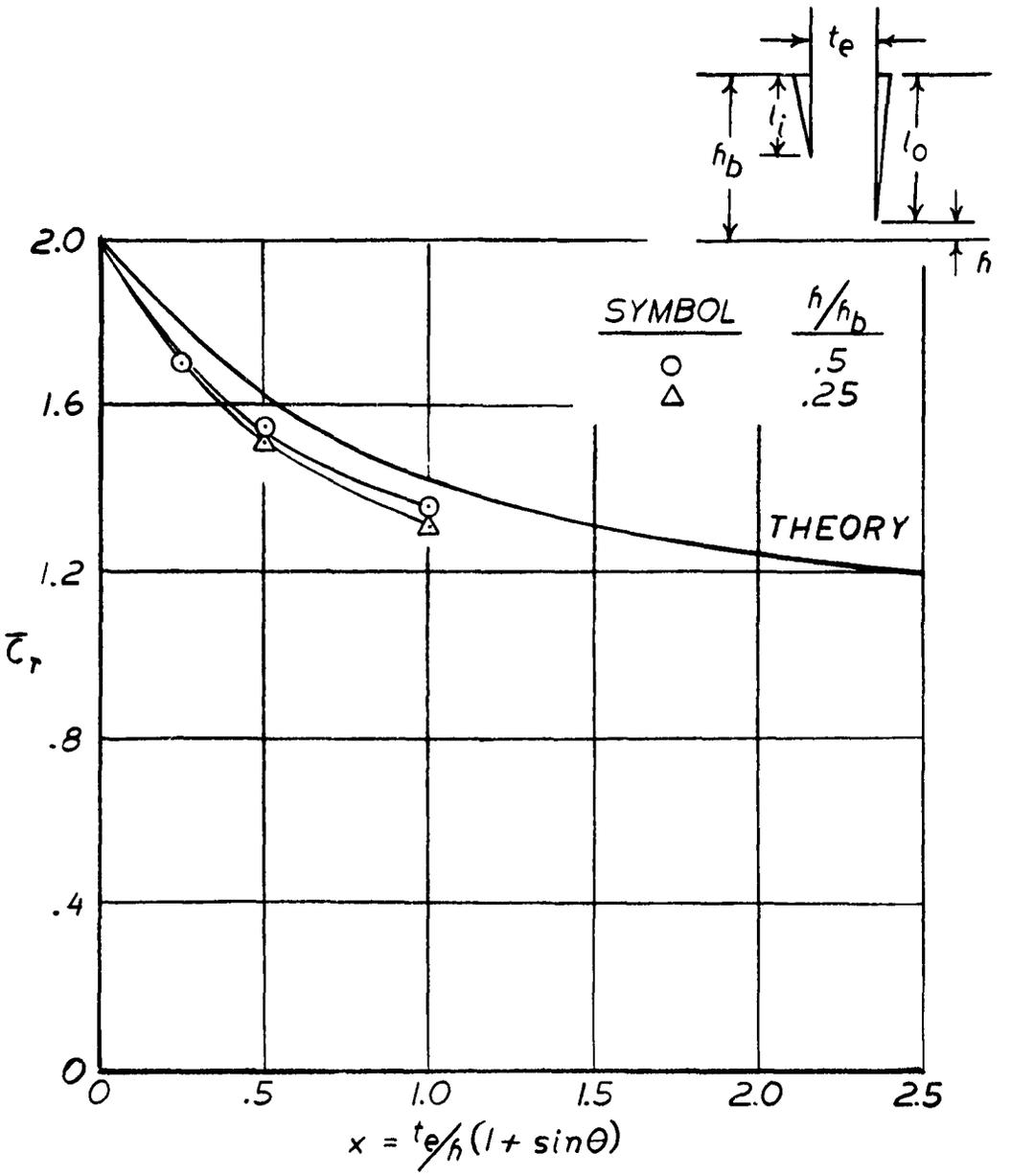

FIG. 7-12

JET REACTION COEFFICIENT

RIGID FLAP DATA COMPARED TO
STANTON-JONES EXPONENTIAL THEORY
$\theta = 0°$ $t_e = 2$ IN.

$l_i/l_o = 1.0$

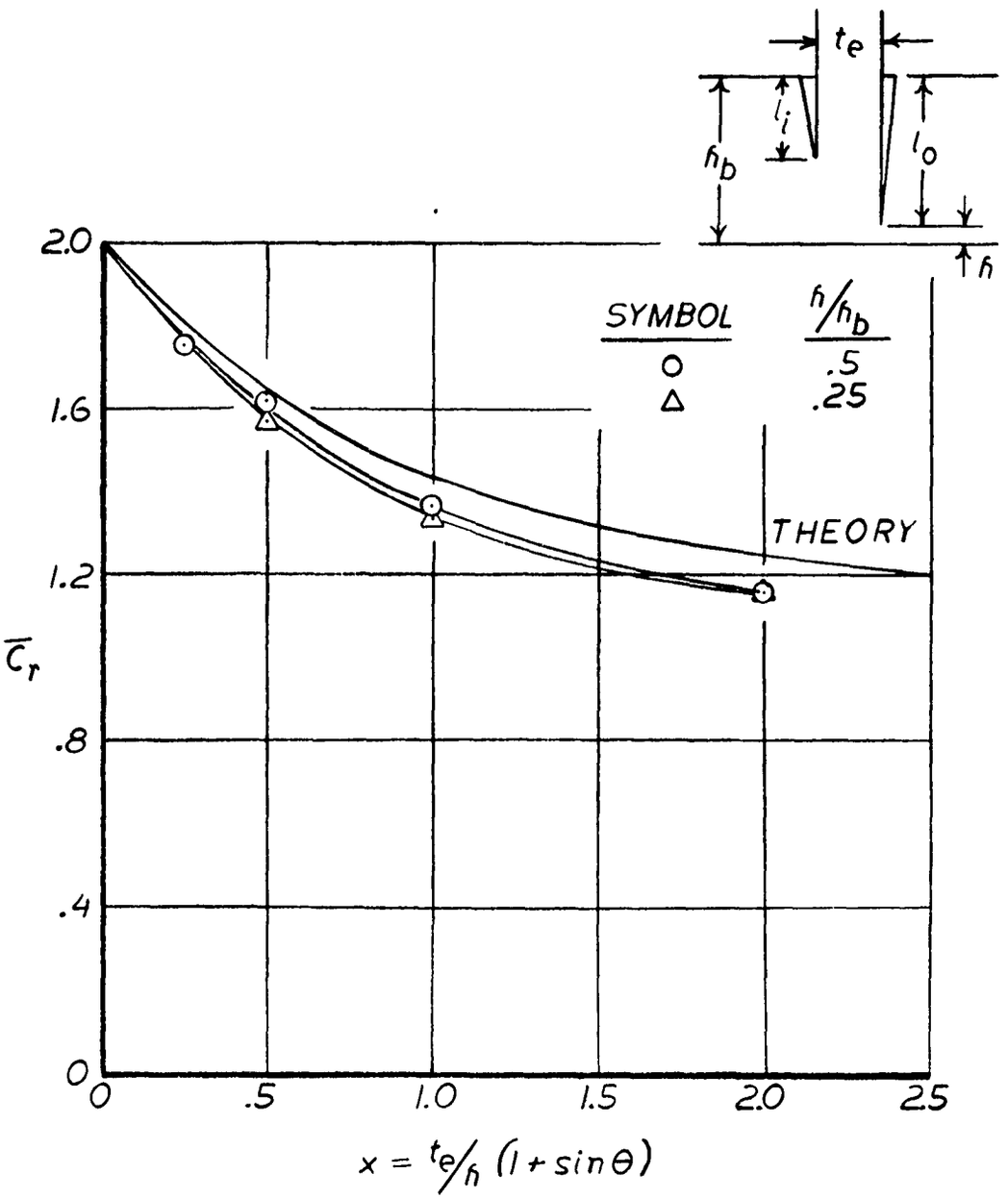

FIG. 7-13

MINIMUM HOVERING GROUND EFFECT POWER FACTOR

HYDRO-SKIMMER CONFIGURATION WITH RIGID FLAPS
$\theta = 0°$

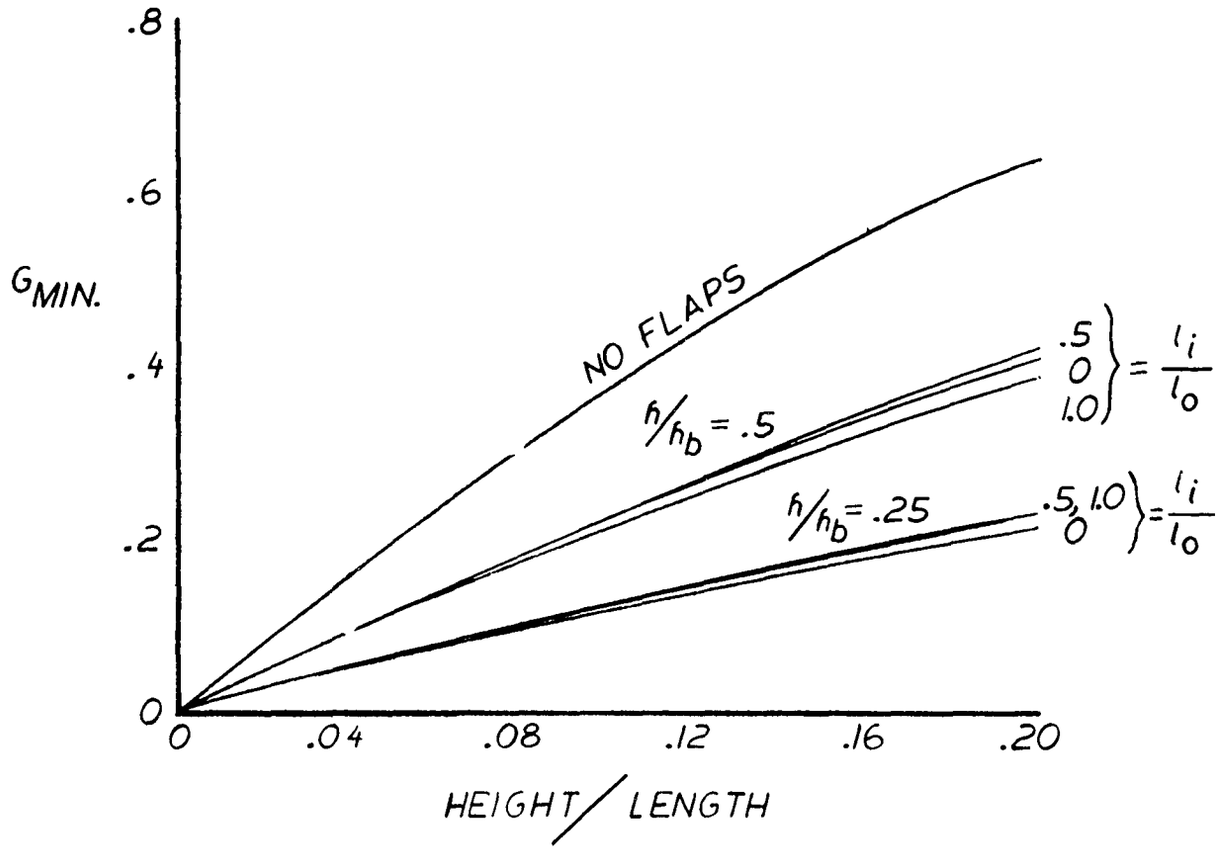

The skin was expected to flex and yield to the imposed stresses. The sides and ribs, however, created such stiffening of the skin that it was not completely free to flex. Due to rapid cyclical nature of the applied loads, the skins developed fatigue cracks at the corners and at the ribs. Some of these cracks progressed slowly across the entire width of the flap. Figure 7-14 shows the start of such a crack and Figure 7-15 shows a complete split of one section of flap.

These cracks naturally weaken the flaps, permitting excessive deflection under air load with attendant leakage of air, and also yield to wave impact much more easily than they should. Since this failure was very gradual, it is difficult to say just where the data lost validity. After examination of these flap failures, it was realized that this concept needs further development before complete evaluation is warranted. It seemed advisable to rerun some of the tests due to strain data interpretation difficulties and indeterminate side leakage of air. Since the fiberglass reinforced urethane rods appeared to be the most promising structurally, tests on these flaps only were repeated. Only the data from these reruns are presented in this report.

The tests were run at the conditions noted:

h = 3.6 in. (wave mean height line)
and .125 in. (essentially at the trough of the wave)

speed = 1 and 3 cycles per second

jet total pressure = 4 and 8 inches H_2O (nominal)

In addition, the wave was moved through a cycle in small steps to determine the static loads on the flaps.

COEFFICIENT DATA

The leakage around the sides of the belt (in spite of the seals installed) was estimated by running the blower with a ground board resting on the waves and no flaps installed. Check runs were made with the sides of the ground board taped to the sides of the cart (no side leakage) and with the board untaped. The ground board was of the same width as the wave and belt, so that the untaped

FIG. 7-14

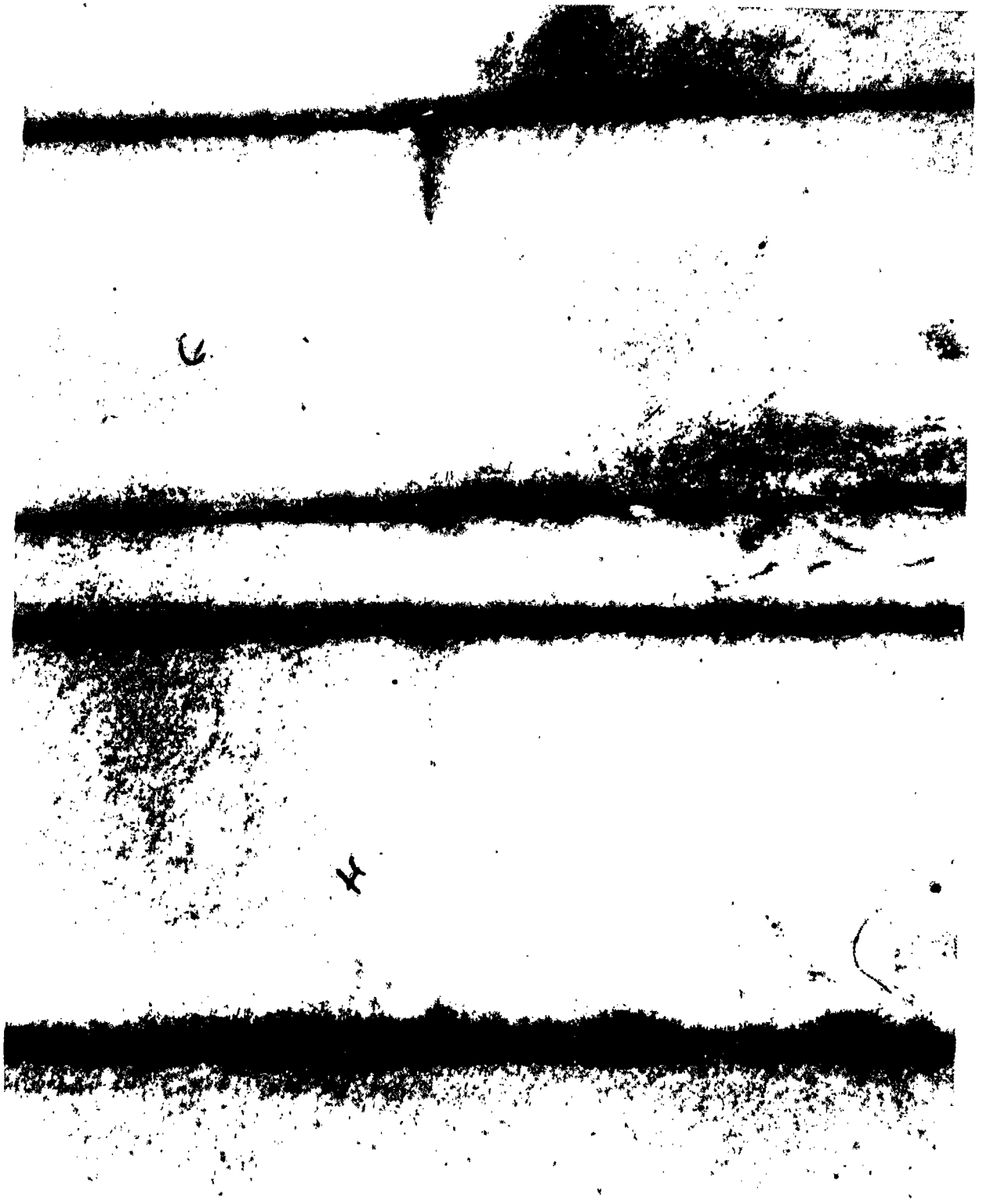

TYPICAL FLAP FAILURE AT CORNERS

FIG. 7-15

EXTREME FLAP FAILURE

ground board tests had the same leakage as the wave with no board on it. In this fashion the base pressure with side leakage could be compared with the base pressure with no leakage. Figure 7-16 compares the untaped C_b with a no leakage curve faired through the taped ground board point and the previous unpublished data.

The slight x displacement between the two data points at x = 0.26 is because the higher base pressure with the ground board taped depresses the foam of the wave more than with the ground board untaped. The height is thus slightly greater. The data point for the ground board taped is the same as for previous one and two jet data. The leakage situation is such that C_b obtained as a function of x is as if the operation were taking place at a lower effective value of x. For example, at x = 0.269, the untaped data point, C_b = 0.324. The value of x for which a perfectly sealed configuration would yield C_b = 0.324 is x = 0.235, a reduction in effective x of 14.5% based on the actual value of x. Similarly, a reduction of 9.5% is obtained if x = 0.433. An average of these two reductions, 12%, was used to correct the flapped data; i.e., the flexible flap data was plotted as a function of x at values of effective x 12% lower than the actual values. This correction takes into account the leakage around the edge of the wave-belt and plots the data as if there were no leakage at all.

Data were recorded with the wave stationary and a trough directly under each jet. This procedure satisfied two intentions. The first was to provide an initial crosscheck, under static conditions, of the dynamic recording system and the manometer board to insure the proper functioning of the dynamic system. The second was to permit estimation of vehicle performance while operating over a flat surface.

The wave-off data are shown in Figures 7-17, 7-18 and 7-19 in the form of C_b, $\overline{C}_v$ and $\overline{C}_r$. Note that the height term in x is the trough-to-flap-tip dimension. For the case where the height is 0.125 inch the value of x is far off scale to the right. It is believed, however, that the coefficients have essentially reached equilibrium values before going off scale, and that for any x beyond the end of the scale a constant value may be used as indicated by the faired curve.

It is evident that at all values of x the flaps are not completely sealing the cushion of air. There is air leaking out between the rods. During the tests it was noted that the rods were vibrating at the tips under the influence of the air flow and of the vibration transmitted through the test stand from the centrifugal blower.

FIG. 7-16

DETERMINATION OF LEAKAGE CORRECTION

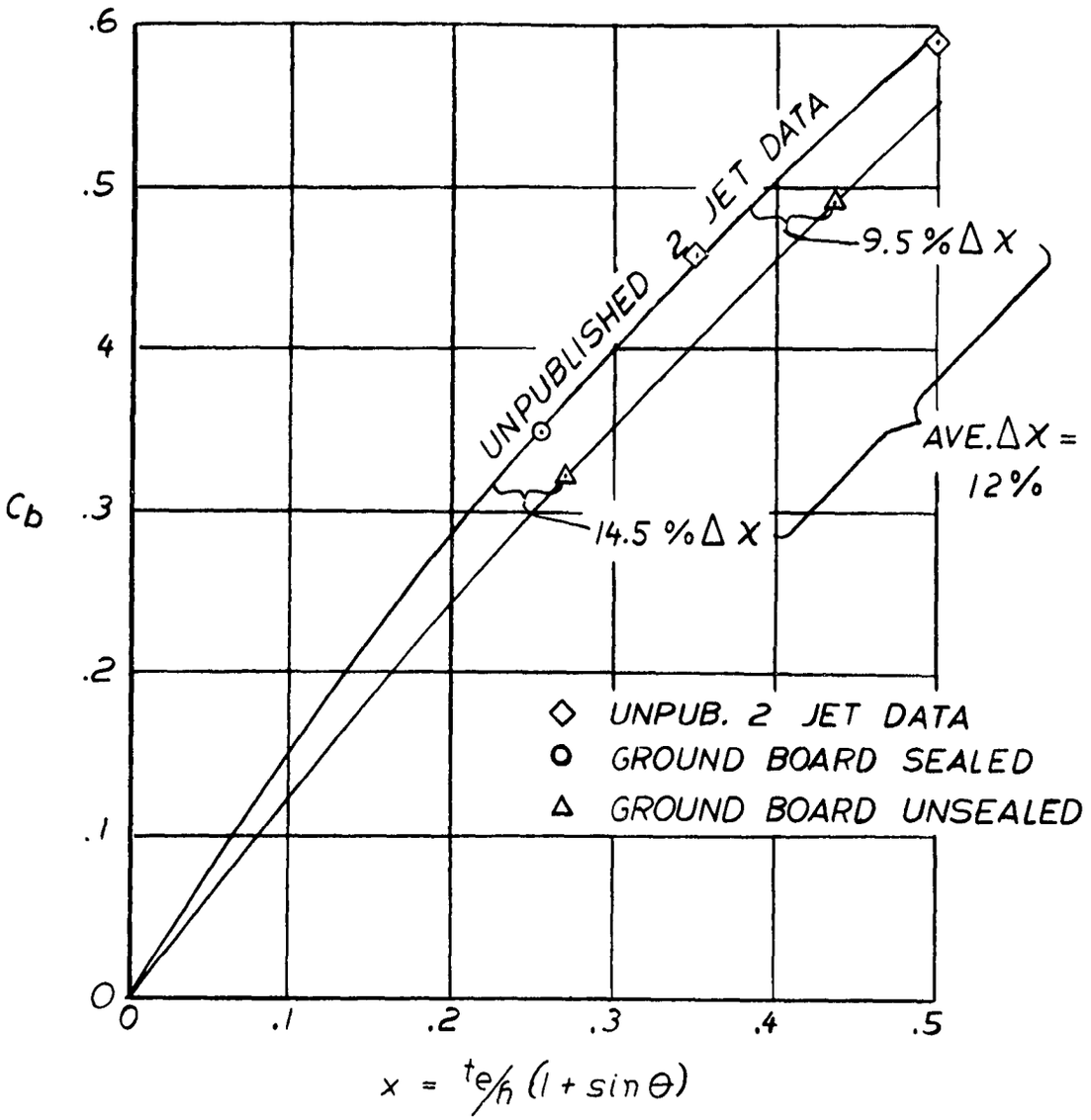

FIG. 7-17

BASE PRESSURE COEFFICIENT

WAVE OFF DATA

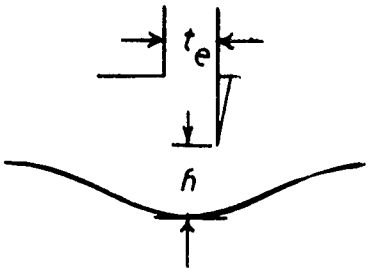

SYMBOL	P_{t_j}
○	4 IN. H_2O
△	8

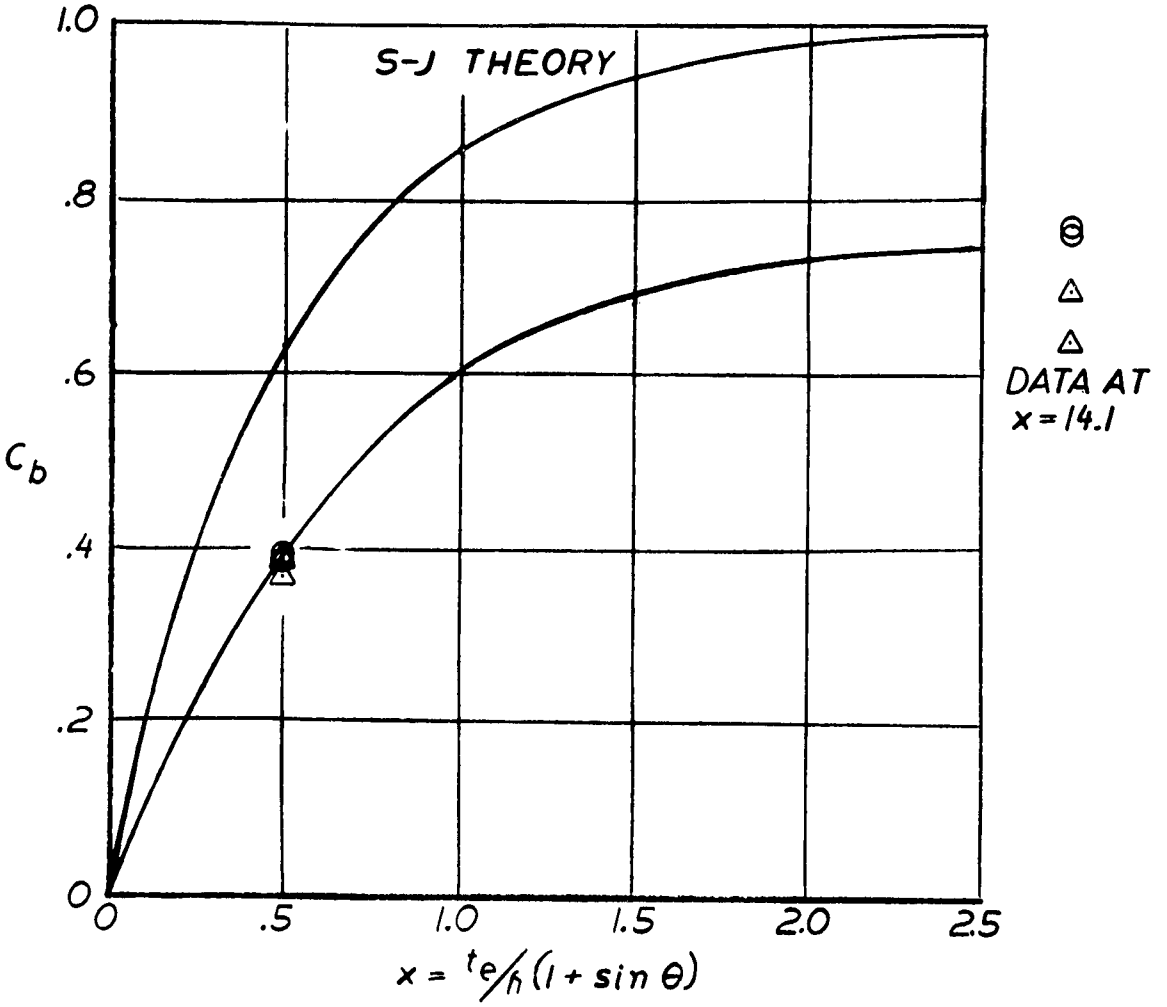

FIG. 7-18

JET VELOCITY COEFFICIENT

WAVE OFF DATA

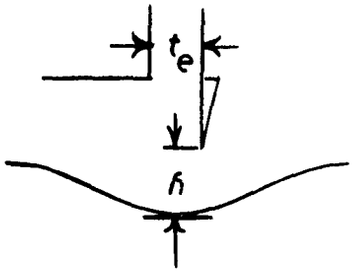

SYMBOL	P_{t_j}
○	4 IN. H_2O
△	8

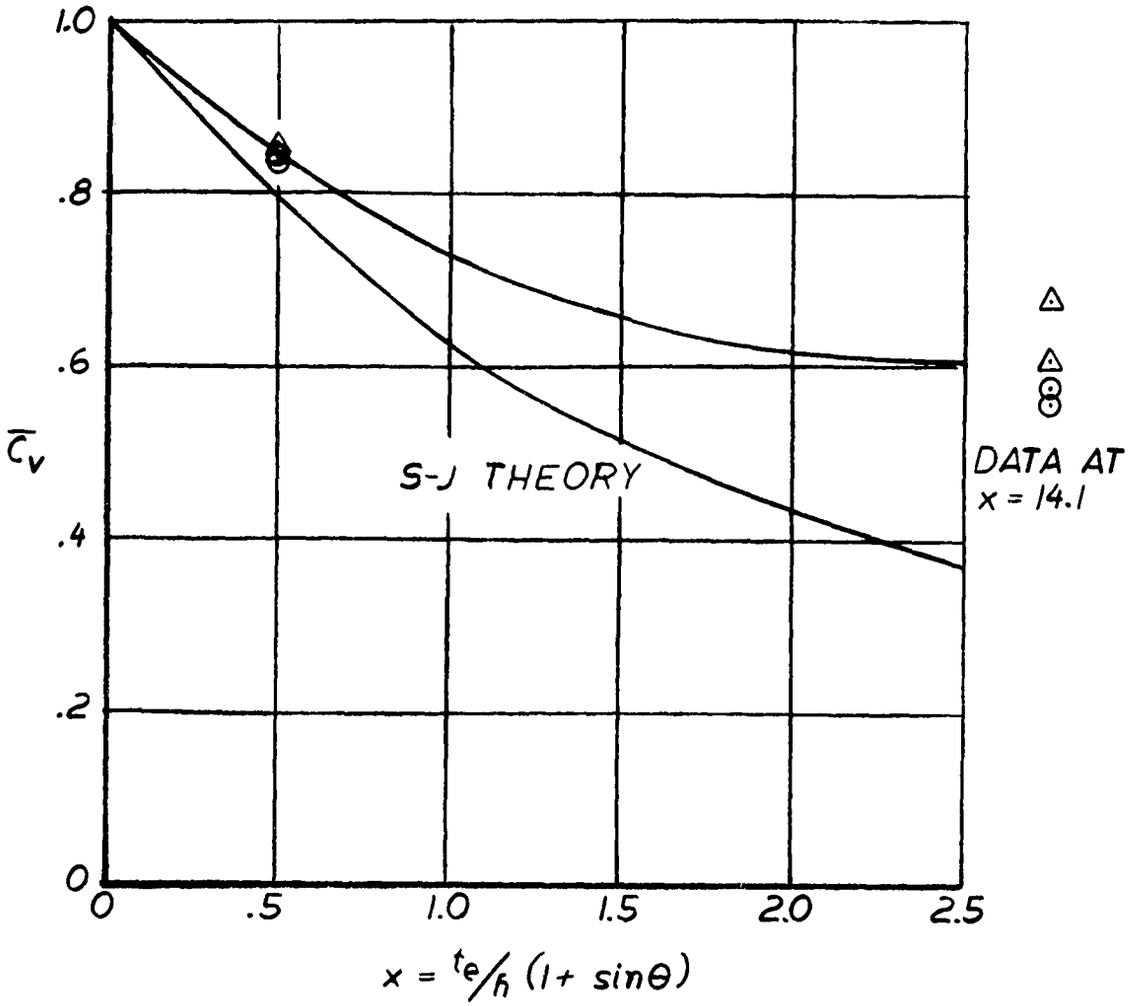

FIG. 7-19

JET REACTION COEFFICIENT

WAVE OFF DATA

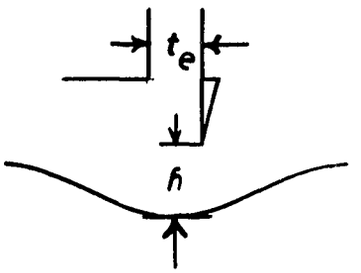

SYMBOL	P_{tj}
○	4 IN H_2O
△	8

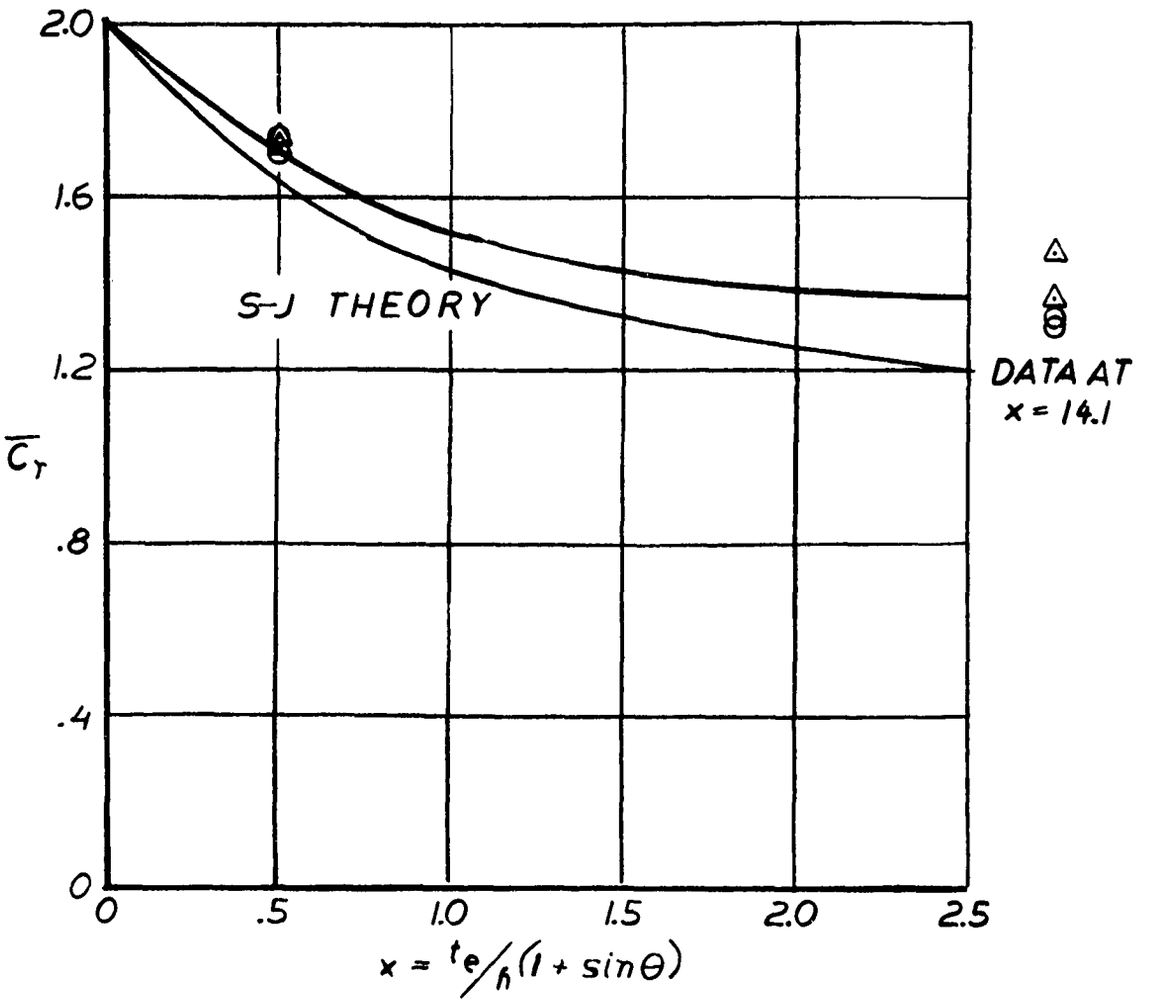

This would tend to permit more open area near the tips than if the rods were vibration free.

The dynamic data are presented in Figures 7-20, 7-21, and 7-22. The values of x at which the data are plotted are the same as in the wave off data; that is, height is measured from the trough to the flap tip. Again, the coefficients appear to have reached equilibrium values before going off scale. The data at the large x tend to cluster according to frequency, but the single fairing closely approximates both frequencies tested.

The equilibrium value of C_b is slightly lower than the value for wave off conditions. This is probably due to the nature of the deflection of the rods that make up the flap. They deflect towards the side after they buckle. The random fashion of the deflection permits sizeable leakage areas to develop intermittently, thus permitting more air to escape than would be expected from the fact that there is zero clearance from the flap tip to the wave over much of the cycle.

The close similarity in total leakage is demonstrated in Figure 7-23 which treats volume flow leakage as if the test stand were a plenum chamber (height = h_b). The discharge coefficient C is defined by the following equation:

$$Q = C\, h_b \sqrt{\frac{2p_b}{\rho}} \quad X \text{ (width of test section)}$$

In this relation p_b is analogous to the total pressure in a conventional plenum chamber.

The wave off C data tend to group according to jet total pressure while the dynamic data group by frequency. However, both sets of data may be approximated by a single line.

When the flap tips are close to the surface and the flaps are long relative to the tip clearance (h/h_b approaching zero) it is believed more appropriate to study the flow situation as a plenum chamber. When h/h_b is "large", the flow picture approaches that of an annular jet. It is not possible to state where the cross-over occurs from the data currently available.

FIG. 7-20

BASE PRESSURE COEFFICIENT

DYNAMIC DATA

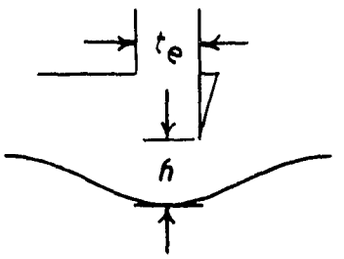

SYMBOL	CPS	P_{t_j}
△	1	8 IN. H_2O
○	1	4 "
△	3	8 "
○	3	4 "

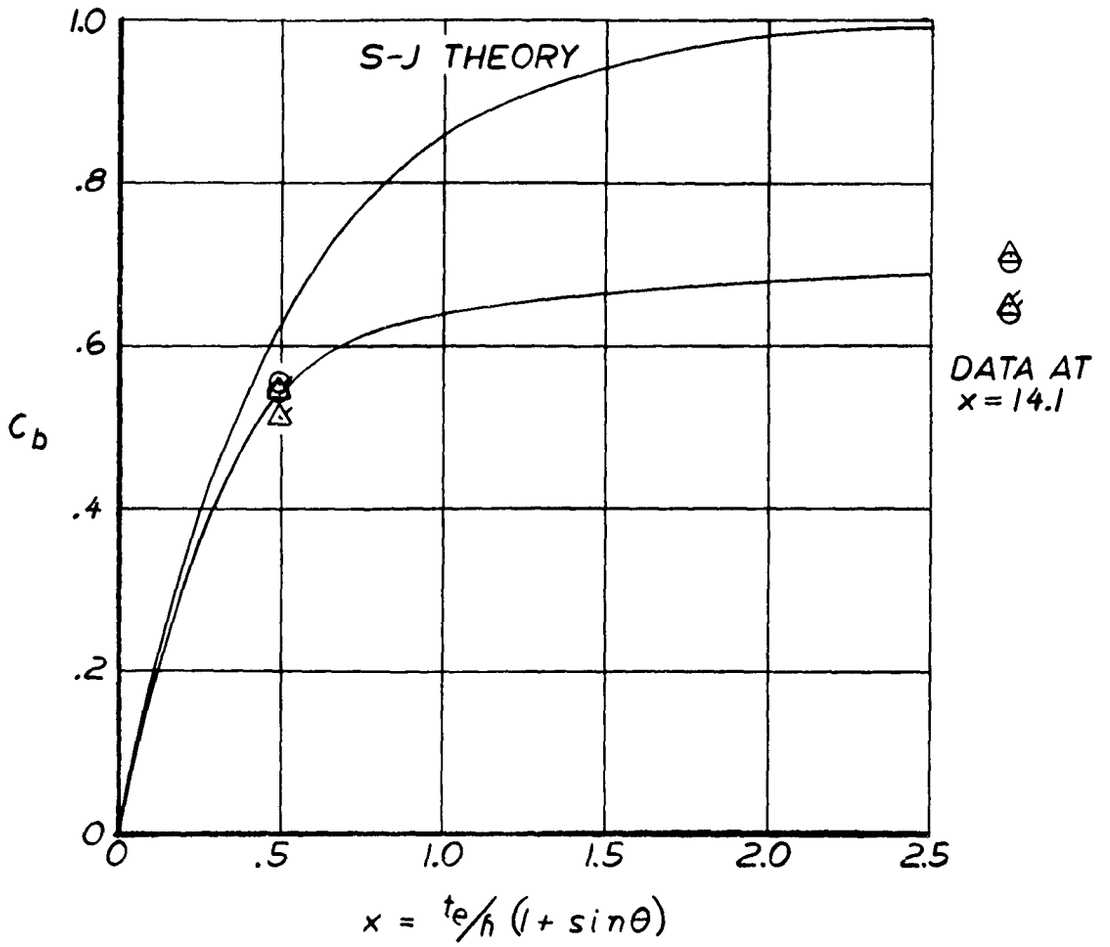

FIG. 7-21

JET VELOCITY COEFFICIENT

DYNAMIC DATA

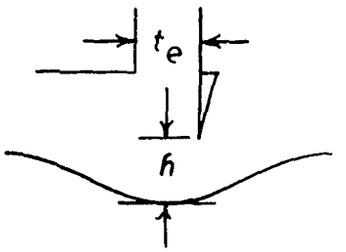

SYMBOL	CPS	P_{t_j}
△	1	8 IN. H_2O
○	1	4 "
△	3	8 "
○	3	4 "

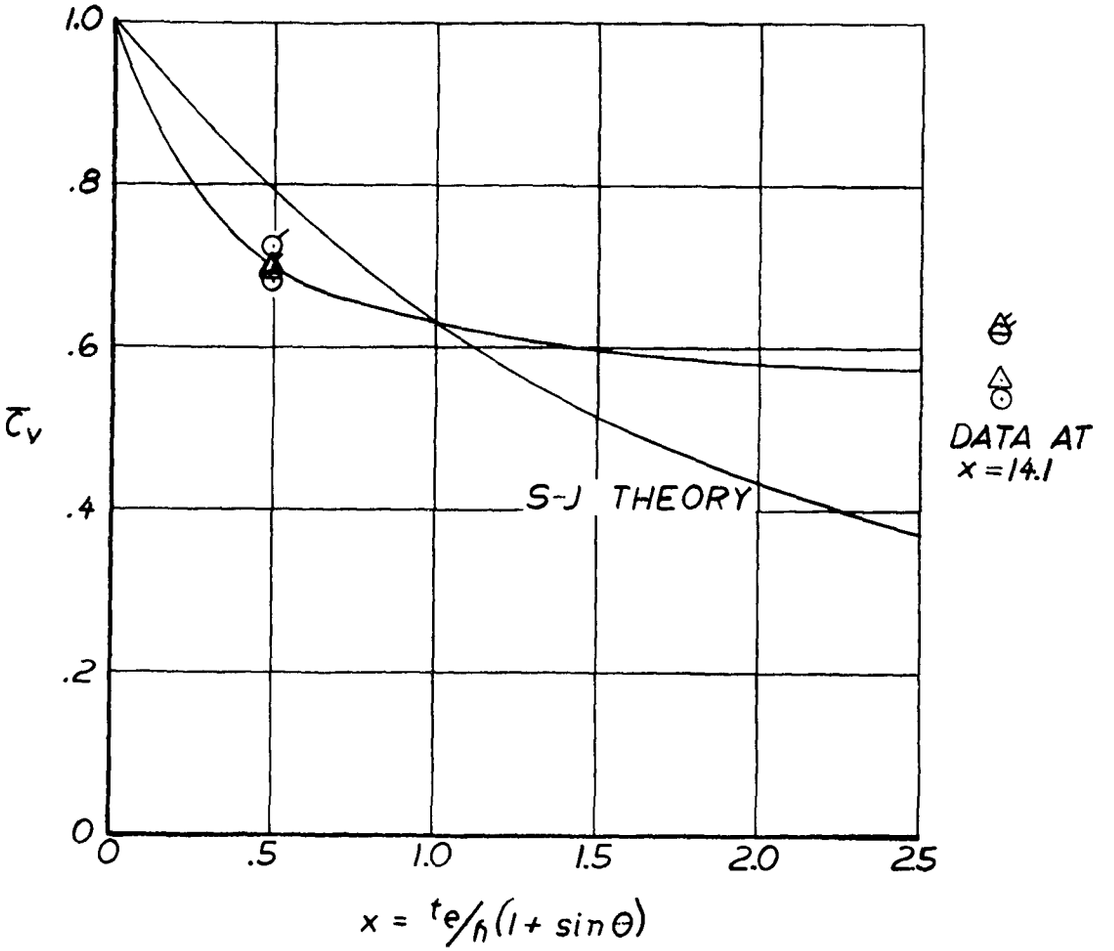

FIG. 7-22

JET REACTION COEFFICIENT

DYNAMIC DATA

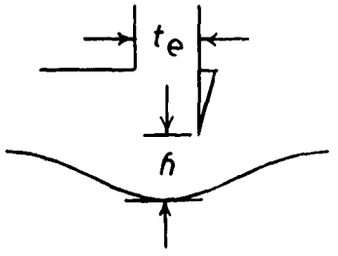

SYMBOL	CPS	P_{tj}
△	1	8 IN. H_2O
○	1	4 "
⧋	3	8 "
◎	3	4 "

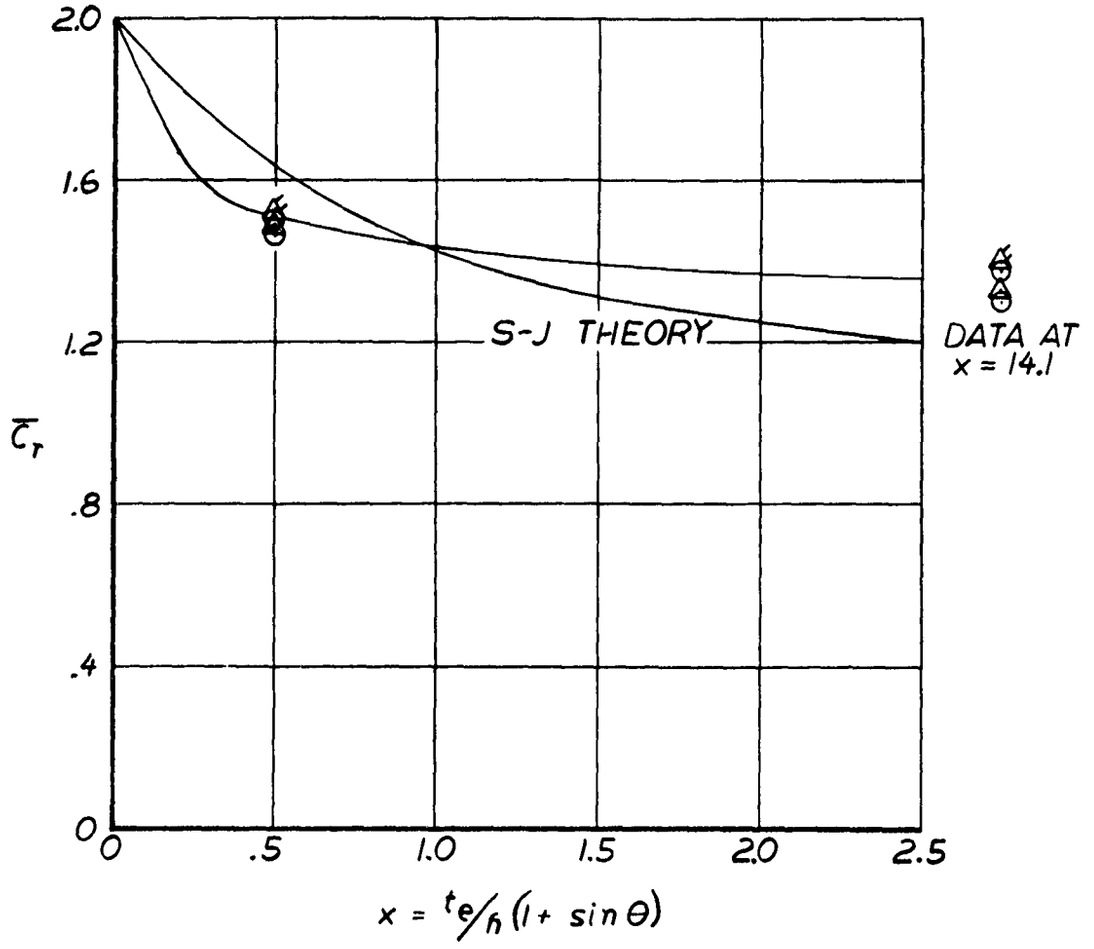

FIG. 7-23

DISCHARGE COEFFICIENT

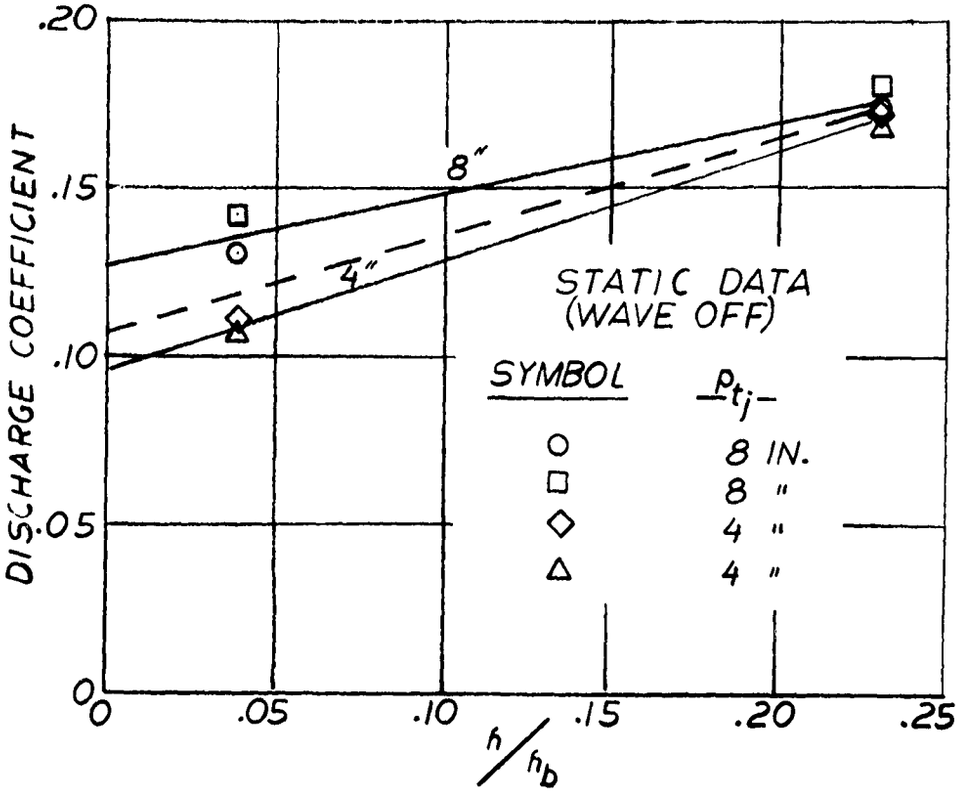

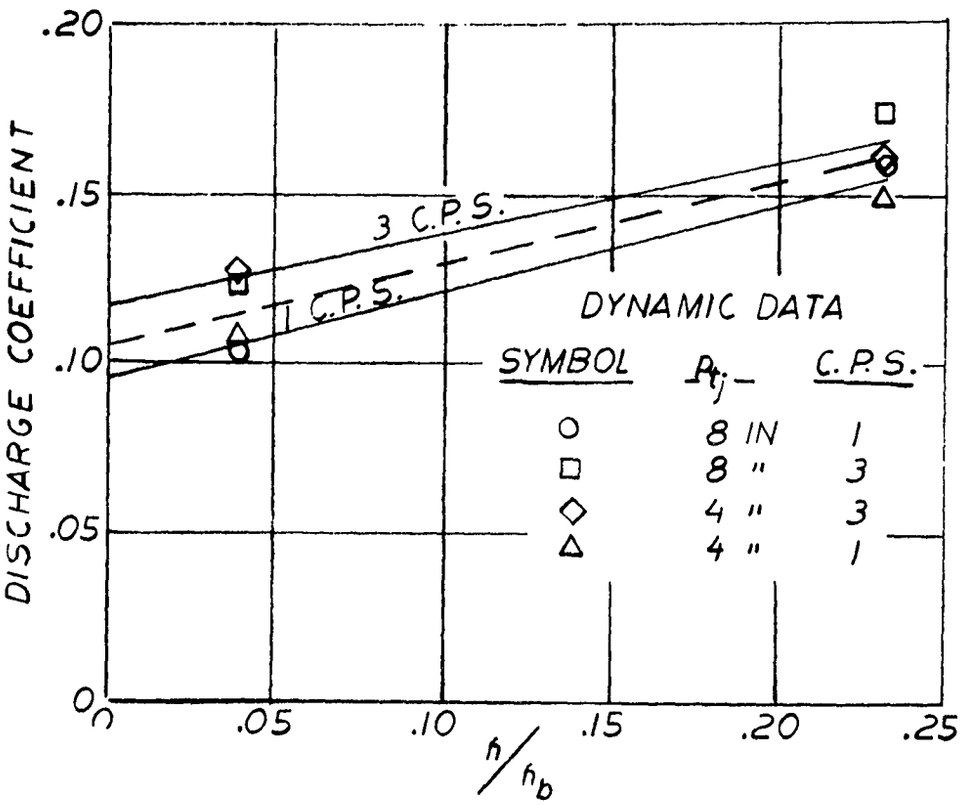

FORCE DATA

Average flap forces are plotted in Figure 7-24 against frequency of wave encounter with jet total pressure as a parameter. The data are marked as to flap position on a hydroskimmer vehicle--bow or stern. The zero frequency data points result from the stepwise pull through runs.

In the drag data, the 8 inch total pressure points seem to be consistent, but the 4 inch data are scattered. Using as guides the lines drawn through the 8 inch points, the 4 inch data were interpreted as shown.

The rods tested were actually too strong for the conditions tested on two counts. The pressure for which the rods were designed was 50 lb/ft^2 while the actual maximum base pressure attained was 35 lb/ft^2. It was realized that the pressure capacity was too high but due to uncertainties as to the pressure attainable with the flaps, there was a safety margin built in. In addition, the original attachment of the 12 inch rods was found lacking in strength so that in the final configuration there was only 10.7 inches of free length of rod. Using the relation developed in Section VI

$$p = 16{,}300 \left(\frac{a}{\ell}\right)^3$$

it can be seen that the pressure capabilities of the flap were increased by the inverse cube of the length. Also, uncertainties in the structural analysis and fabrication led to a net pressure capability of approximately 100 lb/ft^2.

The coefficient of sliding friction between the wave and the flaps was determined by pulling the flaps over a strip of greased wave cap material and measuring the pull and normal force. The value of this friction coefficient was between 0.07 and 0.10. Since there was at least this much scatter in the data, no attempt was made to separate frictional drag from structural.

Had the rods been exactly optimum (just able to withstand the base pressure), the drags measured for the stern flaps would have been essentially zero, since any load over that applied by pressure would have caused the rods to buckle. In some vehicle designs it might even be desirable to eliminate the stern flap for the purpose of obtaining thrust from the rear jet.

FIG. 7-24

FORCES ON 2FT. BEAM FLAP

P_{tj}

○ = 8"H_2O

□ = 4" "

FLAGGED SYMBOLS DENOTE BOW FLAP FORCES
UNFLAGGED SYMBOLS DENOTE STERN FLAP FORCES
AVERAGED DATA

h = 0.125 IN.

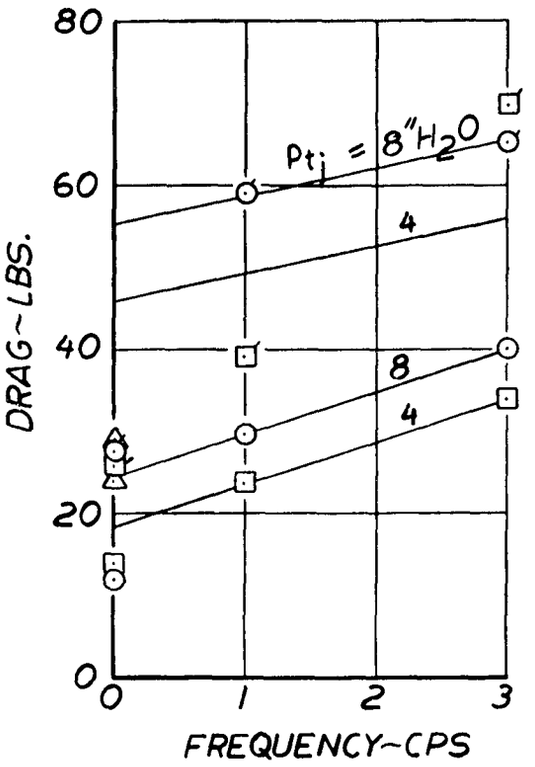

h = 3.6 IN.

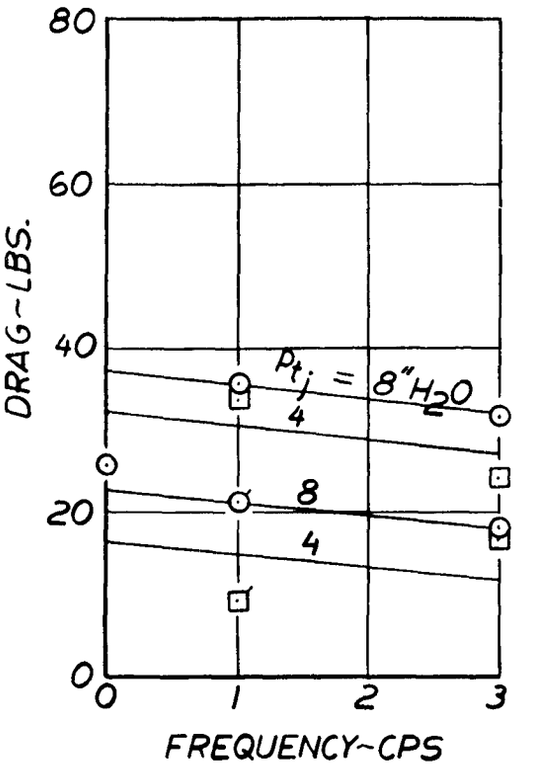

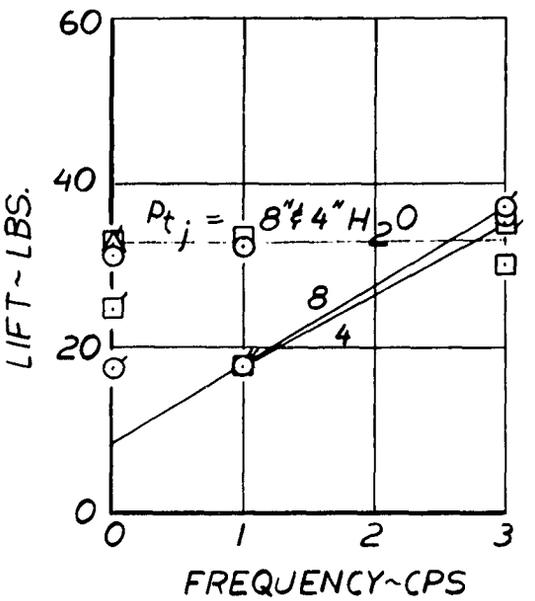

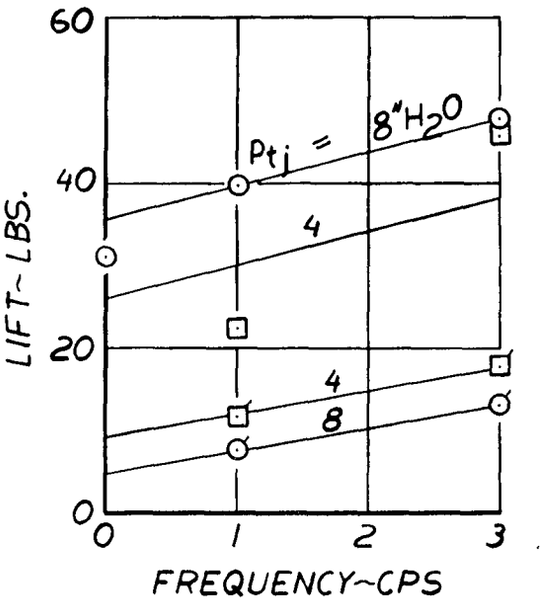

If there is a pressure exerted against the bow flaps, a static force exerted in the opposite direction would have to first overcome the pressure load on the flap and then overcome the basic structural rigidity of the flap in order to buckle it. Thus the static load with pressure against the opposite side would be approximately twice that required to buckle the flap with no pressure on the flap. The basic static load relations developed in Section VI can be used to ratio the measured drags for other lengths of flap and other pressures than those used in the test conditions because the measured drags already include this factor of two. Admittedly, this process neglects dynamic drag loads, but it is believed to be a good approximation since there is little evidence of a strong dynamic effect in Figure 7-24.

The optimum drag for the bow flap can thus be determined from the static load derivation in Section VI.

$$D = 0.0141 \quad D_{basic} \ell^2 \quad p^{4/3}$$

where D_{basic} is the drag measured in the dynamic tests. Figure 7-24)

The optimum bow flap drag loads for 8 and 4 inch jet total pressures and for both heights are shown in Figure 7-25.. The forces are further refined in this figure by being presented as drag per foot of flap beam. The dimension (a) of the optimum flap found from the relations of Section VI is

$$a = .263 \text{ inch}$$

The measured drag may be plotted as a function of the wave penetration parameter, $\frac{w}{\ell}\left(1 - \frac{h}{w}\right)$ to permit estimation of drags at other wave heights, flap lengths and flap tip heights above the wave trough. For purposes of generalization a band of drags were taken to permit a demonstration of sensitivity of power to error in drag estimation. The mid frequency point of the drag curves for 8 and 4 inches total pressure and both heights on Figure 7-24 was taken as indicative of basic drag.

The basic drag per foot of flap beam is shown in Figure 7-26 as a function of the wave penetration parameter. The band of basic drag is extrapolated to a value of wave penetration parameter of 1.0, which corresponds to the condition where the wave height is equal to the flap length and the flap penetrates to the wave trough.

DRAG PER FOOT OF FLAP BEAM

OPTIMUM FLAP GEOMETRY FOR PRESSURE AND FLAP LENGTH TESTED

p_b = 34.9 LB/FT^2

LENGTH = 10.7 IN.

AVERAGED DATA

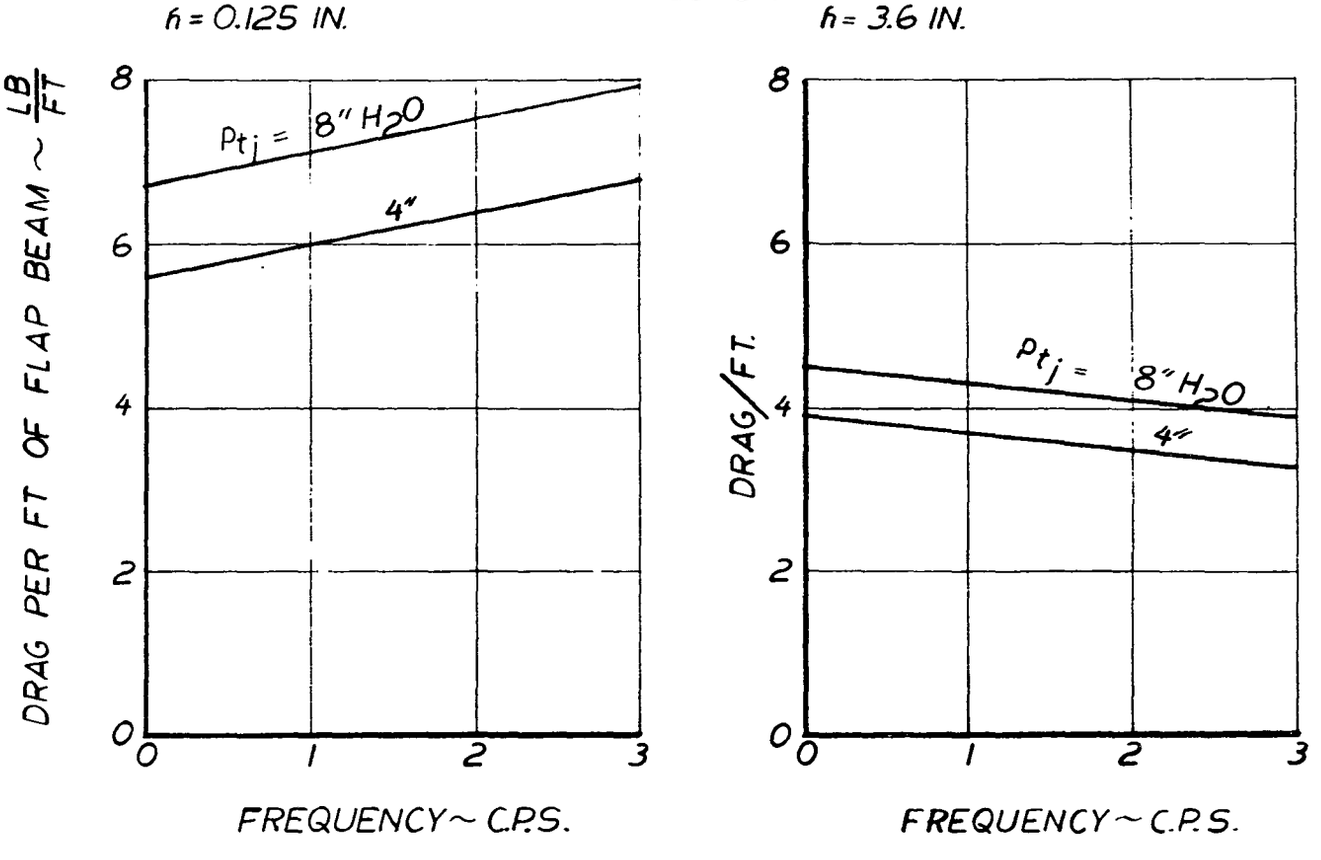

FIG. 7-25

FIG. 7-26

BASIC DRAG PER FOOT OF FLAP BEAM ~ LB/FT

TO BE USED FOR ESTIMATING DRAG FOR PRESSURES AND FLAP LENGTHS OTHER THAN THOSE TESTED

$$D = .0141\, D_{BASIC}\, l^2\, p^{4/3}$$

l = LENGTH (IN.) $\qquad$ p = PRESSURE (PSI.)

W = WAVE HEIGHT (IN.)

h = FLAP CLEARANCE TO TROUGH (IN.)

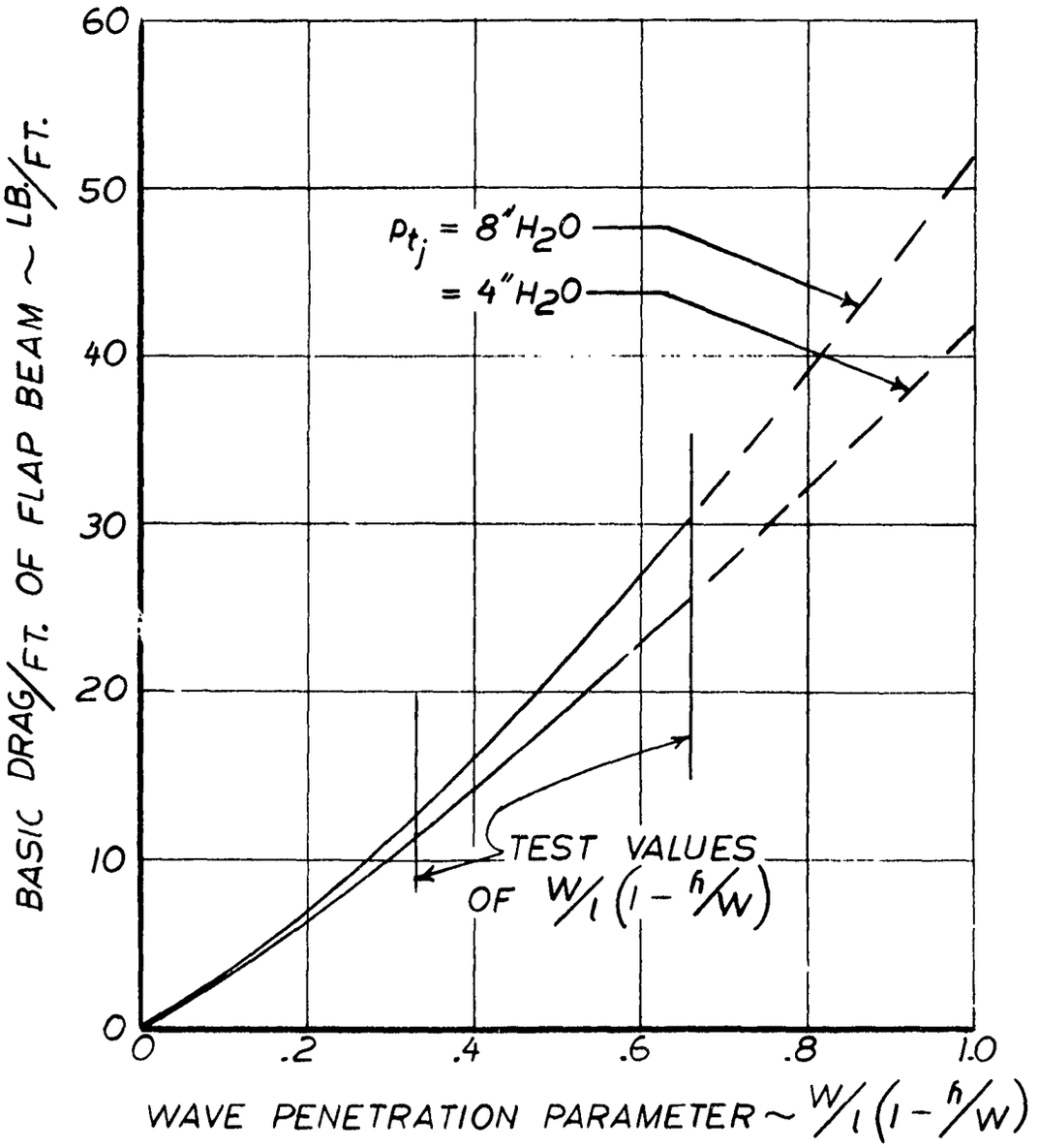

To summarize the drag generalization briefly, the plot of basic drag per foot of flap beam against wave penetration parameter permits the extension of the basic drag to other combinations of wave height, flap tip height and flap length than those tested, and the relation

$$D = 0.0141\ D_{basic}\ \ell^2\ p^{4/3}$$

permits the extension to other flap lengths and base pressures than those tested.

There are no expressions available for estimating the lift which results from flap deflection, such as exist for drag. Therefore, the lift data from Figure 7-24 are shown as L/D ratio in Figure 7-27 plotted against wave penetration parameter. Based on the limited data, the curves appear to maximize and then approach a constant value. Both curves tend back toward zero as wave penetration parameter increases, but it is more logical for them to level off than to actually return to zero in the region where drag is becoming greatest.

EFFECT OF FLAPS ON VEHICLE PERFORMANCE

The most graphic way to predict how flexible flaps can benefit hydroskimmer performance is to examine the effect on a particular vehicle. The vehicle on which this will be effected was described in Section VI. The performance will be shown in four graphs. The conditions in each are: (a) no flaps, flat calm sea; (b) flaps installed, flat calm sea; (c) no flaps, state three sea; (d) flaps installed, state three sea. The first two show the power saving while operating over a level surface with no skeg or flap drag, and the second two show the effect of inclusion of skeg drag and flap drag. Figure 7-28 shows power requirements for the 45,000 lb vehicle over a calm sea with no flaps. The cushion power is seen to decrease with increasing velocity while the momentum drag power increases, as do the aerodynamic and wave drag power requirements. The peak in the total power curve is due to the decrease in wave drag as the vehicle exceeds the so-called "hump" speed. Since the bow and stern jets are not symmetrical there is a thrust on the vehicle which is counteracted by reverse thrust from the propellers. This causes the small power increase as V approaches zero.

FLAP LIFT TO DRAG RATIO

TO BE USED FOR ESTIMATING LIFT FOR PRESSURES AND FLAP LENGTHS OTHER THAN THOSE TESTED
USE WITH FIG. 7-26

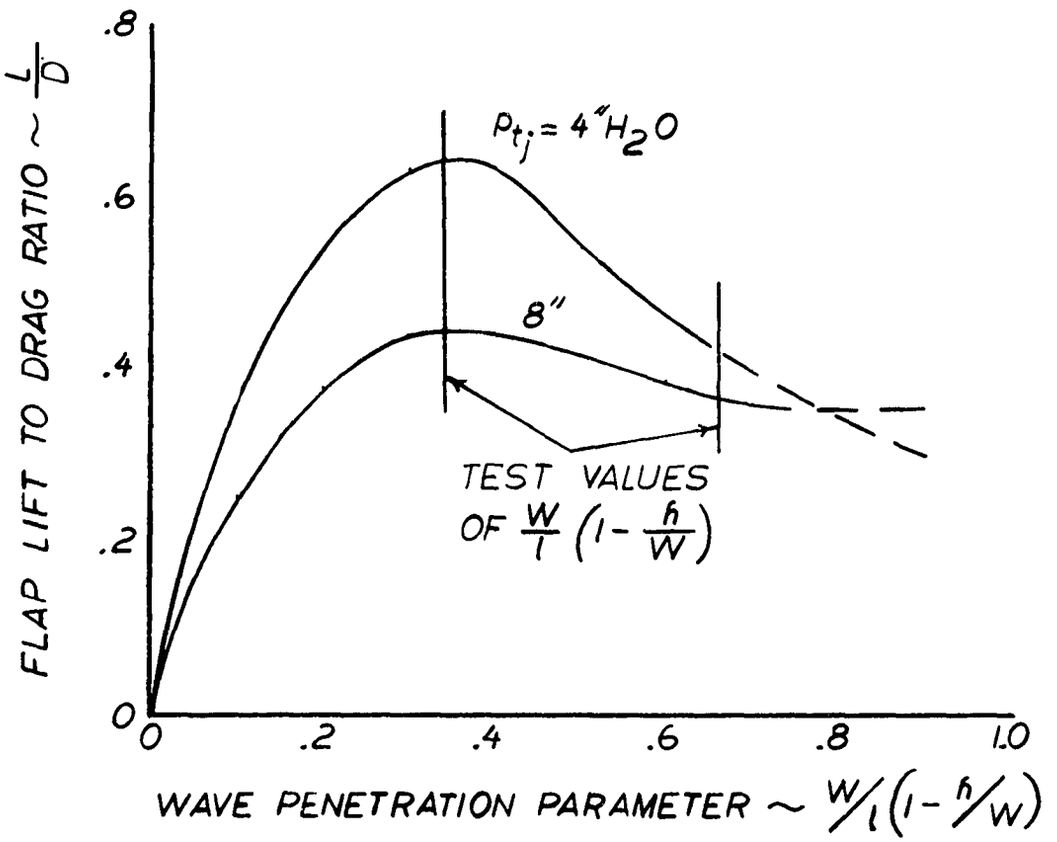

FIG. 7-28

HORSEPOWER VS. VELOCITY

NO FLAPS $h_b = 4.5$ FT.
FLAT CALM SEA

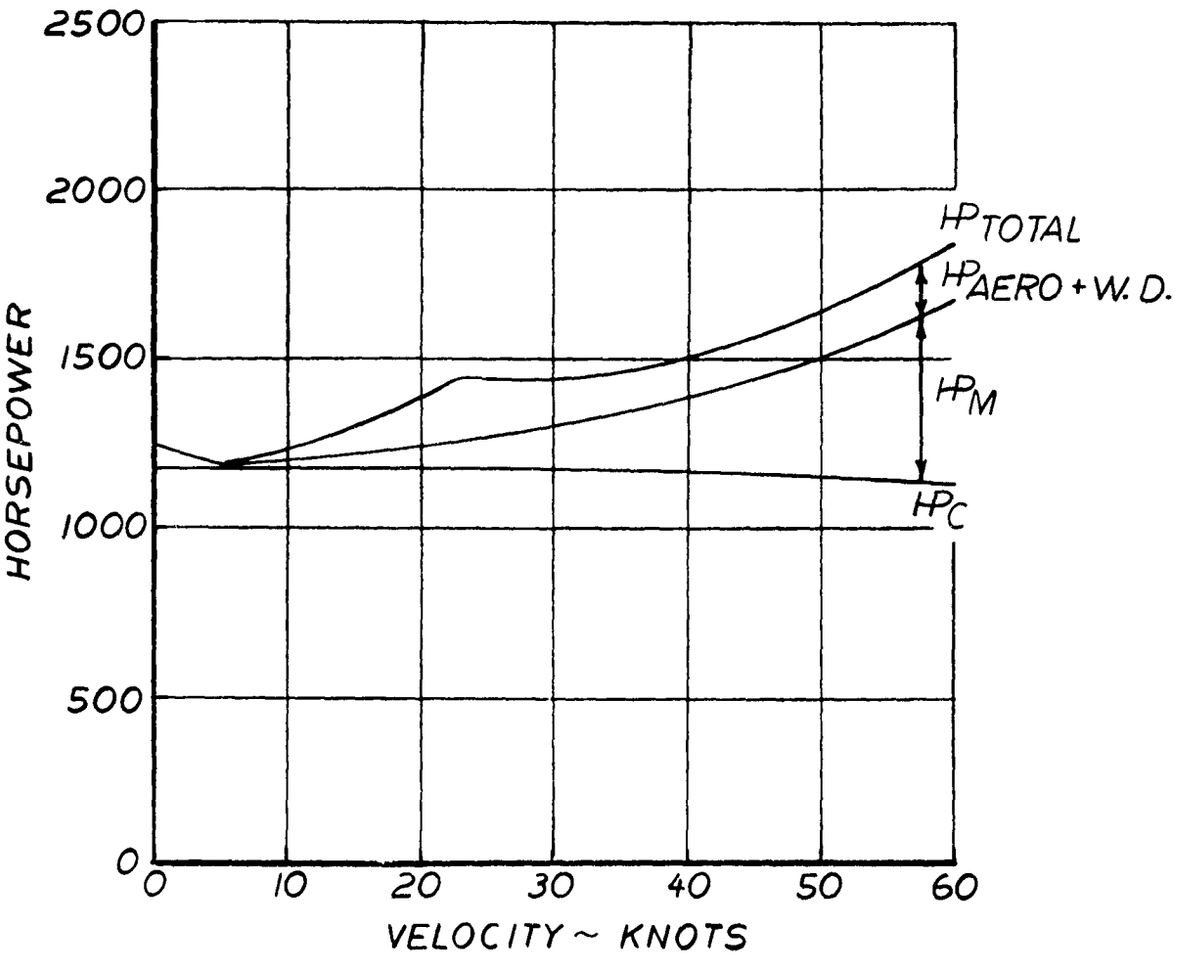

Figure 7-29 demonstrates the substantial reduction in power requirements obtained by installing flexible flaps for the same conditions as in Figure 7-28. The reductions in cushion and momentum drag power requirements are effected by the reduction in volume flow afforded by the flaps. Note that the wave drag and aerodynamic drag power used in this Figure are the same as in Figure 7-28. These terms should actually be slightly different because of higher base pressure and less effect of jet flow on the external flow field, but these effects will be minor. The overall reduction in vehicle power requirements is a factor of approximately three at a speed of 60 knots.

The symmetrical leakage of air out the bow and stern flaps results in no net thrust in the vehicle at zero velocity. Hence, no power is required for reverse thrust.

While operating in the state three sea, the no flap power requirements are shown in Figure 7-30. Skeg drag power requirements are included in this Figure. The asymmetry of the bow and stern jets create thrust at zero velocity. Also, the skeg jets, which are now in use, create thrust.

Power requirements with flaps installed over a state three sea are shown in Figure 7-31. Friction drag power requirements are included in this curve in addition to the skeg drag. The total power requirement is shown as a shaded band of minimum and maximum drags shown in Figure 7-26. At a speed of 60 knots power required is reduced by a factor of approximately 1.5. At zero velocity the flow out the bow and stern is symmetrical, causing no thrust. However, the sket jets are operating, creating a thrust.

The flap rod size required for the study vehicle is very much larger than those tested. At this size it is practical to hollow the rods without materially affecting their strength. This makes possible the fabrication of large light weight flaps. The flap lift, although uncertain in value, appears to approximately counterbalance flap weight. Thus, neither flap weight nor lift have been included in the estimates of power required.

Thus, at a speed of 60 knots the total vehicle power requirements can be reduced by a factor ranging from about 3 to about 1.5 depending on sea state.

FIG. 7-29

HORSEPOWER VS. VELOCITY

h_b = 4.5 FT.

h = .25 FT. TO FLAP TIP
FLAT CALM SEA

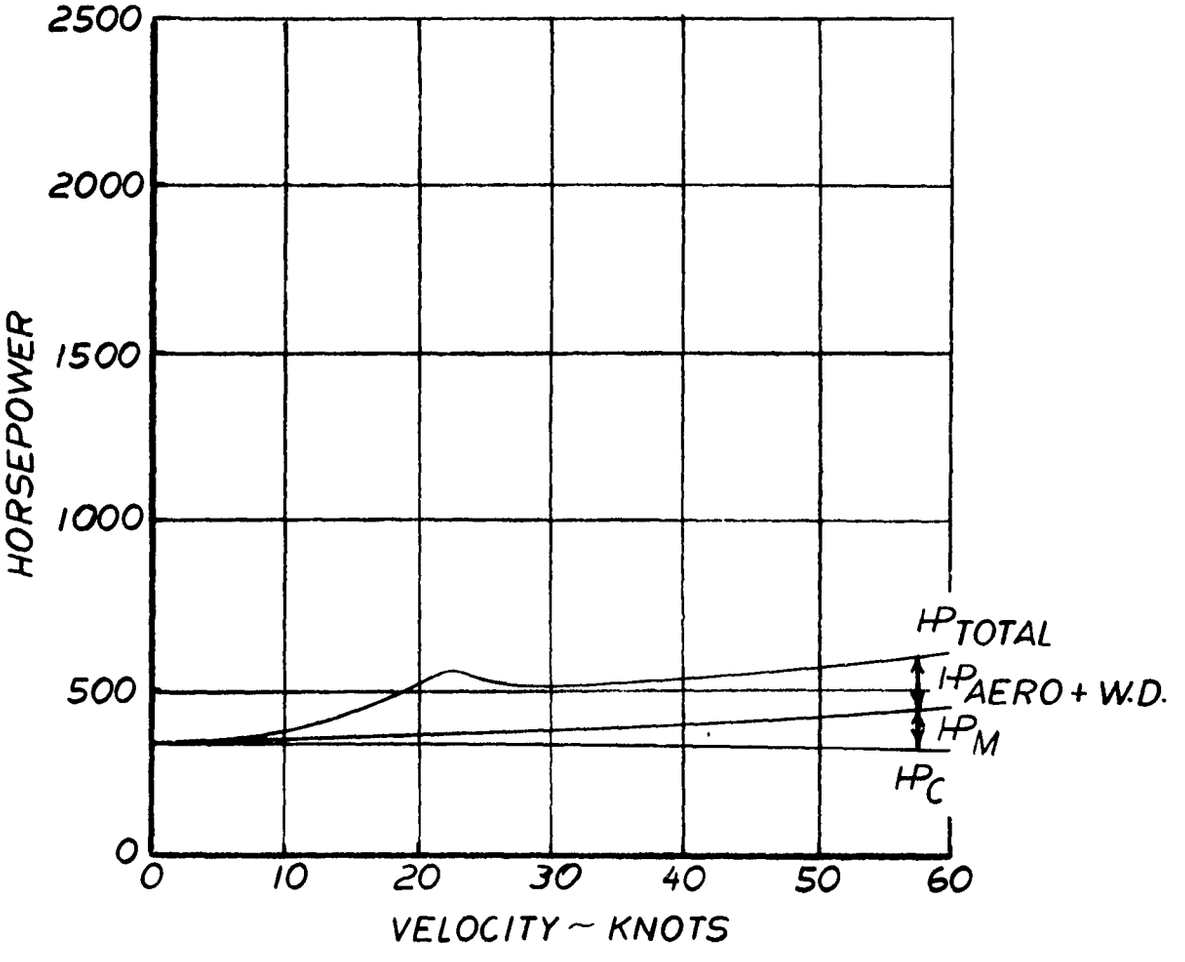

FIG. 7-30

HORSEPOWER VS. VELOCITY

NO FLAPS
4.5 FT. FROM BASE TO WAVE MEAN HEIGHT
STATE 3 SEA

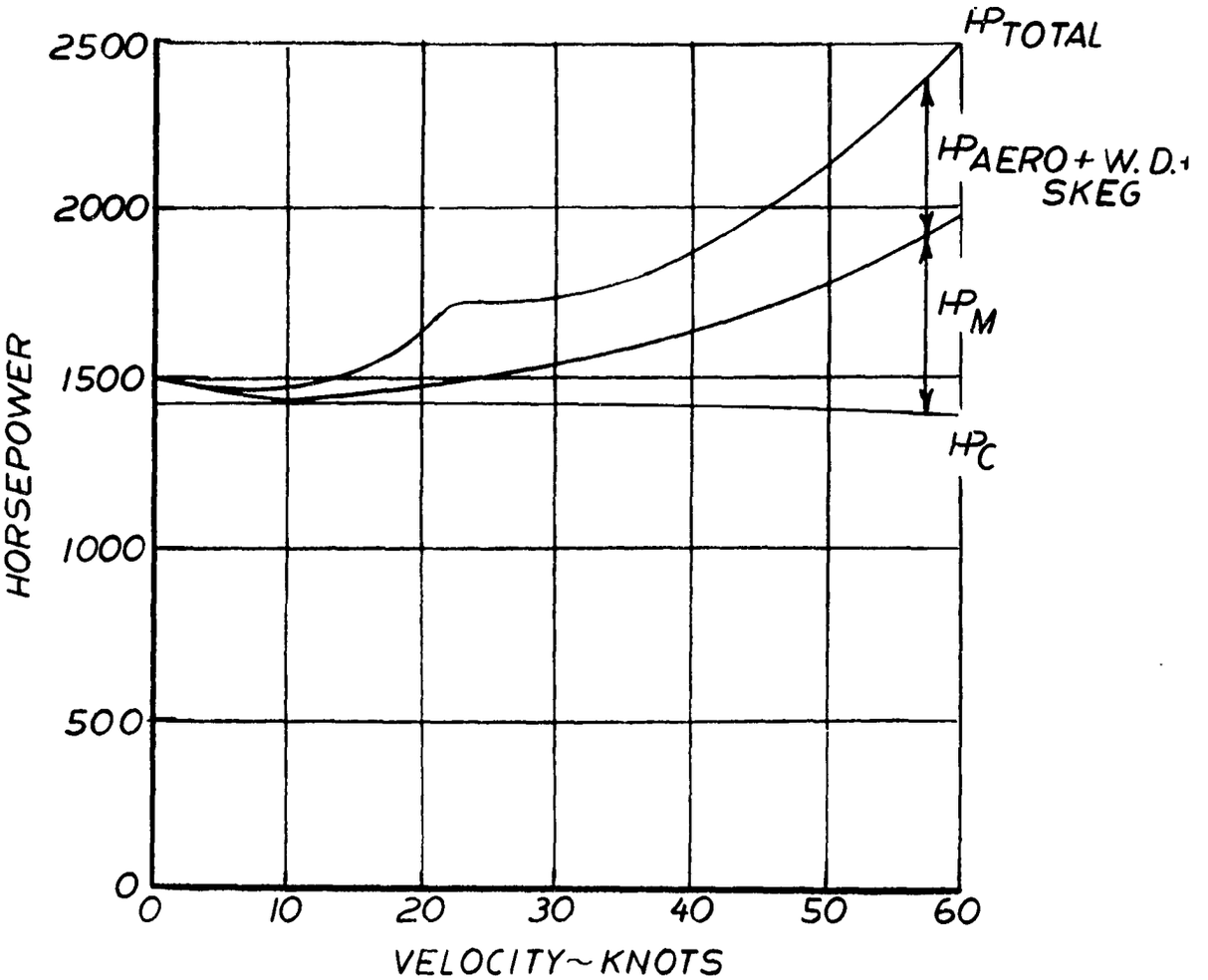

FIG. 7-31

HORSEPOWER VS. VELOCITY

4.5 FT. FROM BASE TO WAVE MEAN HEIGHT
FLAP TIP .25 FT. ABOVE WAVE MEAN HEIGHT
STATE 3 SEA

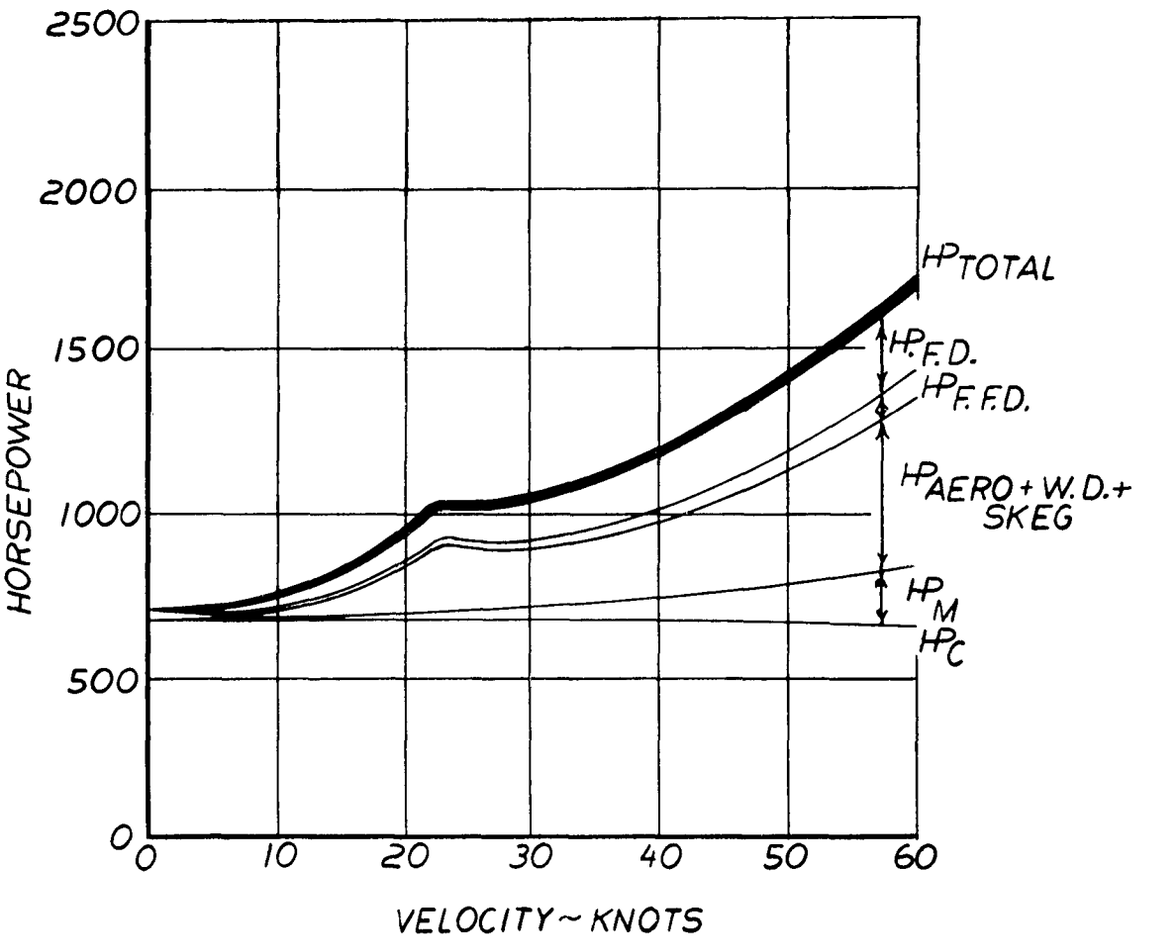

SECTION VIII

CONCLUSIONS AND RECOMMENDATIONS

The work accomplished under this contract indicates clearly that the application of flexible flaps to hydroskimmer type craft will result in savings in power, complexity, and cost with resultant gains in economy and payload. The power saving can be used to obtain higher cruise heights, thus extending the rough water capability of the craft. One or more of the following alternatives is recommended as the best way to proceed with an actual operational demonstration of the flexible flap potential:

1. Installation of flaps on the Bell hydroskimmer--tests and comparisons with original configuration.
2. Installation of flaps on the Hughes Hydrostreak STV. High operating height compared to Bell machine may produce more valuable data.
3. Installation of large scale flaps on 20 ton hydroskimmer currently under consideration by Bu Ships. Ducting and structure may have to be redesigned to realize full flap potential.
4. Design, construction, and test of a small hydroskimmer specifically for flap tests. The "tailoring" of a complete vehicle design to the low volume flow requirements of the flexible flap should result in achieving a very convincing demonstration with minimum time and cost.

The recommended design for flaps to be used in Alternative 1 is as follows:

(a) fiberglas reinforced urethane rods

(b) rod section width = 0.26 inch

(c) rod section depth = 0.42 inch (from the base pressure of approximately 23 lb/ft^2)

(d) fiberglas rod spacing = 0.26 inch

(e) flap length = 12 inches (parallel to jet outer wall)

SECTION IX

REFERENCES

1. Carmichael, B. H.
HOVERING TWO-DIMENSIONAL ANNUAL JET PERFORMANCE EXPERIMENTS
Aeronutronic Publication U-1053
November 1960

2. Stanton Jones, R.
SOME DESIGN PROBLEMS OF HOVERCRAFT
IAS Paper No. 61-45
Presented at the IAS 29th Annual Meeting, New York, N.Y.
23 through 25 January, 1961

3. Strand, T.; Royce, W. W.; and Fujita, T.
PERFORMANCE THEORY FOR HIGH SPEED GROUND EFFECT MACHINE
Vehicle Research Corporation Report No. 11
1 June 1961

4. Timoshenko, S.
THEORY OF ELASTIC STABILITY
Engineering Societies Monograph
McGraw-Hill Book Company, Inc., 1936

5. HYDROSKIMMER TECHNICAL DISSERTATION
Aeronutronic Publication P11151 (U)
30 June 1961

6. Hoerner, S. F., Dr. Ing.
FLUID DYNAMIC DRAG
Published by the Author
1958